UNIVERSITÉ DE SHERBROOKE
Faculté de génie
Département de génie chimique et de génie biotechnologique

ÉTUDE DE LA FORMATION DE BOUES DANS LA CELLULE HALL-HÉROULT

Thèse de doctorat
Spécialité : génie chimique

Mojtaba FALLAH FINI

Sherbrooke (Québec) Canada
7 mai 2020

MEMBRES DU JURY

Gervais SOUCY

Directeur

Martin DÉSILETS

Codirecteur

Duygu KOCAEFE

Évaluatrice externe

Véronique DASSYLVA-RAYMOND

Évaluatrice externe

Jocelyn VEILLEUX

Évaluateur

RÉSUMÉ

La production d'aluminium comme un procédé métallurgique énergivore, joue un rôle majeur dans l'économie du Québec. Un facteur qui peut augmenter la consommation d'énergie correspondante est la formation de dépôts résistifs (des boues) à la surface de la cathode. Par conséquent, l'objectif de cette thèse est de clarifier davantage la nature complexe de la formation de boues dans le procédé Hall-Héroult, en tant que le procédé principal de production d'aluminium.

Les objectifs de recherche sont:

a) étudier l'effet possible de la nuance de cathode sur la formation ou la dissolution des boues;
b) déterminer l'importance relative de trois paramètres opérationnels, à savoir la température d'opération, le ratio de cryolite (CR) ainsi que la nuance de cathode;
c) étudier de façon expérimentale des boues induites chimiquement (c'est-à-dire précipitation des espèces cryolitiques dues au changement de la chimie du bain comme la consommation d'alumine ou la polarisation de concentration de sodium).

La méthodologie expérimentale comporte une configuration expérimentale à l'échelle du banc d'essai, cinq nuances cathodiques différentes, une conception de plan expérimental factoriel complet ayant trois variables et deux niveaux pour chaque paramètre, à savoir la température d'opération (940 et 960 ° C), le ratio de cryolite (2,2 et 3,8) et deux nuances cathodiques.

Les résultats de cette recherche sont:

i. une combinaison de porosité ouverte et de perméabilité à l'air des cathodes affecte l'épaisseur des couches de carbure d'aluminium;
ii. parmi plusieurs propriétés, la conductivité thermique et la porosité ouverte des cathodes affectent la tendance à la formation de boues en raison de la perte de chaleur au fond de la cellule et des phénomènes interfaciaux;
iii. l'influence significative de la température d'opération par rapport au ratio de cryolite et à la nuance de cathode;
iv. la précipitation des espèces cryolitiques solides est accélérée grâce à la polarisation de concentration plus élevée et le taux d'épuisement de l'aluminium plus rapide;
v. le temps de réalimentation des boues est plus élevé pour les cathodes à porosités ouvertes plus élevées en raison de l'interaction des boues, avec des couches de carbure plus épaisses et des espèces carbonées au fond de la cellule.

Mots-clés : Procédé Hall-Héroult, aluminium, électrolyse, thermodynamique, cathode, cryolite, boue, carbure d'aluminium

ABSTRACT

The aluminum production, as one of the most energy consuming metallurgical processes, has a major role in the Québec's economy. One factor that can increase the corresponding energy consumption is the formation of resistive deposits, such as sludge, on the surface of the cathode lining. The aim of this PhD thesis is to shed some light on the complex nature of sludge formation in Hall-Héroult process, as the main process for production of aluminum.

The research objectives are:

a) to study the possible effect of the cathode grade on sludge formation or dissolution;
b) to evaluate the relative importance of three operational parameters, namely the operational temperature, the cryolite ratio (CR) as well as the cathode grade;
c) to carry out an experimental investigation of chemically induced sludge (i.e. precipitation of cryolitic species due to change of bath chemistry such as alumina consumption or sodium concentration polarization).

The experimental methodologie includes an experimental bench scale set-up, five different graphitized cathode grades, a full factorial experimental plan design having three variables and two levels for each parameter, namely the operational temperature (940 & 960 °C), the cryolite ratio (2.2 and 3.8), and two cathode grades.

The results of this research are:

i. a combination of open porosity and air permeability of the cathodes affects the thickness of deposited aluminum carbide layers;
ii. among several properties, thermal conductivity and open porosity of the cathodes affect the sludge formation tendency of the cathode lining due to heat loss at the bottom of the cell and interfacial phenomena;
iii. there is overwhelming influence of operational temperature versus the cryolite ratio and cathode grade;
iv. the precipitation of solid cryolitic species is expedited thanks to a higher concentration polarization and a faster aluminum depletion rate;
v. the back-feeding time of sludge layers is higher in cathodes with higher open porosities because of the interaction of the sludge with thicker carbide layers and carbonaceous species at the bottom of the cell.

Keywords: Hall-Héroult process, aluminum, electrolysis, thermodynamics, cathode, cryolite, sludge (muck), aluminum carbide

REMERCIEMENTS

En premier lieu je remercie professeur Gervais Soucy et professeur Martin Désilets pour m'avoir supporté tout le temps même avec leur horaire surchargé. Je vous en serai perpétuellement reconnaissant.

En deuxième lieu force est de reconnaître a) les apports techniques d'André Bilodeau et Serge Gagnon en laboratoire, b) les supports analytiques des membres de la plateforme de recherche et d'analyse des matériaux (PRAM), à savoir Carl St-louis, Sonia Blais, Stéphane Gutierrez et Charles Bertrand, c) les apports techniques et théoriques des coauteurs des articles, soit Patrick Pelletier et Didier Lombard de Rio-Tinto ainsi que Loig Rivoaland et Regis Paulus de Carbone Savoie, et enfin et surtout d) les supports analytiques et émotionnels de Olivier Drevelle.

Il faut également apprécier mes collègues et mes pairs Jean-René Landry, Martin Brassard, Colin Dessemond et François Allard qui m'ont aidé durant mes études.

Ensuite, force est de constater que je n'aurais jamais pu accomplir tout cela sans l'aide de ma famille et mes copains. D'abord, je suis éternellement redevable à ma sœur professeure Saeideh Fallah-Fini. Quoique soit les succès que j'ai obtenus au cours de ma vie, je te les dois.

De surcroît, il faut mentionner ma chère amie Faranak et son copain Bijan qui étaient à mes côtés durant les temps difficiles. Je souhaite aussi montrer toute ma gratitude à mon amie Gabriela, son époux Thierry et leur chinchilla Tigars. Enfin, je ne peux pas oublier mes amis qui étaient toujours bienveillants envers moi, à savoir Azin Aghdaei, Massoud Karami, Tony Kunnari, Rejean Loiselle, Steeve Turmel, Konstantin Ntokas, Alexandre Marquis, Pierre Bigonesse, Mairy D-Mendoza, Hamid Hassanisaber et tous ceux que j'aurais pu oublier.

Finalement, j'aimerais remercier toutes mes professeures de langue française, surtout Vicky Poirier, grâce à qui j'ai obtenu le diplôme d'études en français langue seconde et j'ai appris assez de subtilités de la langue française de manière à oser écrire et présenter ma thèse en français.

TABLE DE MATIÈRES

LISTE DES FIGURES

LISTE DES TABLEAUX

LEXIQUE DES RÔLES DES AUTEURS[1]

Conceptualisation : formulation ou évolution d'objectifs et de buts de recherche.

Analyse formelle : application des techniques statistiques, mathématiques, informatiques ou d'autres techniques formelles pour analyser ou synthétiser les données.

Acquisition de financement : acquisition du soutien financier du projet.

Investigation : réalisation des expériences ou la collection de données / preuves.

Méthodologie : développement ou conception de méthodologie.

Administration de projet : gestion et coordination de la planification et de l'exécution des activités de recherche.

Ressources : fourniture de réactifs, de matériel, d'échantillons de laboratoire, d'instruments, de ressources informatiques ou d'autres outils d'analyse.

Supervision : supervision de la planification et l'exécution des activités de recherche.

Validation : vérification de la réplication / reproductibilité globale des résultats / expériences et autres résultats de recherche.

Visualisation : préparation, création et / ou présentation de l'œuvre publiée.

Rédaction - premier brouillon : la rédaction de l'ébauche initiale.

Rédaction - revue et révision : révision critique, commentaire ou révision.

[1] Brand, A., Allen, L., Altman, M., Hlava, M. & Scott, J. 2015. Beyond authorship: attribution, contribution, collaboration, and credit. *Learned Publishing,* 28(2), pp. 151-155, https://doi.org/10.1087/20150211.

LISTE DES ACRONYMES

ACD ..... Distance entre cathode et anode (*anode to cathode distance*)

BET .....Surface spécifique (méthode Brunauer, Emmett et Teller)

CR .....Ratio molaire de cryolite = [NaF]/[AlF_3] (*cryolite ratio*)

CVD ..... Chute de voltage cathodique (*cathodic voltage drop*)

CW ..... *Center working*

IFT ..... *Interfacial tension*

MEB (*SEM*) ..... Microscopie électronique à balayage (*scanning electron microscopy*)

MHD ..... Magnétohydrodynamique

PF ..... *Point feeding*

SW .....*Side working*

DRX (*XRD*) .....Diffractométrie à rayons X (*X-ray diffractometry)*

XRF ..... Spectroscopie de fluorescence aux rayons X (*X-ray fluorescence spectroscopy)*

CHAPITRE 1 INTRODUCTION

1.1 Mise en contexte et problématique

1.1.1 Production d'aluminium primaire

Ayant 9 usines avec une production annuelle de 2,9 millions de tonnes d'aluminium primaire, le Canada se trouve au quatrième rang mondial après la Chine, la Russie et le Moyen Orient, parmi les plus grands producteurs d'aluminium primaire [AluQuébec, 2019]. Rio Tinto, Alcoa et Alouette, les trois principaux producteurs d'aluminium québécois, nourrissent plus de 7,000 familles québécoises, ce qui fait de l'industrie de l'aluminium un facteur important dans l'économie québécoise et canadienne [AluQuébec, 2019]. En outre, d'après les estimations, d'ici fin 2019, la Chine (produisant environ 57% de la production mondiale d'aluminium primaire en mai 2019) sera responsable d'une augmentation d'environ 3 millions de tonnes de la capacité de production d'aluminium primaire [Djukanovic, 2018; International-Aluminium-Institute, 2019]. En raison d'un tel essor mondial par rapport à la production d'aluminium, les producteurs d'aluminium sont en constante recherche d'améliorations concernant la réduction des coûts de production. Quant à la production d'aluminium primaire, ça fait 134 ans que, malgré tous les efforts des industriels, celle-ci est basée sur le procédé Hall-Héroult sans modifications majeures [Habashi, 2002].

1.1.2 Procédé Hall-Héroult

Dans le procédé Hall-Héroult, l'alumine (Al_2O_3) est dissoute dans un mélange de sels fondus (c'est-à-dire le bain) à une température typique d'environ 960 °C. Le bain contient typiquement la cryolite (Na_3AlF_6), toutefois d'autres sels (par exemple, CaF_2, AlF_3, LiF ou MgF_2) sont également ajoutés afin d'en modifier certaines caractéristiques comme la température de fusion, les émissions polluantes, etc. [Haupin, 1991; Richards, 2007]. L'électrolyse du bain est faite dans une cellule électrochimique utilisant des courants entre 200 kA et 600 kA selon la technologie utilisée. La Figure 1-1 présente les composantes typiques de la cellule du procédé Hall-Héroult. Ce dernier a vu plusieurs années de légères modifications afin d'en réduire la consommation d'énergie électrique et d'en améliorer l'efficacité de courant [Welch, 2007; Tarcy et coll., 2011; Haraldsson et Johansson, 2018]. Entre autres, un phénomène majeur est responsable de l'augmentation de la consommation d'énergie et l'inefficacité de courant, à savoir la formation et la solidification de boues. La boue, en anglais « *sludge* », est

principalement un mélange de bain et de particules d'alumine non dissoutes qui se forme à l'interface entre le bloc cathodique et l'aluminium fondu [Fallah Fini et coll., 2017]. Il existe plusieurs scenarios pour la formation de boues : i) l'agglomération des particules d'alumine; ii) l'introduction de croûte d'anode ou de matériau de recouvrement anodique au fond de la cellule lors du changement d'anodes; iii) l'extension du talus protecteur sur la surface de la cathode; iv) la formation de bain solide autour des anodes neuves et l'introduction de celui-ci au fond de la cellule, v) la formation de boues en raison du changement de chimie du bain [Fallah Fini et coll., 2020a].

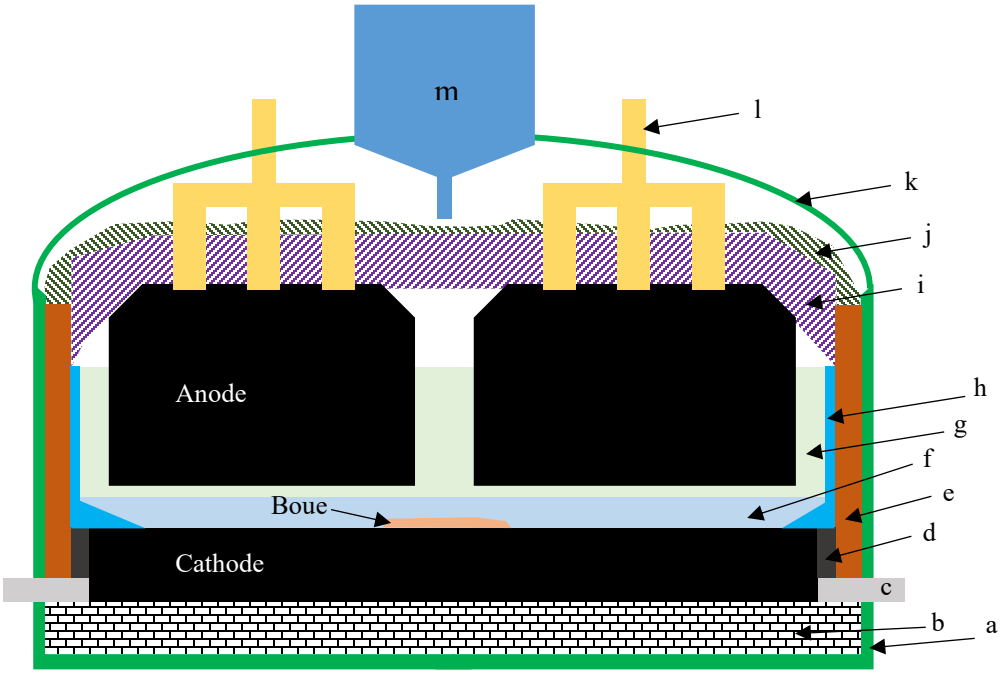

Figure 1-1. Cellule d'électrolyse d'aluminium; a) caisson en acier, b) isolation, c) barre collectrice, d) pâte de brasque, e) bloc de carbure de silicium, f) aluminium, g) bain, h) talus et pied de talus, i) croûte d'anode, j) matériau de recouvrement d'anode, k) capot, l) tige d'anode, m) système d'alimentation d'alumine

1.1.3 Nuances de blocs cathodiques

Dans le procédé Hall-Héroult, trois éléments sont composés de matériaux carbonés, à savoir l'anode, la pâte de brasque et la cathode (Figure 1-1). Hormis l'anode et la pâte de brasque qui dépassent la portée de cette thèse, la cathode est composée des matériaux carbonés, y compris l'anthracite (une roche sédimentaire contenant ~ 93% de carbone), le graphite (un des allotropes

du carbone constitué de feuillets de graphènes[2] retenus par des liaisons de van der Waals), le coke (produit par distillation de la houille en atmosphère réductrice) ou le brai (un liant, soit un résidu pâteux de la distillation du goudron) [Sørlie et Øye, 2010]. Les nuances cathodiques sont catégorisées d'après la structure atomique, ce qui est le résultat des traitements thermiques. La nuance semi-graphitique, constituée essentiellement d'anthracite (e.g. ~ 80 wt%) et de graphite (e.g. 20-30 wt%), est cuite à une température avoisinant 1200 °C. La nuance graphitique, constituée de graphite, est cuite à une température avoisinant 1200 °C. La nuance graphitisée, constituée de coke, est cuite à une température avoisinant 3000 °C. Le liant des espèces carbonées pour toutes les nuances est le brai [Charette et Kocaefe, 2012]. Les usines utilisaient auparavant des cathodes semi-graphitiques. D'ailleurs, vu l'augmentation d'intensité électrique des cellules, plusieurs ont choisi des cathodes graphitiques ou graphitisés de manière à réduire la chute de voltage. Cependant, sachant la faiblesse des forces de van der Waals, les blocs graphitisés sont plus fragiles à l'usure. Donc, les industriels essaient d'innover et de préparer des nuances possédant les propriétés désirées, dont faible résistivité électrique, faible tendance à la détérioration chimique, forte résistance en compression et forte énergie de cohésion [Sørlie et Øye, 2010; Charette et Kocaefe, 2012].

1.1.4 Problématique

Envisageant le fait que l'exportation d'aluminium chinoise ait atteint un haut niveau record ainsi que la nécessité d'optimiser la performance énergétique du procédé Hall-Héroult, le comportement de la boue et ses désavantages doivent être étudiés. Selon Fallah Fini et coll. [2020a], plusieurs facteurs influencent la formation et la dissolution de la boue, y compris le niveau de surchauffe (c'est-à-dire la température d'opération), la chimie du bain, la nuance de bloc cathodique, la technologie d'alimentation d'alumine, les caractéristiques physico-chimiques de l'alumine, l'hydrodynamique et les phénomènes d'interface.

Quant à la littérature scientifique, il y en a beaucoup qui porte individuellement sur l'impact de ces derniers. Cependant, il n'existe aucune publication qui montre l'importance relative des paramètres d'opération, dont la température, la chimie du bain (CR), la nuance de cathode et la teneur en alumine. De plus, force est de constater que malgré l'importance de la formation de boues, les données se rapportant à un tel phénomène sont dispersées dans des articles

[2] Une couche, d'un atome d'épaisseur, d'atomes de carbone de maille hexagonale

scientifiques et dans des publications de conférence depuis de nombreuses années. Ceci démontre l'absence d'une revue de la littérature approfondie décrivant non seulement la formation de boues, mais incluant également ses désavantages et les paramètres correspondants.

De surcroît, étant donné que l'utilisation des cathodes graphitisées entraîne des économies d'énergie et des intensités de courant cathodiques plus élevées [Lorentsen, 2014], ces types de cathodes affectent indirectement la formation ou la dissolution de boues moyennant ses caractéristiques thermoélectriques, géométriques et physicochimiques. Faute de recherche concernant le dernier sujet susmentionné, les producteurs d'aluminium l'ignorent en dépit de son rôle délicat par rapport aux stratégies de contrôle des cellules. D'ailleurs, il y a certains articles qui portent sur la théorie de la formation de boues à cause du changement de chimie du bain; toutefois, aucun article n'est dédié à l'observation expérimentale de ces types de boues et à ses caractérisations chimiques.

1.2 Questions de recherche

Sachant que la formation de boue et sa dissolution dans le procédé Hall-Héroult dépendent de plusieurs facteurs, la question de recherche de ce projet a trois parties :

a) Lequel des trois paramètres d'opération principaux (c'est-à-dire, la température d'opération, le ratio de cryolite (CR) et la nuance de cathode) est le plus important par rapport à la formation de boue?

b) Lesquelles des propriétés des blocs cathodiques peuvent affecter la formation ou la dissolution de boue?

c) Comment la formation de boue à cause du changement de chimie du bain peut-elle aider la dissolution de boue ayant une teneur en alumine élevée?

1.3 Objectifs du projet de recherche

Afin de répondre à la question de recherche, deux objectifs ont été poursuivis :

a) Étudier l'impact de différentes caractéristiques des nuances de cathode sur la formation et sur la dissolution de boue à l'interface entre le bloc cathodique et l'aluminium.

b) Déterminer le paramètre le plus important entre la température d'opération, le ratio de cryolite et la nuance de cathode par rapport à la formation de boue.

1.4 Contributions originales

Au niveau des contributions originales, ce projet a fourni cinq articles scientifiques et publications de conférence par rapport au phénomène de la formation de boue et sa dissolution. Par ailleurs, les résultats de ce projet de doctorat approfondissent notre compréhension des comportements des cellules industrielles.

1.4.1 Revue de la littérature sur la formation de boue et ses désavantages

Ce projet a fourni deux articles de revue de la littérature concernant la formation de boue, étant donné la rareté des documents publics touchant la formation-dissolution de boues dans le procédé Hall-Héroult, et sachant que la formation de boue est un facteur important par rapport à la durabilité de la production d'aluminium au Canada. Le premier (annexe A), étant un exposé concis qui traite plutôt de l'existence du problème de boue, sa thermochimie, etc., a été présenté dans le cadre de la conférence *ICSOBA 2017* à Hambourg, en Allemagne, en octobre 2017 [Fallah Fini et coll., 2017]. Le deuxième (Chapitre 2), publié dans le journal *Mineral Processing and Extractive Metallurgy Review,* est un papier exhaustif incluant les différents mécanismes pour la formation et la dissolution de boue, et les dynamiques complexes entre les multiples phénomènes (par exemple, ceux d'interface et de transfert de chaleur/masse).

1.4.2 Impact de la nuance de cathode sur la dissolution de boue

D'après les résultats préliminaires (présentés à la conférence *Light Metals 2018* en Arizona [Landry et coll., 2018]), la croissance de la couche de carbure d'aluminium varie selon la nuance de cathode. Cette variation par rapport à la formation de couche de carbures a été utilisée afin d'expliquer comment on observait plus de boue dans certaines cellules industrielles. En premier, les profils variables des boues semblent être liés aux conductivités thermiques des blocs cathodiques, ce qui aide la perte de chaleur à travers les blocs et par conséquent, augmente la possibilité de solidification de la boue (publié comme un article dans le journal *Metallurgical and Materials Transactions B* en 2019 [Landry et coll., 2019]).

En deuxième lieu, vu que : a) la porosité ouverte de la cathode peut faciliter l'infiltration du bain des boues vers les espèces carbonées au fond de la cellule, et b) le bain est un environnement approprié pour la dissolution des couches de carbures, la diffusion du bain vers la surface du carbone et la formation de carbure s'intensifient davantage. En outre, la réaction des espèces carbonées avec le bain et la formation de carbure augmentent encore le ratio de cryolite et la

température de liquidus du bain. Par conséquent, en cas d'un bloc cathodique plus poreux, une couche isolante de carbure et de bain solide plus épaisse couvre la surface cathodique. Cette dernière, non seulement ralentit la dissolution des boues, mais en diminuant la densité de courant locale, diminue également la production locale d'aluminium en dessous des boues, ce qui a un effet de fendage[3] et enlève partiellement les boues [Herstad et coll., 1983a; Keller, 2005]. Cette interprétation a été soumise au journal *Minerals Engingeering* en janvier 2020 [Fallah Fini et coll., 2020b].

1.4.3 Surchauffe comme paramètre clé de la formation de boue

Après avoir revu de nombreuses recherches effectuées sur les paramètres affectant la formation des boues et ses désavantages, trois concepts semblent absents, à savoir l'importance relative des paramètres d'opération, l'influence de la nuance cathodique et la formation expérimentale de boues induites chimiquement. Afin de combler ces trois objectifs, un plan d'expériences a été suivi en ayant comme résultats, entre autres, le rôle énorme de la température d'opération, c'est-à-dire le niveau de surchauffe, parmi les trois variables, soit la température d'opération, le ratio de cryolite (CR) et la nuance de cathode.

1.4.4 Précipitation des espèces cryolitiques et ses interactions avec de la boue

Malgré certains articles qui portent sur la théorie de la précipitation des espèces cryolitiques à cause du changement de chimie du bain, également appelées des boues induites chimiquement, aucun article n'est dédié à l'observation expérimentale de ces types de boues et à ses caractérisations chimiques. Ces précipités sont provoqués par des changements dans le ratio local de cryolite accompagné par l'épuisement de l'alumine. Dans une cellule industrielle, une polarisation de concentration de sodium se produit en raison de la migration du sodium vers l'interface bain-métal. Par conséquent, la température locale du liquidus augmente et des espèces cryolitiques solides précipitent à la surface du métal. De plus, la faiblesse de la teneur en alumine peut également accroître la température du liquidus et accélérer la solidification des espèces susmentionnées. Cette étude, présente pour la première fois, l'observation de ce type de matériaux solides ainsi que ses propriétés thermophysiques calculées grâce au logiciel FactSage et aux techniques de caractérisation des matériaux.

[3] En anglais « *wedging effect* »

1.5 Plan du document

Cet ouvrage se constitue de quatre parties. En premier, une revue de la littérature exhaustive concernant les différents mécanismes pour la formation et la dissolution de boue de manière à mettre en évidence l'originalité du projet. Les méthodologies appliquées forment alors le chapitre 3, suivi par les résultats présentés dans trois chapitres séparés selon les trois articles scientifiques. Finalement, la conclusion indique le sommaire des points les plus importants de cette thèse.

CHAPITRE 2 ÉTAT DE L'ART

2.1 Avant-propos

Auteurs et affiliation :

Mojtaba Fallah Fini : étudiant au doctorat, Département de génie chimique et génie biotechnologique, Université de Sherbrooke, Québec, Canada.

Jean-René Landry : étudiant à la maîtrise, Département de génie chimique et génie biotechnologique, Université de Sherbrooke, Québec, Canada.

Gervais Soucy : professeur titulaire, Département de génie chimique et génie biotechnologique, Université de Sherbrooke, Québec, Canada.

Martin Désilets : professeur titulaire, Département de génie chimique et génie biotechnologique, Université de Sherbrooke, Québec, Canada.

Patrick Pelletier : scientifique de recherche brasquage, Solutions Technologiques Aluminium – CRDA, Rio Tinto, Québec, Canada.

Loig Rivoaland : responsable de projets transverses, Carbone Savoie, Vénissieux, France.

Didier Lombard : champion innovation & consultant matériaux / brasquage, Solutions Technologiques Aluminium – LRF, Rio Tinto, Saint Jean de Maurienne, France.

État de l'acceptation : Version finale publiée.

Revue : *Mineral Processing and Extractive Metallurgy Review: An International Journal.*

Référence : Fallah Fini et coll. [2020a]

Lien d'accès : http://dx.doi.org/10.1080/08827508.2018.1536658

Contributions à la thèse :

Ce document est la première revue de littérature sur la formation des boues dans les cellules Hall-Héroult. Les principaux facteurs affectant la formation ou la dissolution des boues sont énoncés et discutés. Cet article : a) fait ressortir l'importance relative du phénomène de formation de boues et ses désavantages, b) catégorise la littérature pertinente, et c) explique tous les facteurs et les impacts correspondants sur la formation ou la dissolution de boues.

Contributions des auteurs[1, 2]:

Mojtaba Fallah Fini : conceptualisation (100%), investigation (80%), méthodologie (100%), rédaction du premier brouillon (90%), révision (100%), visualisation (100%), validation (50%); total (75%)

Jean-René Landry : investigation (20%), rédaction du premier brouillon[3] (10%), revue (100%), validation (50%); total (25%)

Gervais Soucy : validation, ressources, revue, révision, surveillance, administration de projet, acquisition de financement

Martin Désilets : validation, surveillance, revue, révision

Didier Lombard : ressources, revue, révision

Patrick Pelletier : ressources, revue, révision

Loig Rivoaland : ressources, revue, révision

Titre français :

Formation de boues dans les cellules Hall-Héroult : désavantages et facteurs importants

Résumé :

Cette revue de littérature discute de la formation des boues dans les cellules Hall-Héroult. La formation de boue et sa transformation en dépôts résistifs sont parmi les principaux problèmes pour les producteurs d'aluminium. Les boues interviennent dans la dynamique complexe des cellules d'électrolyse tout en augmentant la demande en énergie et en réduisant l'efficacité de courant. Les données se rapportant à un phénomène d'une aussi grande importance sont éparpillées dans les actes de conférences *TMS Light Metals* et dans les journaux scientifiques ; d'où la nécessité d'une revue en profondeur comprenant les principaux facteurs tels que la température (surchauffe du bain), la chimie du bain, la nuance de bloc cathodique, l'alimentation d'alumine, l'hydrodynamique et les phénomènes d'interface.

[1] Pourcentage approximatif just entre les premiers deux auteurs
[2] Trouver lexique des rôles des auteurs à la page xi.
[3] La section concernant la nuance cathodique « 2.2.4 Influence of cathode carbon materials »

2.2 Sludge Formation in Hall-Héroult Cells: Drawbacks and Significant Parameters

Keywords: Sludge; bottom crust; muck; Hall-Héroult cells; resistive deposits

2.2.1 Abstract

This literature review discusses the sludge formation in the Hall-Héroult process. Sludge formation and its transformation into resistive cathodic deposits are one of the focal concerns of the aluminum producers. Sludge formation interacts with the complex dynamics of the electrolysis cells while increasing the energy demand and decreasing the current efficiency. The data on such important phenomenon is scattered through years in proceedings of TMS Light Metals and journal articles; hence requiring an in-depth review including the influence of important parameters such as temperature (i.e. superheat), bath chemistry, cathode type, alumina feeding characteristics, hydrodynamics and interfacial phenomena.

2.2.2 Introduction

According to the world's annual production of aluminum and its trend in recent years [Bray, 2018], China has become a formidable producer of aluminum in the last couple of years and this has forced other producers to reduce their production costs. Besides, the Hall–Héroult process has gone through years of investigation and subtle modifications since its commercialization at the beginning of the 20th century [Grjotheim et Welch, 1989; Tarcy et coll., 2011]. Looking at the trend of such developments reveals that the Achilles' heel of the aluminum electrolysis has always been its high consumption of electrical power and improvement of current efficiency (Figure 2-1).

In an ideal aluminum electrolysis process and according to Faraday law for 1 kAh of electrical current, 0.3356 kg of aluminum is produced [Grjotheim et Kvande, 1993]. On top of that, at a typical temperature of 960 ºC, the ideal process energy for production of 1 kg of aluminum with a current efficiency of 100% is about 6.3 kWh [Thonstad et coll., 2001]. However, in reality (Figure 2-2), a current efficiency of ≈ 95% and a typical process energy of 13-15 kWh per kg of aluminum is observed. Among other factors, two major phenomena decrease the current efficiency and increase the energy demand. The first phenomenon (which drastically reduces the current efficiency) is the back reaction of solubilized metallic species with CO_2 gas followed by the production of CO gas and dissolved Al_2O_3. The second major phenomenon is the formation

of resistive deposits on the surface of the cathode. Such deposits create more resistance and increase the required electrical energy. Figure 2-2 shows the different types of solid species found inside aluminum electrolysis cells.

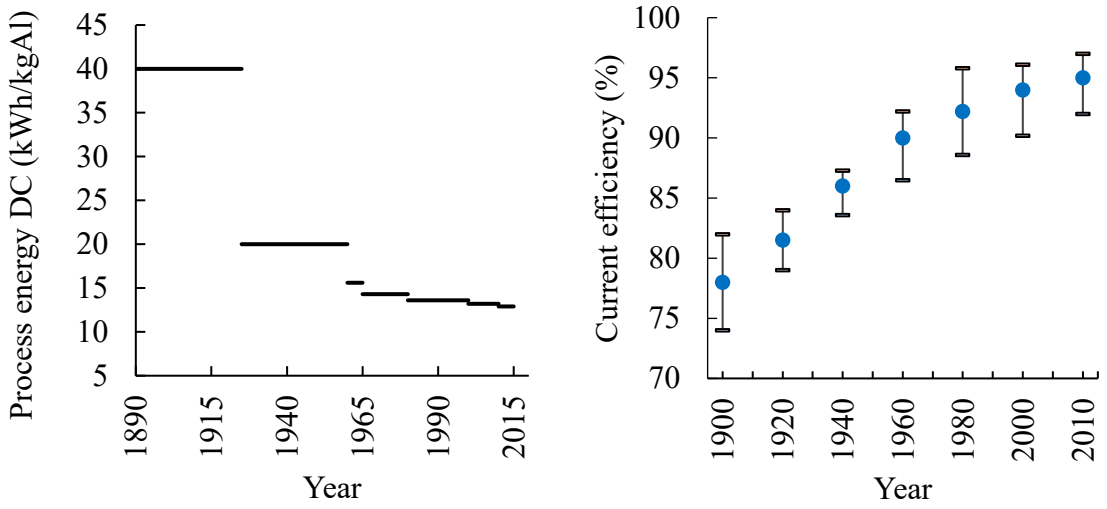

Figure 2-1. DC electrical energy consumption and current efficiency in Hall-Héroult process [Welch et Kinery, 2000; Tabereaux et Peterson, 2014; International-Aluminium-Institute, 2019]

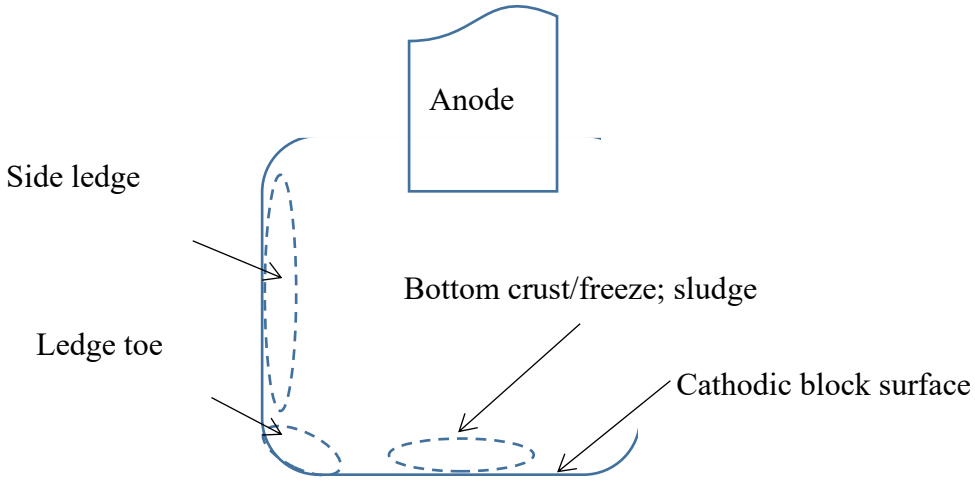

Figure 2-2. Typical loci of common deposits within a typical aluminum electrolysis cell

The side ledge is a beneficial layer because it not only protects the cell walls from the bath/aluminum corrosion but also prevents the infiltration of aluminum into the cell lining. Nevertheless, a proper heat balance is required to avoid the extensive elongation of the side

ledge on the surface of cathodic block (i.e. extended ledge toe). The frozen side ledge mostly consists of cryolite and therefore its melting has an important effect on the chemistry of the bath. On the contrary, the detrimental solid deposits are the bottom deposits namely, bottom crust/freeze and sludge. The behavior of these solid deposits has been investigated for quite a while and it is one of the focal points of research on aluminum electrolysis [Gasik et Gasik, 2003]. In this literature review, first a general overview of the sludge formation and its drawbacks are presented, followed by the most important factors that could affect the formation or dissolution of such deposits.

2.2.3 Sludge formation and its drawbacks

According to Tabereaux et Peterson [2014], the following steps are followed upon addition of 1–2 kg of alumina particles onto the surface of the bath by point feeders. At first, the bath wets some of the particles and dissolves them immediately. However, some of the particles form agglomerates surrounded by a frozen bath layer. Later, the alumina particles absorb the sensible heat and their temperature increases from 100°C to 960°C. At this stage, the process is heat transfer controlled while the frozen bath layer around some of the agglomerates gradually disintegrates. Finally, alumina particles dissolve into the bath and distribute in the cell by the turbulent flow. Nevertheless, not all the alumina particles dissolve and when undissolved clumps of alumina sink to the bottom of the cell, beneath the metal pad, a dense and viscous phase called sludge is formed. In addition, there are other probable scenarios for the formation of sludge, including the falling of anode cover materials and collapse of the top crust. For example, each anode change, including the removal of the anode butt and installation of new anodes, creates abundant opportunities for around 200 kg of anode cover materials to fall into the cell [Taylor et Welch, 2004]. Furthermore, during the anode change and feeding procedure, clumps of top crust are often introduced into the cell, leading to the formation of sludge. AlF_3 feeding may also affect sludge formation, although such possibility was much more significant in old technologies in which AlF_3 was added in sudden and huge quantities of about 50 kg. In the latter case, the sludge contains an excessively high amount of AlF_3 and its dissolution will take a much longer time than the alumina-rich sludge [Utigard, 1987].

The other possible route for the formation of sludge is related to the influence of bath chemistry on the phase equilibria. A simple demonstration of such behavior is presented in Figure 2-3. As it is evident in case of keeping the same operational temperature in the cell, upon the depletion

of the alumina content in an unsaturated bath, a mixture of the bath and alumina is prone to be precipitated as is shown by the horizontal arrow in Figure 2-3. Such precipitates, upon accumulation on the bath-metal interface, may be able to penetrate through the metal pad or slip to the sides of the bath-metal interface and join the ledge toe. Furthermore, the sodium concentration polarization at the bath-metal interface also may help such deposits to solidify furthermore, by increasing the interfacial liquidus temperature (Figure 2-3).

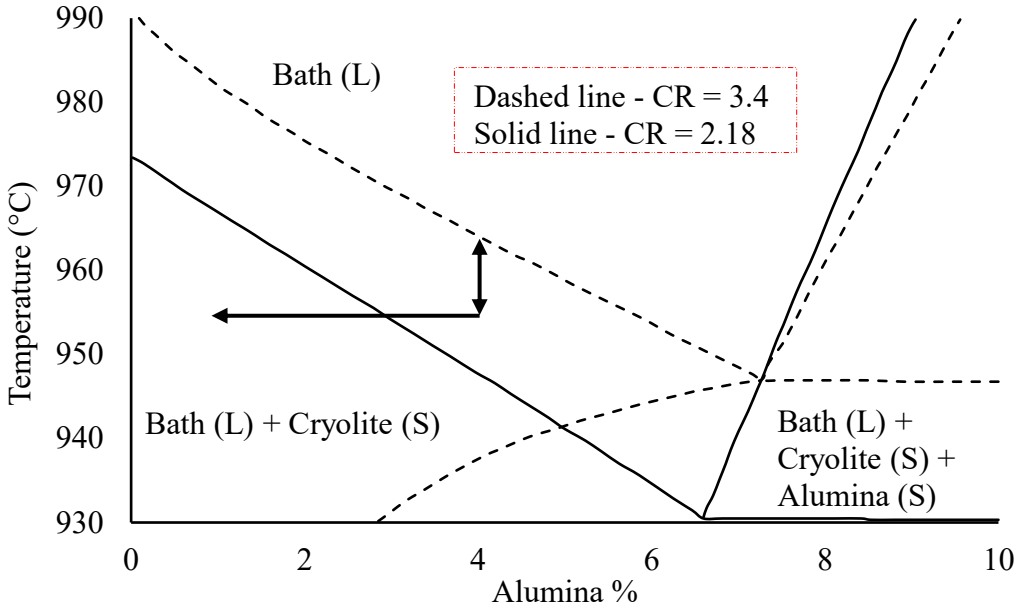

Figure 2-3. The horizontal and vertical arrows show the formation of solid cryolitic species because of depletion of alumina and sodium concentration polarization at the bath-metal interface respectively.

Sludge, formed upon alumina agglomeration, is a viscous paste-like combination of alumina particles and alumina-saturated bath with a typical density of 2400 kg/m^3 [Thonstad et coll., 1980; Grjotheim et Kvande, 1993]. The acidity of the sludge is less than mother bath (typically 2-5% excess AlF_3 [Grjotheim et Kvande, 1993] or CR of 1.4-1.8 [Thonstad et coll., 1972]). The lower acidity of sludge compared to the mother bath can be either attributed to its equilibrium with a metal pad that has a high sodium content [Keller et coll., 1988] or precipitation of cryolite due to the higher interfacial liquidus temperature [Solheim, 2002]. As Figure 2-3 depicts, the precipitation of cryolitic species not only dissolves the solid alumina content of the sludge but also increases the cryolite ratio of the sludge (i.e. less acidity). Dissolution of alumina in the precipitated cryolite, creates saturated bath with low density that may find its way to the mother bath by forming a film between aluminum and side ledge or through the aluminum pad

[Solheim, 2002]. Such vertical gradient of CR has been noticed in laboratory experiments and industrial samples [Allard et coll., 2014a; 2014b]. If the amount of heat loss from the bottom of the cell is enough (i.e. if it gets below the liquidus temperature of the sludge) and the sludge is not back-fed fast enough, such sludge can create a resistive deposit on the surface of the cathode usually called bottom crust or deposit. Bottom crust typically has a density of 3200-3700 kg/m^3, a porosity of 1-20 % and acts as an electrically resistive layer [Veneraki et coll., 1973; Thonstad et coll., 1982]. The size and shape of the alumina particles within the bottom crust are larger than and different from the size of the fed alumina because of the alumina phase transformation catalyzed by presence of an alumina-saturated bath [Landi et coll., 1968; Kachanovskaya et Arakelyan, 1976]. Another type of bottom deposit that mostly consists of cryolite, is called bottom freeze (Table 2-1). Bottom freeze is generally created when the solidified bath close to the sidewalls extends on the surface of the cathode. The other possible path for creation of bottom freeze is the falling of the frozen bath around the newly installed anodes (i.e. anode freeze) [Utigard, 1999].

Table 2-1. Typical composition of different bottom solid phases found in industrial cells [Allard et coll., 2015]

Type	AlF_3 (wt%)	CaF_2 (wt%)	Al_2O_3 (wt%)
Bottom freeze	2-13	4-6	2-10
Sludge	2-10	2-5	20-50
Bottom crust	2-5	2	65-85

Formation of sludge is not a desirable phenomenon because it affects significant operational factors including current efficiency, operational temperature, bath chemistry, current density and the stability of the metal-bath interface [Welch, 1995; Fallah Fini et coll., 2017]. A typical sludge phase has an electrical conductivity of 1.0 S/cm ± 0.2, which is about twice when compared to bath and 30,000 times when compared to molten aluminum [Keller, 2005; Geay et coll., 2013]. Such electrical resistivity diverts the local current density and creates areas with higher current density and consequently higher cathode wear [Liao et Øye, 2013]. Besides, sludge formation consequently influences the carbide content in the bath, carbon particles dispersion, bath superheat and loss of current efficiency [Thonstad et coll., 2001]. Extensive sludge formation increases the occurrence of anode effects, during which the anode is poorly wetted by the electrolyte resulting in an extensive carbon dusting. Presence of dispersed carbon

particles in the bath not only increases the electrical resistivity of the bath (i.e. higher energy consumption) [Bugnion et Fischer, 2016], but also causes higher solubility of aluminum and loss of current efficiency by reaction with dissolved aluminum and formation of aluminum carbide [Wang et coll., 1994; Ødegård et coll., 2013b].

Moreover, sludge also tampers with the hydrodynamics of the cell. The higher electrical resistivity of the sludge-covered cathode area diverts the local electrical current to flow horizontally towards the edges of the sludge. Such horizontal current flows perturb the dominant vertical current flows leading to additional instability of the metal-bath interface [Tarapore, 2013]. The oscillation of metal-bath interface has a dramatic effect on the optimum operation of the cell considering the large aspect ratio of the cell and higher resistivity of the bath compared to metal pad [Davidson et Lindsay, 1998]. Moreover, the shear amount of metal-bath interfacial stress leads to higher aluminum solubility (i.e. fogging effect), which consecutively accounts for higher back reaction and loss of current efficiency [Thonstad et coll., 2001]. In addition, such metal/bath instability results in change of anode-cathode distance (i.e. uneven ACD), cell voltage drop (CVD) and heat balance which dramatically affect the current efficiency and energy consumption [Welch et Kuschel, 2007].

As it was mentioned, there are various parameters involved in the formation or dissolution of the sludge; therefore, it is necessary to review the influence of important factors such as cathode grade, hydrodynamics, interfacial phenomena, temperature, bath chemistry, physicochemical characteristics of alumina and feeding strategy. Furthermore, considering the complex nature of alumina dissolution, which is strongly interlinked with the bath chemistry, level of superheat, alumina feeding strategy, etc., it is quite evident that the cycle of sludge formation and dissolution is a common phenomenon in the smelters around the world. However, before individual investigation of each parameter, it is helpful to review the previous studies on sludge formation in both laboratory and industrial scale (Table 2-2 and Table 2-3).

Table 2-2. Observations on central deposits from industrial electrolysis cells

Observation	Average chemistry of the deposit	Reference
- Graphitic cathode - Whitish rounded spots with thickness of 0.5-9 mm - Under the feeder containing α-alumina platelets 50-700 µm - Cathode surface coverage 3-9 %	CaF_2 ~ 5.2 wt%; CR ~ 2.5; a1umina ~ 18 wt%	[Coulombe et coll., 2016]
- Graphitized cathode - Dark stripes covered by whitish material with thickness of 3-50 mm - Scattered on the bottom surface containing α-alumina platelets 5-80 µm - Cathode surface overage 16%	CaF_2 ~ 4.1 wt%; CR ~ 2.4; a1umina ~ 44 wt%	[Coulombe et coll., 2016]
- Black carbonaceous material surrounded by carbide - Visible aluminum droplets and α-alumina platelets	CaF_2 ~ 2.8 wt%; Excess AlF_3 ~ 2.4 wt%; a1umina ~ 42 wt% Impurities (Si: 120, P: 40 ppm)	[Geay et coll., 2013]
- Thickness few mm - Under the feeder - Just thin deposits on the middle of the cell	CaF_2 ~1.3 wt%; CR ~2.5; alumina 21.8 wt%	[Allard et coll., 2014b]
- Thickness few mm positioned under the feeder	CaF_2 ~ 5 wt%; CR ~ 2.5; alumina ~ 26 wt%	[Allard et coll., 2014a]

Observation	Average chemistry of the deposit	Reference
- Spots of thin layer on the surface		
- Bottom crust (65-85 wt% alumina) formation requires enough ΔT (15-20 °C) - Majority of α-alumina platelets were 10-400 µm, few 3-4 mm - α-alumina platelets have a yellowish tint	65-74 wt% alumina	[Thonstad et coll., 1982]
- The dissolution of bottom crust is hindered due to its insulating effect. - The difference in liquidus temperature of sludge (950-964 °C) is mostly due to the CaF_2 content.	1-5 wt% AlF_3; 1.6-3.5 wt% CaF_2; 35-60 wt% alumina; 40-60 wt% cryolite	[Liu, 1995]
- Viscosity of the sludge increases dramatically at 25% alumina - As bottom crust grows the size of the alumina particles increase	Alumina 23-53 wt% (60-90 wt% α-alumina); Higher CR than the bath (1.4-1.7); 0.3 wt% Al_4C_3; 0.03 wt% Al	[Thonstad et coll., 1972]
- There is a fairly rapid mass exchange between the sludge and the bath - The mass transfer is likely due to the thin film between side ledge and metal	-	[Thonstad et coll., 1980]
- Alumina content of the sludge is dependent on feeding strategy - Upon hardening, the sludge rejects AlF_3	Soft sludge: Excess AlF_3 ~ 3 wt%, alumina 42 wt% Bottom crust: Excess AlF_3 ~ 0.7 wt%, alumina 69 wt%	[Taylor et coll., 1990]
- The sludge particles are relatively large and thick irrespective to the feed's degree of calcination.	-	[Abd El All et coll., 1980]

Table 2-3. Experimental laboratory scale investigations of central deposits

Bath composition	Operational characteristics	Central deposit characteristics and remarks	Reference
74 wt% cryolite, 11 wt% AlF_3, 5 wt% CaF_2, 9 wt% α-alumina, 1 wt% γ-alumina, CR = 2.2, 3.0 and 4.0	Graphitized cathode, 960 °C, electrolysis at 0.7 A/cm^2 for 6 h; with two conditions of alumina underfeeding and overfeeding	- Surface deposit: 21 wt% alumina, CR ~ 2.3 - Sludge: 24.8 wt% alumina, CaF_2 0 wt%, CR ~ 2.3 - In cases with higher CR less amount of sludge or no sludge was noticed	[Allard et coll., 2014a; 2014b]
Industrial bath, 5% CaF_2, 10 wt% alumina, CR = 2.2	Graphitized and graphitic cathodes, 955 °C, electrolysis at 0.9 A/cm^2 for 2-5 h; high/low heat transfer rate at walls of the cell; with two conditions of alumina underfeeding and overfeeding	- The blocks with higher thermal conductivity showed less sludge formation; - Lower heat transfer at the walls leads to more bottom sludge formation; - At similar conditions there is hardly any difference between the chemical composition of central deposits for two types of cathodes; - At similar conditions, graphitized cathode had more central deposits	[Coulombe et coll., 2016]
5 wt% CaF_2, 5 wt% alumina, CR = 1.5-4.0	Inversed polarity electrolysis cell; Anthracitic and graphitic cathodes, 1000 °C, electrolysis at 0-0.7 A/cm^2 for 4 h	- Higher current density leads to thicker deposits (2-3 mm) at 0.15-0.20 A/cm^2 - At higher current densities, aluminum droplets act as wedges and partially remove the deposit - For graphitic cathodes, the deposit contains more aluminum droplets - Carbide formation is a function of current density and CR	[Herstad et coll., 1983a, 1983b]

Bath composition	Operational characteristics	Central deposit characteristics and remarks	Reference
		- For a system with CR ~ 4.0, the deposit is a network of alumina particles trapping cryolite - For a system with CR ~ 1.5, the deposit is larger and bulky; there is no network structure; the deposit contains carbon and silicon (5%)	
Saturated alumina and cryolite 10 wt% excess AlF_3 2-4% LiF	Inversed polarity electrolysis cell; alumina particles size 40-150 µm; 1020 °C with cold finger at 975-997 °C	- When heated above the liquidus temperature, the sludge kept its dimension and just lost some of the bath - Alumina content was 65-85 wt% and large crystallized α-alumina particles (up to 5 mm) were visible - Presence of aluminum metal decreased the size of the crystals up to 75%; changed the colorless crystals to yellowish/brownish; changed the random orientation of crystals into thin right-angled growth - Crystals are connected by recrystallization of interstitial dissolved alumina - In case of more acidic baths, the deposit adherence to the cathode is stronger and the alumina plates are thinner - Presence of LiF decreases the cathodic deposit coverage - Sludge dissolves 2.5 times faster than bottom crust	[Thonstad et coll., 1982]

Bath composition	Operational characteristics	Central deposit characteristics and remarks	Reference
		- Dissolution rate of bottom crust is quite close to the dissolution rate of pure alumina.	
5 wt% excess AlF_3, 2 wt% alumina, 5 wt% CaF_2	960 ºC	- A sludge with alumina content >10 wt% acts like a fluid and wets the cathode; On slightest cooling alumina crystallizes - A sludge with alumina content <10 wt% forms bottom crusts that preserve their structure after heat losses	[Gerlach et Winkhaus, 1985]
Pure cryolite	1020 ºC Sludge samples with 25-50 wt% alumina under 4 cm of molten aluminum covered by pure cryolite Stirring rate of cryolite: 20-80 rpm	- Dissolution of sludge is hindered by the thickness of the metal pad - In direct contact of sludge and cryolite, the dissolution rate is of first order in unsaturated bath - Presence of metal pad creates an almost zero order dissolution rate (i.e. mass transfer is controlled through a bath film between the metal and the walls)	[Thonstad et coll., 1980; 2013]
40 wt% alumina 60 wt% cryolite	Stable top crusts (35-55 wt% α-alumina) formed at 985 °C were kept for 48 h in sludge phase at 1000 °C and they were removed	- If stable top crust (35-55 wt% α-alumina) forms sludge, such sludge will take much more time to dissolve in comparison to crusts formed by floury alumina (unstable crust).	[Ødegård et coll., 1985, 2013a]

Bath composition	Operational characteristics	Central deposit characteristics and remarks	Reference
		- The transformation of γ-alumina to α-alumina is rapid and is catalyzed by cryolitic vapors/liquids; the order of catalytic effect is as follows: $AlF_3 > Na_3AlF_6 > NaF > CaF_2$	
No bath.	Cubes of top crust (1 g) were placed under the molten aluminum at 980 °C	- At 980 °C for 1 hour: sludge with lower α-alumina content (< 25 wt%) remains stable; sludge with intermediate α-alumina content (25-45 wt%) deforms and sludge with very high α-alumina content (97 wt%) disintegrates forming a film under the metal pad. - At longer times (96 h), the sludge with intermediate α-alumina content also disintegrates but sludge with lower α-alumina content remains stable.	[Kheiri et coll., 1987]

2.2.4 Influence of cathode carbon materials

The cathode is related to the sludge formation tendency through its thermo-electrical, geometrical and physicochemical characteristics. The most important characteristics of the cathode that may play a major role in the formation/dissolution of the sludge are the thermal conductivity, electrical resistance, porosity and design.

The propensity of a cell to form sludge is strongly related to the quality of alumina dissolution and secondly to the heat loss at the bottom of carbon cathode block. Approximately 50 % of the total heat loss occurs through the cell sidewall and bottom, therefore the thermal properties of the carbon cathode lining become a significant parameter [Solheim, 2018]. Consequently, as long as the sludge does not freeze due to the excessive heat loss at the bottom of the cell, it can be back fed through several phenomena including interfacial and hydrodynamics movements. As a result, it is not wrong to say that the primary purpose of the cell heat balance is to avoid the formation and freezing of the sludge [Grjotheim et Kvande, 1993].

Heat transfer across the cathode construction materials is proportional to the thermal resistance of each layer of material. The thermal conductivity of the carbon materials increases with the level of graphitization and it is a function of the age of the cell and temperature. The thermal conductivity of anthracite increases with temperature, but graphitized materials' thermal conductivity decreases with temperature. However, graphitic materials show contradictory behaviors (i.e. decrease or increase). The intriguing point here is that the behavior of cathode blocks does not always follow a definite increase or decrease pattern. Such different behavior can be attributed to the complex phenomena that each cathode block undergoes during the operation life such as carbide/deposit formation, sodium/thermal expansion, sodium/bath penetration and surface corrosion of cathode block. [Sørlie et Øye, 2010]

The thermal conductivity of the side walls also affects the dynamics of the cell through its interaction with the buffer layer of frozen cryolite (i.e. side ledge). The thickness of the side ledge is influenced by the heat transfer rate. Side walls with lower thermal conductivities transfer the heat from the side ledge at a slower rate, hence cells using such materials may be more prone to have higher superheat levels and sludge dissolution ability. Nevertheless, the more conductive side wall materials may also be prone to dissolve the sludge but with another mechanism [Coulombe et coll., 2016]. Such mechanism involves the extensive formation of the

ledge toe (i.e. bottom freeze) and its contact with the sludge. The interaction of such cryolite rich phases and the sludge produces liquid deposits less dense than the aluminum metal, helping the back-feeding of sludge into the main bath [Solheim, 2002].

In addition to thermal conductivity, the electrical resistance of the cathode block also plays a major role in the complex dynamics of the cells. Song et coll. [2016] have shown, by using a modelling approach, that a cathode material with higher electrical resistivity may cause a higher cathode voltage drop; however, such high resistivity, forces the current paths to follow the most energy efficient path, which is a straight line towards the cathodic bar (i.e. less horizontal current). According to this criterion, the magnitude of horizontal currents versus the cathode type in decreasing order is graphitized, semi-graphitized, full graphitic, 50/50 anthracite/artificial graphite, 70/30 anthracite/artificial graphite and full anthracite. Moreover, horizontal currents can be decreased by up to 20 % with a cathode bottom inclination of 2°. Likewise, other types of modifications such as addition of cylindrical or trapezoidal protrusions on the bottom surface of the conventional cathodes may help to achieve lower and more uniform metal velocity [Wang et coll., 2014; Song et coll., 2017a, 2017b]. Better metal stability can also be achieved by the use of copper inserts which not only reduce the CVD but also can halve the amount of horizontal current density; however, application of such copper inserts may also lead to an extended ledge elongation on the cathode surface because of the high thermal conductivity of copper [Singh et coll., 2017; Von Kaenel et coll., 2017]. Consequently, the use of copper inserts in modern cells has created a renewed interest for cathodes with lower thermal conductivity (e.g. graphitic grades) letting a better control over the thermal balance of the cell (i.e. limiting sludge formation and freezing) [Rivoaland, 2016].

In addition to thermal, electrical and geometrical characteristics of the cell, the physicochemical characteristics of the cell linings such as porosity, tortuosity and air permeability may play a major role in the dynamics of the cell [Wang et coll., 2009]. The later properties define the effective diffusivity of gaseous sodium through the linings and carbon materials (i.e. changing the chemistry of the thin bath that separates the ledge from the metal). The changed chemistry within the aforementioned thin film affects the corresponding interfacial phenomena, which play a major role in the dissolution/formation of sludge and are extensively explained in another section of this article. Furthermore, there is a direct relationship between the carbide formation, porosity of the cathode block and the sludge formation [James et coll., 1995; Landry et coll.,

2018]. Such relationship could be easily explained by the fact that as sludge is formed, it acts as a medium for the dissolution of the carbide. Later, when the sludge is gradually back-fed, the carbide finds its way into the cell and changes the batch chemistry [James et coll., 1995; Fallah Fini et coll., 2017]. In addition, innovative cathode design such as drained cathodes may also eliminate the problem of sludge formation. Drained cathodes only require a film of molten aluminum on the surface of the cathode and consequently the sludge dissolution happens with more ease. Pawlek [2010] has reviewed some of the proposed innovative cell designs and patents of drained cells.

2.2.5 Fluid dynamics

It is quite well established that without proper agitation around the fed alumina particles, alumina feed cannot dissolve and distribute evenly in the bath. Irrespective to the interfacial movements which are explained separately in this article, the most effective dynamic forces in an aluminum electrolysis cell are anodic bubble movements and magnetic agitations. Bubble induced agitation is the most effective phenomenon to dissolve the alumina particles since detrimental hydro-magnetic waves at the bath-metal interface leads to excessive dissolution of metallic species in the bath and alter the anode cathode distance (i.e. more back reaction and loss of current efficiency) [Thonstad et coll., 2001]. In order to minimize the detrimental effect of MHD forces, a typical layer of 25 cm of molten aluminum is maintained during the operation [Tabereaux et Peterson, 2014].

Modern cell technologies all use magnetic compensation systems to reduce the bath-metal agitation and to keep the anode cathode distance as even and low as possible. On the other hand, the application of other technologies such as the insertion of copper rods in the cathode bars has dramatically reduced the metal pad movements [Von Kaenel et coll., 2017]. In such situation, alumina dissolution and distribution in the cell are mostly dependent on the bubble movements. In order to exploit the turbulence of bubble movements, application of slotted anodes has been practiced [Moxnes et coll., 1998]. The slots in the anodes guide the bubbles towards the central channel before leaving the cell in order to exploit the bubble turbulence most efficiently.

Although the hydrodynamics of the cell affects the alumina dissolution and distribution, the formation of sludge also tempers with the hydrodynamics of the cell. As the sludge is formed, it acts as an electrical insulation on the cathode block and this creates local horizontal current

distribution. Such horizontal current lines create local vortexes that disturb the total hydrodynamics of the cell [Tarapore, 2013].

While talking about the hydrodynamics of the electrolysis cells, it is important to mention that one of the oldest questions in the aluminum industry has always been how the sludge is back fed to the mother bath. In order to answer this question, there have been three theories, namely interfacial phenomena (i.e. a thin bath film between the ledge and metal pad [Thonstad et coll., 1980], direct contact of the bath and sludge [Welch, 1995] and finally the metal pad movements [Torklep et coll., 1997; Kalgraf et Torklep, 1998]. Irrespective to the interfacial theory, which is explained extensively in its proper section, the other two theories are directly related to the hydrodynamics of the cell.

The direct contact of sludge and the bath was mostly practical in old feeding systems, such as side work and center break ones in which the cells were mostly run by sludge dissolution and on average just 25% of the fed alumina was dissolved shortly after introduction into the cell [Thonstad, 1977; Welch, 1995]. Nevertheless, in cases that a significant amount of sludge is formed, metal tapping (i.e. lower level of metal) can expose the sludge directly to the bath and expedite the sludge dissolution. Sludge dissolution is a long and time-consuming process since the sludge is not in direct contact with the bulk bath, so consequently, lowering the liquid metal height not only creates a direct contact between the sludge and the bath but also increases the metal pad hydromagnetic movements [Sele, 1977]. Such temporary elevated hydromagnetic movement, while the bath and sludge are in direct contact, is an excellent approach to deal with the extensive amount of sludge. Moreover, according to sediment transport theory [Torklep et coll., 1997; Kalgraf et Torklep, 1998], the increased horizontal movement of metal pad on the fresh sludge, by creating a considerable drag force, may be able to lift up the sludge particles, as big as 1 mm, and move them through the metal pad into the bath.

In severe situations, in order to dissolve the sludge as soon as possible, the synergistic effect of hydrodynamics, superheat and bath chemistry is implemented. In such cases, it is common to practice lower metal depth, less acidity (i.e. reduction of AlF_3 addition) and higher temperature (i.e. superheat level) [Hove et Kvande, 1982; Stam et coll., 2008]. Increasing the metal tapping not only increases the hydromagnetic movements but also, by increasing the anode cathode distance, increases the superheat level. On the other hand, the decreased amount of AlF_3 addition

increases both the alumina solubility and the rate of alumina dissolution [Grjotheim et Kvande, 1993].

2.2.6 Interfacial phenomena

Interfacial phenomena are quite a significant factor in the Hall-Héroult process, since the main cathodic reaction occurs at an interface. Interfacial phenomena may affect the dynamics of the cell through numerous ways. Interfacial tension (IFT) gradient, induced by change in local temperature or bath chemistry, can play a major role in creating certain circulation within the metal-melt interface. Interfacial forces may resist the formation and movement of the gas bubbles or dampen the oscillation at the bath-metal interface; however, surface active species may speed up the renewal of the interface and enhance the mass transfer [Utigard et coll., 1989]. Besides, the interfacial tension between the bath and metal is a barrier against the undissolved alumina agglomerates and other precipitated cryolitic species.

It is well established that as surface-active sodium ions travel towards the metal/bath interface, such concentration polarization lowers the IFT of metal/bath [Utigard et coll., 1989]. On the other hand, since there is a difference between the current density exactly under the anode, and the areas at its vicinity, such IFT gradient causes an outward movement from under the anode (Figure 2-4). Moreover, since usually the deposited sludge has a lower AlF_3 content than the bulk of the melt, and the fact that higher excess AlF_3 increases the interfacial tension, another IFT gradient exists between the metal/bath and metal/sludge. This latter IFT gradient induces a film movement from the sludge towards the bulk melt. Besides, since sodium is continuously lost to the cathode lining, the thin layer of melt in contact with the cathode linings must have a higher AlF_3 (i.e. higher interfacial tension) compared to metal/bath interface. Such higher IFT induces a film of the bath to move downwards from the metal/bath interface (lower interfacial tension) towards the metal/sludge interface (higher interfacial tension). [Utigard et coll., 1989; Utigard et Toguri, 1991].

Based on such interfacial movement patterns, a slow back-feeding of the sludge through a thin film of the bath between the ledge and the metal pad has been proposed by Thonstad et coll. [1980]. Such speculation is based on the two following observations. First, in a laboratory experiment, it was found out that dissolution rate of sludge was approximately independent of bath agitation rate and diffusion controlled. Secondly, after cooling down the experimental set-

up, a thin bath film was always surrounding the metal pad. Later on , Thonstad et coll. [1980] also noticed a fairly rapid transfer rate of sludge in industrial cases. Based on such industrial observations, and assuming an interfacial layer of 0.25-1.0 mm thick, Utigard [1987] has calculated a net back-feeding of 5.5-88 liters of sludge per hour through the thin bath film, which corresponds well with the high exchange rate observed in previous commercial cases [Thonstad et coll., 1980].

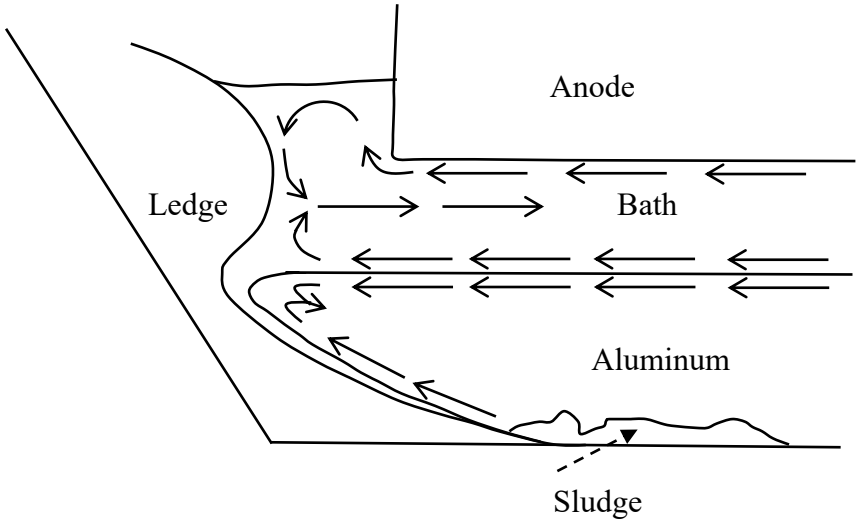

Figure 2-4. Interfacial movements within the aluminum electrolysis cells [Utigard et Toguri, 1991] "Copyright 1991 by The Minerals, Metals & Materials Society. Used with permission."

On the other hand, as it was mentioned before, AlF_3 feeding may also cause sludge formation and such sludge interacts very differently with the bath. For instance, its dissolution time is much longer than the sludge formed by alumina agglomerates. The elongated dissolution time is explained by the interfacial movement from the low IFT at bath towards the high IFT (due to excessively high amount of AlF_3) at the sludge, exactly opposite of the flow pattern speculated for alumina formed sludge. As AlF_3 gradually dissolves in the film layer, a mixture of solid AlF_3 and AlF_3-rich bath is formed. At a certain point, the density of this solid-liquid mixture becomes less than the aluminum pad and a sudden batch of AlF_3 is introduced into the bath. Furthermore, it is shown that the IFT plummets in the range between pure cryolite and 13 wt% of excess AlF_3; beyond such amount of excess AlF_3, no further significant change is noticed in IFT values [Utigard et Toguri, 1985]. Accordingly, it has been speculated that it is better to operate the electrolysis cells at an excess AlF_3 value of 10-13 wt% in order to keep a tangible driving force to enhance the movement of bath film and back-feeding of sludge [Utigard, 1987].

Moreover, Utigard [1993] has argued that when the low density liquid fraction of the sludge is back-fed, either through the metal pad or through a thin film between the ledge and metal pad, the remaining solid bottom crust is also capable of being removed. He speculates that the dissolution of such bottom crust is dependent on two phenomena that are, first, the downward movement of the bath through the thin bath film that separates the ledge from the metal. Such downward movement is due to the low sodium and AlF_3 activities of alumina-rich cryolite in contact with the bottom crust. Secondly, such low activities, enhance the mass transfer of sodium from sodium-rich cathode block towards the sludge. These two phenomena gradually provide enough bath to gradually dissolve the bottom crust.

Furthermore, in cases when the heat loss at the bottom of the cell is enough to crystallize cryolite, such precipitation increases the local AlF_3 concentration, leading to enhanced movement of the bath within the thin film from the bulk to the bottom of the cell. Consequently, a thin layer of solid cryolite may form and extend astonishingly fast (up to 10 cm/day) on the surface of the carbon cathode [Utigard, 1987]. At high bath acidity, irrespective to the problem of increased bath resistivity, increased anodic/cathodic overvoltage, less alumina solubility and lower rate of alumina dissolution, it is also possible that a solid layer of cryolite precipitate on the bath-metal interface [Utigard, 1987]. Such phenomenon has been noticed in cases with very high amount of excess AlF_3 and low superheat levels due to the sodium overvoltage at the bath metal interface and increased interfacial liquidus temperature [Sleppy et Cochran, 2013]. The precipitation of cryolite at the metal-bath interface may be enhanced in systems that possess high amount of excess AlF_3, stable bath-metal interface (i.e. magnetically compensated) and no lithium [Haupin, 1997].

Additionally, Solheim [2002] has calculated the amount of cryolite and alumina that may crystallize at the bath-metal interface in case of sodium concentration polarization, considering the fact that lower superheat level as well as higher excess AlF_3, favor the crystallization. According to Haupin [1997], the increased electrical resistance due to the precipitated cryolitic species at the bath-metal interface, ultimately dissolves such layer (by creating local heat) creating a cycle of precipitation and dissolution in a repetitive manner. In addition, if such cryolitic crystals form sludge, those may act as a solvent for alumina particles. The dissolution of alumina particles in the precipitated cryolite crystals not only decreases the acidity of the sludge, but also lowers the liquidus temperature and density of the liquid fraction of the sludge

[Solheim, 2002]. The consequence of such phenomena for the molten mixture of cryolite and alumina is either rising through the metal pad in small batches or dissolution in the thin film that exists between the ledge and metal pad.

2.2.7 Temperature

Probably the most effective parameter in the formation/dissolution of sludge is the operational temperature. The operational temperature of the cell is directly related to the heat balance of the cell and the primary purpose of checking the heat balance of the cell is to avoid the formation and freezing of the sludge [Grjotheim et Kvande, 1993]. Based on the phase behavior of the bath (i.e. bath chemistry), operational temperature is also related to the superheat level of the bath according to Figure 2-5. For more detailed information for the influence of temperature on the formation and dynamics of different deposits within the electrolysis cells refer to Fallah Fini et coll. [2017].

Moreover, it deserves to be mentioned that the summation of the dissolution energy and sensible heat is enough to decrease the temperature of the melt by 15˚C if 1 wt% of alumina (with respect to total mass of the bath) at room temperature is introduced into the cell [Welch et Kuschel, 2007]. Such calculations show that heat transfer within the cell is crucial for proper dissolution of the alumina and further prevention of sludge formation [Hove et Kvande, 1982]. On the other hand, as it was mentioned before, the dissolution/disintegration of the frozen bath layer around the agglomerated alumina particles is heat transfer controlled. On top of that, in order to reduce the required sensible heat for the dissolution of alumina particles, preheating of the alumina particles has been proposed [Kobbeltvedt, 1997].

Also, in order to enhance the chance of back-feeding of the sludge, it is always necessary to keep the temperature of the bottom of the cells at least at the eutectic temperature of the operating bath [Utigard, 1999]. The latter consideration is due to the fact that the liquid bath in contact with sludge is saturated in alumina and the lowest temperature that allows the dissolution of sludge in the bath is the eutectic temperature. However, the liquid fraction of the sludge is rich in sodium which increases the threshold saturation temperature (i.e. eutectic temperature).

Another important parameter regarding the operational temperature of the cell is related to the rate of heat transfer through the cell walls affecting the growth or melting of the side ledge. Coulombe et coll. [2016], by using a bench scale set-up, have demonstrated the influence of the

heat transfer rate at the sidewalls of the cell on the sludge formation/dissolution tendency. It has been shown that more sludge is formed at low heat transfer rate from the cooled wall of an experimental cell, in comparison to tests with higher heat transfer rate. They justify such contradictory results by claiming that for tests with higher heat transfer rate, the side ledge extends on the bottom surface of the cathode forming an elongated ledge toe. Such ledge toe creeps towards the sludge and upon linking to the sludge, creates a less dense liquid, which is gradually back fed into the bath either through interfacial phenomena or through the aluminum metal. Such conclusion is quite comprehensible since the ledge is mostly consisting of cryolite and its contact with alumina particles can dissolve them and create a low-density alumina-saturated bath with lower liquidus temperature [Solheim, 2002].

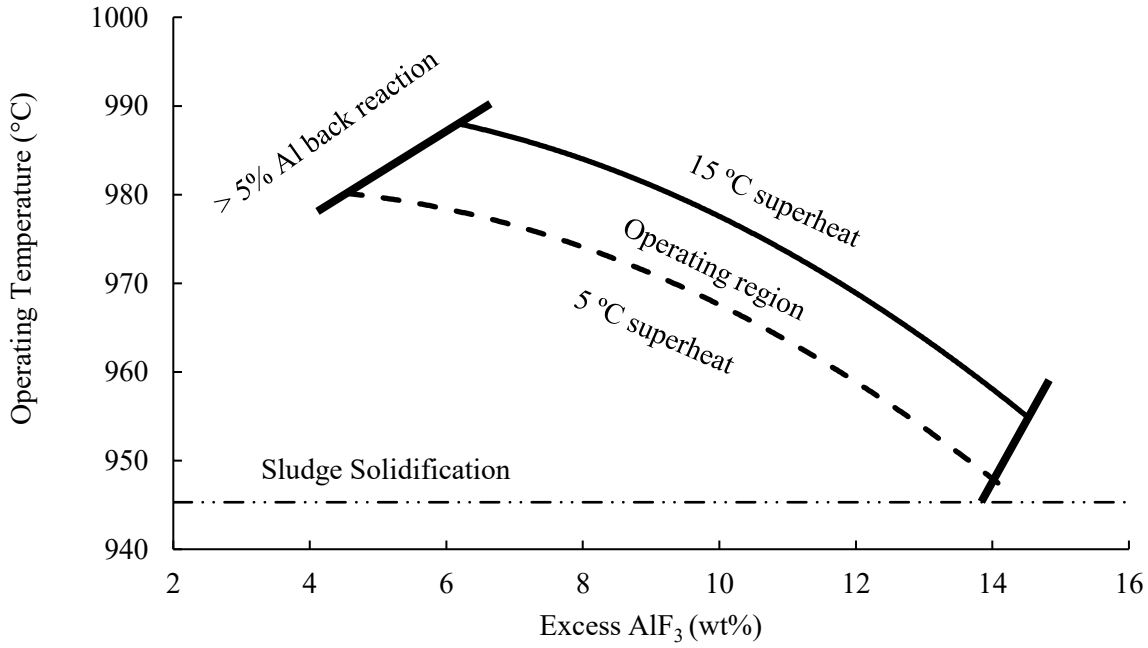

Figure 2-5. The schematic influence of temperature and bath acidity on the operation of the cells; the bath includes 0.5 wt% MgF_2, 3 wt% alumina and 5 wt% CaF_2. [Taylor, 1997]

2.2.8 Bath chemistry

A typical electrolysis cell uses 9-11 wt% AlF_3, 4-6 wt% CaF_2, 1.5-4 wt% Al_2O_3 and in some cases 2-4 wt% MgF_2/LiF [Tabereaux et Peterson, 2014]. Table 2-4 shows the influence of various additives on the physicochemical properties of a typical bath. There is no doubt that the presence of each chemical in the bath affects the phase equilibria. However, the study of the

phase equilibria in each system is out of the scope of this research and avid readers are referred to extensive references [Grjotheim et coll., 1982; Thonstad et coll., 2001].

Table 2-4. Influence of additives on physicochemical properties of the bath; ↑ increase, ↓ decrease [Grjotheim et Kvande, 1993; Habashi, 2003]

Property	LiF	NaF	CaF_2	MgF_2	AlF_3
Liquidus temperature	↓	↑	↓	↓	↓
Alumina solubility	↓	↓	↓	↓	↓
Rate of alumina dissolution	↓	↓	↓	↓	↓
Vapor pressure	↓	↓	↓	↓	↑
Density	↓	↓	↑	↑	↓
Viscosity	↓	↓	↑	↑	↓
Interfacial tension (bath-metal)	↑	↓	↑	↑	↑
Electrical conductivity	↑	↑	↓	↓	↓

The reduction of liquidus temperature is a beneficial phenomenon since it reduces the operating temperature (i.e. less energy consumption) and enhances the current efficiency. This is also beneficial since at constant operating temperature, lower liquidus temperature reduces the chance of sludge solidification. Nevertheless, the combination of lower superheat levels and higher acidity not only reduces the alumina solubility and its dissolution rate but also increases the difference between the melting point of the side ledge and the bath [Utigard, 1993]. Besides, in the systems using LiF as additive, the liquidus and hence the eutectic temperature of the system is lower, allowing for a possible lower bottom temperature in the cell [Utigard, 1999]. Nevertheless, Thonstad et coll. [1982] indicate that the application of LiF in acidic baths exacerbates the bottom crust formation [Thonstad et coll., 1982]. Such problem may be related to the fact that the application of LiF not only reduces the liquidus/eutectic temperature but also reduces the eutectic alumina concentration and dissolution rate of alumina.

All the additives affect the density of the bath. Lower bath density may decrease the terminal velocity of the alumina particles. Keller [1984] mentions that lower density of the bath consequently reduces the density of the alumina agglomerates and hence it can hinder the sludge formation. On the other hand, since the density of aluminum pad (~2300 kg/m^3) does not change significantly with temperature within the range of 940-970 ˚C [Leitner et coll., 2017], most of

the density difference between the bath and metal is accounted for by the cryolitic melt. Dissolution of alumina in the bath reduces the density of the bath up to the eutectic point [Thonstad et coll., 2001] and hence any contact between the sludge and a cryolite rich phase could enhance the back-feeding of sludge. Such cryolite rich phases could be provided by the molten side ledge (i.e. high superheats) or precipitation of cryolite due to sodium concentration polarization at bath-metal interface [Solheim, 2002].

After alumina particles agglomerate and sink through the bath, there is yet another barrier (i.e. interface of metal-melt) for them to reach to surface of the cathode block. According to Table 2-4, all additives increase the metal-melt interfacial tension (IFT). Lower CR and higher alumina content also increase the interfacial tension [Utigard, 1999]. In addition to IFT, the viscosity of the electrolyte also affects the hydrodynamics of fluids through interaction with gas bubble detachment and terminal velocity of undissolved alumina particles. A high viscosity can reduce the metal dissolution within the bath and enhance the alumina dissolution rate by reducing the back-reaction rate. In addition to the above-mentioned factors, evaporation of volatile species also affects the chemistry of the bath. The most volatile species are the sodium and aluminum fluoride or the combination of these species as $NaAlF_4$ [Grjotheim et Kvande, 1993]. Evaporation of such chemicals increases the CR and it is required to control the CR by introduction of fresh materials. Higher CR increases the liquidus temperature and consequently the sludge finds more opportunities to transform into a solid deposit [Allard et coll., 2014a].

2.2.9 Physicochemical characteristics of alumina

One of the other significant factors in normal operation of the electrolysis cells is the physicochemical traits of the alumina feed, since it directly influences the solubility rate of the alumina and the chemistry of the bath. Such characteristics include different phases of alumina, BET (Brunauer-Emmett-Teller) surface area, density, loss on ignition (LOI), particle size distribution and flow funnel time. There are already extensive literature reviews about the influence of alumina traits on its dissolution behavior [Grjotheim et coll., 1982; Grjotheim et Kvande, 1993; Thonstad et coll., 2001; Welch et Kuschel, 2007; Wang, 2009], consequently, only some important points will be addressed here. Furthermore, typical characteristics of the smelter grade alumina feed has been summarized by Tabereaux et Peterson [2014].

Alumina is present in the cryolitic bath samples as dissolved alumina or several crystalline structures (i.e. β, γ, θ, δ, α). The two most common alumina phases are the α-alumina (high temperature calcined) and γ-alumina (low temperature calcined). γ-alumina (also known as sandy alumina) has a lower flow funnel time, higher surface area and higher dissolution rate which makes it more ideal for aluminum electrolysis cells; however, pure γ-alumina creates very hard top crusts (i.e. excessive crust feeding). Hence typical α-alumina (also known as floury alumina) content of smelter grade alumina (SGA) is 2-15% [Tabereaux et Peterson, 2014]. Moreover, the rate of dissolution for different alumina phases is as follows: $\beta > \gamma > \theta > \delta > \alpha$ [Gerlach et coll., 1975]. Upon addition to the melt, γ-alumina exothermally transforms into α-alumina, which is less soluble, and later, endothermally dissolves within the bath [Gerlach et Winkhaus, 1985]. γ-alumina transformation into α-alumina creates thin plates (*ca.* 0.5 µm) while thicker alumina plates (*ca.* 1.5 µm) are the initial feed α-alumina content that has precipitated without dissolution and act as building blocks of the agglomerates [Thonstad et coll., 2001].

What's more, alumina particles which easily flow (i.e. less flow funnel time) tend to disperse over the bath rather than forming clumps, therefore a faster dissolution rate is observed. Flow funnel time is inversely proportional to the percentage of fine alumina particles. High number of fine particles may lead to the creation of densely packed alumina aggregates (i.e. higher density) that in return increase the possibility of sludge formation. Of course, fine particles dissolve individually faster than coarse particles, but their higher flow funnel time and poor wetting properties lead to a slower dissolution rate. Because of such poor wetting properties, electrolyte cannot penetrate within the intergranular voids of the alumina particles and instead, finer particles fill the voids between the coarse particles creating an elongate floating period for the formed rafts. Besides, the volatile content of the alumina (i.e. LOI) in contact with the hot bath not only creates agglomerates that are more porous (i.e. lower density) but also provides a local turbulence that helps to enhance the dissolution rate of alumina. Upon addition of the alumina into the cell, the volatile content of the alumina is released in two steps, 1) a short rapid release of vapor from $Al(OH)_3$ and 2) a more extended vapor release during α-phase transition catalyzed by $NaAlF_4$. [Keller, 1984; Rye et coll., 1990; Isaeva et coll., 2009; Dando et coll., 2010]

Moreover, preheating the alumina (≥ 600 °C) is an effective method to make sure that most of the alumina is dissolved at rates close to single particle dissolution rate; nevertheless, the agglomerates formed at such condition, are much denser and hard to dissolve [Kobbeltvedt, 1997]. According to Rye et coll. [1990], the reason for increased rate of dissolution in case of preheated alumina is the formation of a thinner bath layer around the agglomerates which in return disintegrates faster. The short life span of such alumina agglomerates inhibits extensive sintering, so less dense α-alumina aggregates are formed. It has to be emphasized that the most effective method to enhance the dissolution rate of the single alumina particles as well as the alumina agglomerates is to have enough superheat [Kobbeltvedt, 1997]. In recent years, there have been some attempts to construct preheating equipment that can use the top crust heat loss of the smelters to preheat the alumina particles [Schubert Severo et Gusberti, 2017].

Yang et coll. [2015] have investigated the difference between two grades of alumina namely primary and secondary alumina. Based on observations made with transparent quartz cells, it has been shown that secondary alumina dissolves 50% faster than primary alumina. In order to explain the higher dissolution rate of the secondary alumina, parameters such as higher values of loss on ignition (25-300˚C), fluoride content and burning of adsorbed carbon dust have been proposed. It has been claimed that the burning of adsorbed carbon dust after introduction of the feed can decrease the temperature drop up to 0.5% as compared to primary alumina.

Furthermore, according to Wang [2009], there are contradictory research results pertaining to the effect of BET surface area on alumina particles' dissolution rate. Some results indicate that higher surface area enhances the dissolution rate [Bagshaw et Welch, 2013], whereas some others mention that surface area has a negligible effect on the dissolution rate [Jain et coll., 1983a; Jain et coll., 1983b]. In addition, it has to be emphasized that most of the alumina characteristics such as BET, α-alumina content, LOI and flowability are interlinked which makes the study of individual parameters very hard [Wang, 2009]. On the other hand, it is well established that the dissolution of alumina in the bath is mostly governed by superheat level, bubble agitation and feeding strategy rather than the characteristics of feed stock [Kobbeltvedt, 1997; Welch et Kuschel, 2007; Kuschel et Welch, 2013; Lavoie et coll., 2016].

Archer [1983; 2013] has presented a qualitative model to predict the sludge formation tendency of the alumina feedstock with respect to alumina characteristics that are governed by Bayer

process. Accordingly, two parameters were reported to have medium levels of confidence in the prediction of sludge formation tendency, namely big alumina particles (>149 µm) and Gibbsite content, while the other two parameters (i.e. specific surface area and particle size distribution) showed low levels of confidence. At the end, no data has been reported on the relationship between the fine particles (<45 µm) and the tendency towards sludge formation.

At the end, it must be emphasized that in some cases the situation is much more complex, and a more in-depth analysis is required to investigate the influence of alumina characteristics on the dynamics of the cell. Consequently, some dramatic and unpredictable changes may occur by changing the alumina feed from one batch to another batch. In one case, for example, a change to an alumina feed containing higher gibbsite and moisture content has shown two different behaviors either leading to lower bath acidity (i.e. from 10.6% to 8.8%) or no change in bath acidity [Meyer et coll., 2012]. On top of that, investigation of some parameters such as pore size distribution or particle size distribution has failed to account for the unpredictable response of the smelter. Such contradictory behavior requires further studies to a) compare the difference between the effect of moisture content of various alumina phases; and b) investigate the different behavior of moisture content depending on particles' pore size distribution.

2.2.10 Alumina feeding strategy

Upon the introduction of alumina into the aluminum smelting cells, alumina particles (depending on their physicochemical characteristics and feeding strategy) either undergo a rapid path of dissolution, with no problem of sludge formation, or agglomerate and follow a slower regime of dissolution [Solheim, 2014]. As Table 2-5 indicates, there are three main feeding strategies, namely center worked (CW), side worked (SW) and point feeding (PF).

The CW and SW technologies are the oldest feeding technologies which had several drawbacks such as higher anode effect frequency and extensive sludge formation. The benefits of the center worked (CW) cells versus the side worked (SW) cells are a greater volume of bath close to feeding zone and faster recovery from thermal effects. However, the location of sludge in SW cells is better than CW cells since during the heating period, the partially molten side ledge is closer to the sludge formed in the SW cells. On the other hand, the magnetically driven motion of the metal pad tends to force the sludge towards the side ledge hence enhancing the back-feeding [Welch et Grjotheim, 1988]. The main problem of CW cells is the excessive sludge

formation that stems from two operational facts namely, big mass of alumina dumps and big amount of top crust feeding [Welch et Grjotheim, 1988]. Considering that the thickness of the crust is typically 100 mm in the CW and SW cells, sometimes several beam actions are required to break the crust properly. Consequently, in addition to the excessive crust feeding, volume of the bath is also reduced because a lot of bath freezes over the beams. Based on these facts, most of the sludge formation problems in the CW and SW cells arise from the considerable amount of crust that is suddenly dumped into the cell [Welch et Grjotheim, 1988; Grjotheim et coll., 1989; Welch, 1990].

Table 2-5. Comparison between different feeding systems [Grjotheim et coll., 1989].

Property		Feeding system		
		PF*	CW**	SW***
Break and feed	Frequency (1/hr)	10-30	0.3-0.5	0.2-0.3
	Immersion time (s)	0.7-2	2-4	2.5-4
	Discharge mass (kg)	0.5-3	60-100	100-160
	Crust feeding (kg)	0.2	30-50	60-100
	Bath quantity (kg)	30-50	350-450	500-700
Heat demand	(kJ/kg bath)	50	700	800
Sludge tendency		Low	High	Very high

*Point feeding, **Center working, ***Side working

In order to alleviate the muck formation problem, various attempts were made to better adjust the following parameters: bath acidity, alumina quality, temperature (i.e. superheat), dump size, crust-breaking technology, feeding position, bath volume, alumina discharge technology and agitation level of the bath [Welch, 1990]. So far, the most influential technique which not only minimizes the muck (sludge) formation but also addresses several other control issues such as short-term variation in temperature, anode effect frequency and enhancement of current efficiency, has been the implementation of point-feeding systems [Welch et Grjotheim, 1988; Welch, 2007; Tarcy et coll., 2011]. The main concept behind the point feeding systems is to reduce the number of alumina dumps but increase the frequency of alumina addition. Such approach not only helps to avoid excessive sludge formation but also decreases the frequency of anode effect.

Batch size and frequency of alumina addition mainly depends on the corresponding temperature drop and the heat balance of the cell. According to Hove et Kvande [1982], the state of sludge formation is related to the volume of the fed alumina batch, rate of the feeding and duration of feeding time. Walker et coll. [1995] have compared the temperature drop of two industrial cells with two different feeding strategy (i.e. point feeding versus center break). As it is shown in Figure 2-6, the larger quantity and the more sudden addition of alumina lead to excessive and a much wider temperature drop and hence more possibility for sludge formation. According to Welch [1990], every cell has its own dump size to break-frequency ratio which has to be recognized through experience and modelling strategies.

Jain et coll. [1983b] have monitored two distinct behaviors during two feeding regimes. The first regime shown in Figure 2-7 happens when alumina is added in a manner that every alumina particle is well dispersed (i.e. slow feeding rate and small dumps) and a rapid dissolution regime is followed. The second behavior is according to the slow dissolution path, usually happening when alumina is not well dispersed, and agglomerates are formed. If the heat transfer is not enough, the dissolution of agglomerates will be hindered and as Walker et coll. [1995] have shown, agglomerates' density may surpass the density of the molten aluminum.

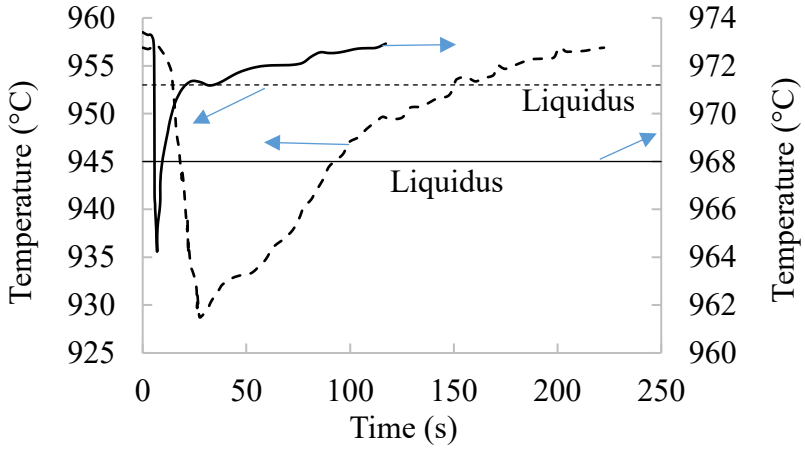

Figure 2-6. Comparison of bath temperature change versus time for two feeding strategies; The solid lines and dashed lines correspond to point feeding and center working respectively [Walker et coll., 1995]. "Copyright 1995 by The Minerals, Metals & Materials Society. Used with permission."

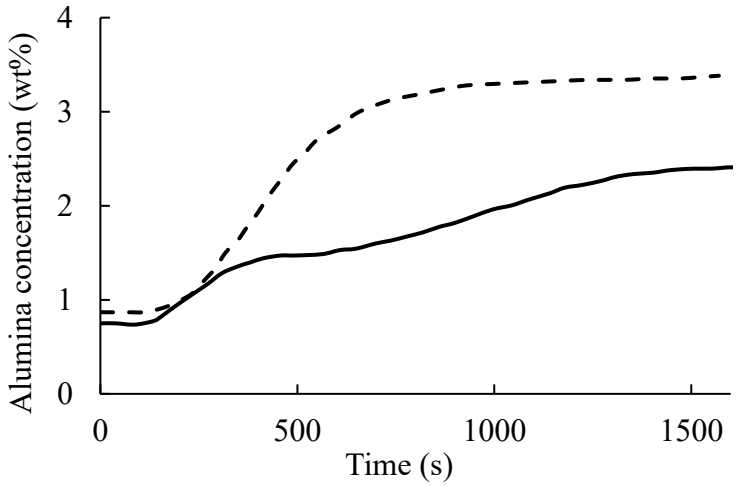

Figure 2-7. Dissolution behavior of one-stage well dispersed (dashed line) and two-stage agglomerated alumina particles (solid line) [Jain et coll., 1983b]. "Copyright 1983 by The Minerals, Metals & Materials Society. Used with permission."

The agglomeration or fast dissolution of alumina particles are also influenced by the feeding height and area [Bagshaw et coll., 1985]. Of course, the addition of alumina in a widely dispersed manner creates occasional rafts; nevertheless, alumina feeding to a confined area enhances the possibility of alumina particles' agglomeration. Moreover, as Figure 2-8 shows, the dissolution rate of alumina particles is quite dependent on impact-induced turbulence and increased penetration velocity of the particles into the bath [Bagshaw et coll., 1985].

Recently Solheim [2014] has argued about the ideal case of feeding strategy which is continuous feeding (i.e. very high frequency + very low quantity). In an ideal continuous feeding, the alumina concentration is constantly kept at low values avoiding any anode effect or sludge formation. Nevertheless, point feeders that are used nowadays are far away from completely dispersed feeding systems. Solheim [2014] has also reviewed several patents and articles concerning the continuous feeding of alumina as well as the problems that may arise by their implementation.

Considering the fact that nowadays most of the smelters in the world use point-feeding systems [Tabereaux, 2000], the frequency and batch size of the alumina is quite dependent on the number of feeders and their location [Walker et coll., 2013]. On the other hand, the number of feeders and their location are determined based on proper dissolution and distribution of alumina, which means that the hydrodynamics of the bath is a crucial parameter [Kobbeltvedt et Moxnes, 2013].

It is well established that in order to enhance the alumina distribution in the bath, the best location for feeders is in the center channel near to the corner of anodes along the anodes' width and close to the inter-anode slots [Welch, 1990; Zhan et coll., 2014]. Such feeding location, not only widens the effective mixing of the bath by bubble movements, but also approximately halves the number of required point feeders [Zhan et coll., 2014].

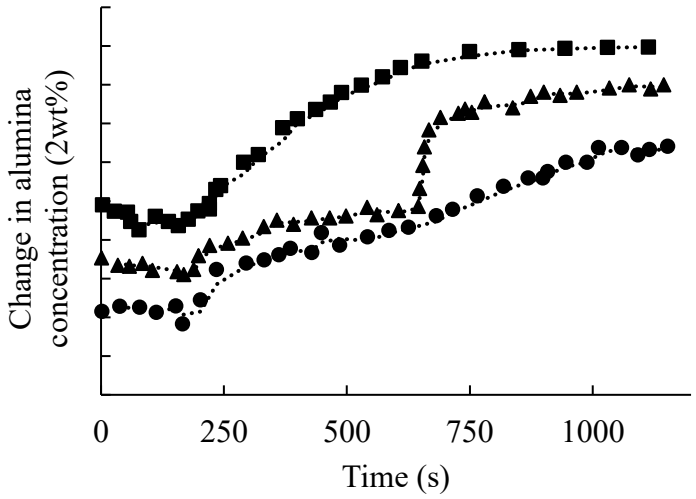

Figure 2-8. Effect of dumping height (h) on the dissolution behavior of alumina; ● (h=2 cm), ▲ (h=10 cm), ■ (h=60 cm) [Bagshaw et coll., 1985]. "Copyright 1985 by The Minerals, Metals & Materials Society. Used with permission."

The other parameter that may determine the batch size and frequency of alumina addition is based on demand-feed technology. This concept is based on the variation of bath resistivity between two extremes of underfeeding (i.e. anode effect) and overfeeding (i.e. sludge formation) [Kvande et coll., 1994; Welch, 2007; Moxnes et coll., 2009; Robilliard et Rolofs, 2013]. Consequently, one common approach is to add the alumina based on the bath resistance, keeping the alumina concentration around a mean value by having underfeeding and overfeeding periods. Flow adapted alumina feeding is yet another recently developed strategy and it tries to optimize the cell operation through keeping a uniform alumina content. In this method, the uniformity of alumina concentration in the cell is adjusted by controlling the local feeding rate of each feeder as a function of anodic current density. Such an approach leads to higher current efficiency, lower anode effect frequency and less sludge formation [Moxnes et coll., 2009].

Another important factor for having a sludge free operation is related to the condition of feeding holes. Kobbeltvedt et coll. [1996] have argued about the plugging effect of feeding holes that leads to the excessive formation of agglomerates/sludge. It is mentioned that alumina may plug feeding holes due to design features or bath splashing. Consequently, the next crust breaking action will push into the bath an amount of alumina higher than expected. As it can be seen in Figure 2-9, there is a vivid variation of temperature in case of plugged feeding holes compared to the almost equal temperature drop of the open feeding holes (i.e. easy to control). Besides, in case of plugged feeding holes, the alumina dissolution behavior shows a two-stage pattern in accord with extensive agglomeration of alumina particles. [Kobbeltvedt et coll., 1996; Lavoie et coll., 2016]

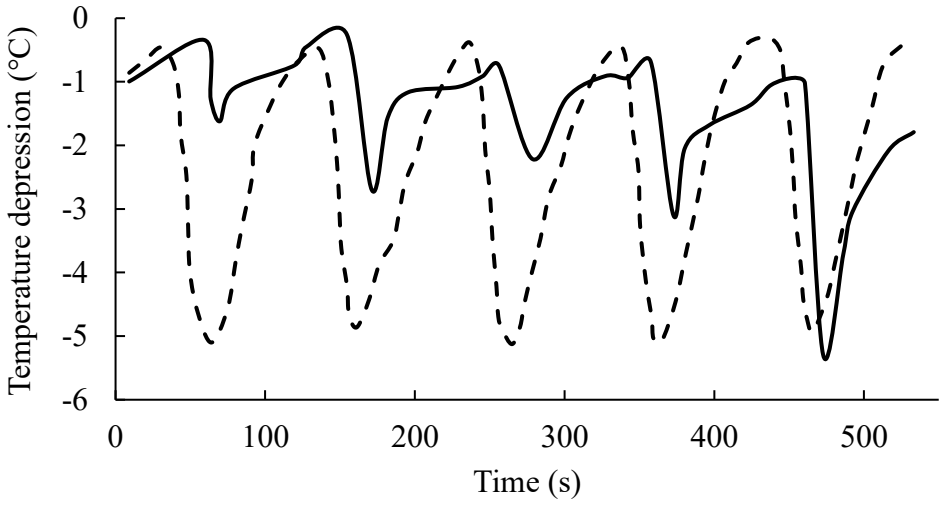

Figure 2-9. The temperature drop when the bath was fed with plugged holes (solid line) and open holes (dashed line) [Kobbeltvedt et coll., 1996]. "Copyright 1996 by The Minerals, Metals & Materials Society. Used with permission."

Considering the above-mentioned factors related to alumina feeding, it has to be emphasized that anode change can also introduce a considerable amount of top crust and anode cover materials (150-250 kg per anode) into the cell [Taylor et Welch, 2004]. Such crust feeding may create a domino of undesirable events such as reducing bath volume, dropping superheat, changing bath chemistry, altering cell's resistivity, and agitating magnetic forces [Grjotheim et coll., 1989]. Besides, anode change may also contribute to the formation of cryolite-rich sludge if lumps of anode freeze (containing less AlF_3 and alumina compared to the main bath) fall on the bottom of the cell [Utigard, 1999].

2.2.11 Conclusions

Sludge formation in Hall-Héroult cells causes numerous operational problems leading to higher energy demand and lower current efficiency. As it is reviewed in this article, sludge formation is quite a complex phenomenon, interlinked with several operational and fundamental parameters. Such parameters include the heat balance, feeding strategy, characteristics of alumina, type and geometry of the cathode, hydrodynamics, interfacial tension and bath chemistry. It is evident that with a proper superheat throughout the cell, not only the fed alumina is dissolved but also in case of sludge formation, the sludge may not find enough time to form resistive hard-to-dissolve bottom crust. However, proper dissolution and distribution of alumina in the cell are also quite dependent on the bath chemistry, hydrodynamics, feeding strategy and the characteristics of the fed alumina.

It has been well established that the introduction of small batches of alumina in short intervals not only keeps the cell's heat balance in check but also provides more opportunities for fine tuning the bath chemistry and hydrodynamics. Anode gas release, magnetic movements and geometry of the cell are the key factors in hydrodynamics of the cell. In modern cells that are typically magnetically compensated, anode gas release has become the main source of agitation in the bath. Withal, recent developments in application of certain protrusions at the bottom of the cell or tilting the bottom of the cell have shown even more potential to reduce the metal pad movements. Nevertheless, the local turbulence of the bath, upon introduction of fresh alumina into the cell is another crucial factor in efficient dissolution and distribution of alumina throughout the anode cathode distance. Of course, it must be emphasized that such local agitation induced by the alumina introduction into the cell is mainly governed by the physicochemical characteristics of the alumina.

Moreover, the undeniable effect of interfacial phenomena in the Hall-Héroult process must not be forgotten since the main cathodic reaction leading to aluminum production occurs at an interface. Considering all the above-mentioned factors, sludge formation is quite common, whether it is related to alumina feeding, anode change, collapse of top crust or change of bath chemistry. The important questions at the end of this review would be first to understand how all these factors interact and enhance or alleviate the problem of sludge formation. The first question has been dealt with in different sections of this article, but the second question is how to avoid sludge formation and enhance the operation of the cells in order to reduce the energy

consumption and increase the current efficiency. The answer to this question is simply to keep all the parameters in check (i.e. keeping enough superheat, controlling the feeding, etc.). Such task has been following a one-hundred-year-old path of improvement and fine-tuning because of interlinked nature of all the operational parameters. The most recent improvements include the continuous monitoring of anodic current density, preheating the alumina and implementing the concept of continuous alumina feeding. These innovations seem to be able to eliminate or drastically reduce the sludge formation soon.

CHAPITRE 3 MÉTHODOLOGIE

3.1 Description du montage expérimental

Les expériences sont effectuées dans le laboratoire d'électrolyse de l'aluminium à l'Université de Sherbrooke. Comportant des fours électriques, des systèmes d'alimentation électrique, des systèmes de contrôle et des systèmes de purge à l'azote ou à l'argon, ce laboratoire dispose de bancs d'essai spécifiques qui permettent d'imiter certaines conditions d'opération industrielles à plus petite échelle. La Figure 3-1 représente le banc d'essai pour l'électrolyse d'aluminium à haute température. Les données expérimentales sont enregistrées dans un fichier Excel sur un ordinateur moyennant LabVIEW^{TM} (un acronyme de *Laboratory Virtual Instrument Engineering Workbench*).

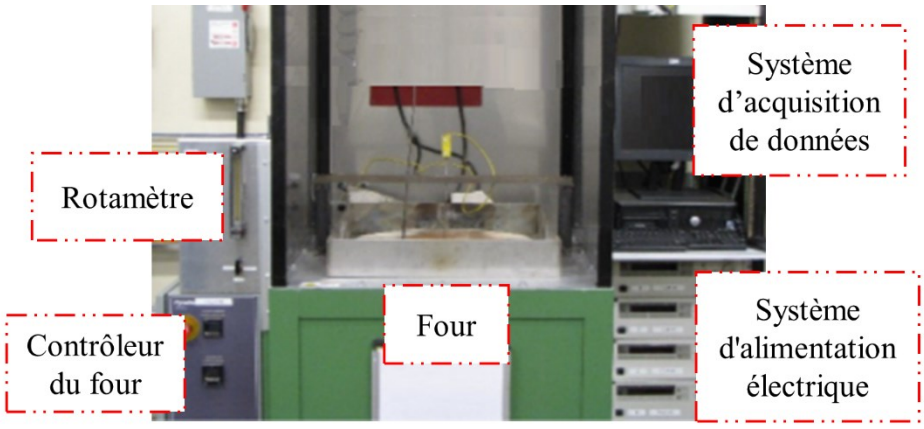

Figure 3-1. Banc d'essai pour l'électrolyse d'aluminium à haute température

Avant chaque expérience, les surfaces latérales des blocs cathodiques, ayant les dimensions illustrées à la Figure 3-2, sont recouvertes de feutre de carbone et quatre plaques en Inconel^{TM} sont ensuite soudées autour de celles-ci afin de réduire la perte de sodium à travers les blocs cathodiques, tel que présenté à la Figure 3-3. Ainsi, afin de protéger les surfaces latérales internes des blocs cathodiques, quatre plaques de SiC/Al_2O_3 sont déposées à l'intérieur du bloc cathodique tel que représenté à la Figure 3-2. Ensuite, un bloc d'aluminium d'environ 480 g est placé au fond du bloc cathodique. La cellule est alors remplie du bain cryolitique broyé tandis que l'anode est positionnée au centre de la cellule (Figure 3-2).

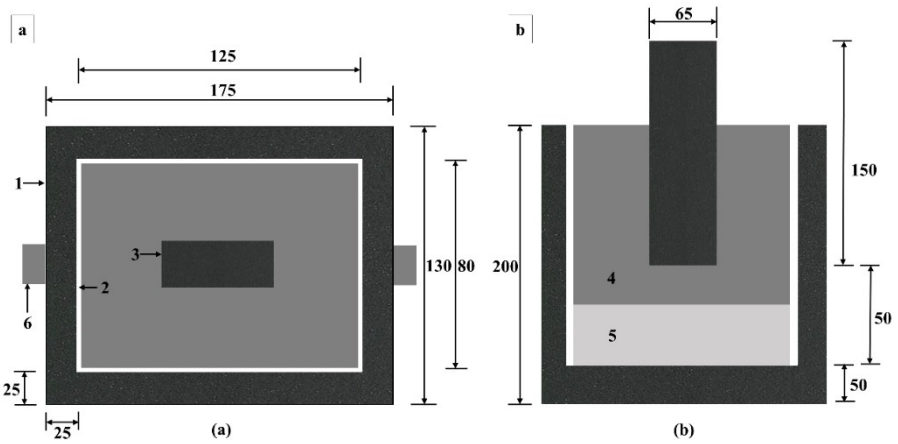

Figure 3-2. Dimensions et composantes d'une cellule expérimentale; vue de haut (a) et vue de côté (b); 1 : bloc cathodique, 2 : plaques de SiC/Al_2O_3, 3 : anode, 4 : bain, 5 : aluminium, 6: barre collectrice; toutes les dimensions sont en millimètres [Landry et coll., 2018].

Figure 3-3. Un bloc cathodique recouvert de feutre de carbone et de plaques en Inconel™

Après que la cellule expérimentale a été remplie de bain (les valeurs exactes se trouvent à la section 3.2 Plans d'expérience), cette dernière est placée au fond du porte-creuset en Inconel™ sur un carreau de carbure de silicium. La Figure 3-4 représente toutes les composantes du montage expérimental, dont la laine en alumine (isolation thermique), les tiges de contact anodiques/cathodiques, le thermocouple recouvert d'une gaine de carbure de silicium[1], l'entrée d'azote (toutes les expériences s'effectuent sous une atmosphère d'azote), et le point d'échantillonnage à travers lequel des échantillons de bain sont prélevés en utilisant un doigt froid en acier.

[1]Saint Gobain, Hexoloy® Silicon Carbide

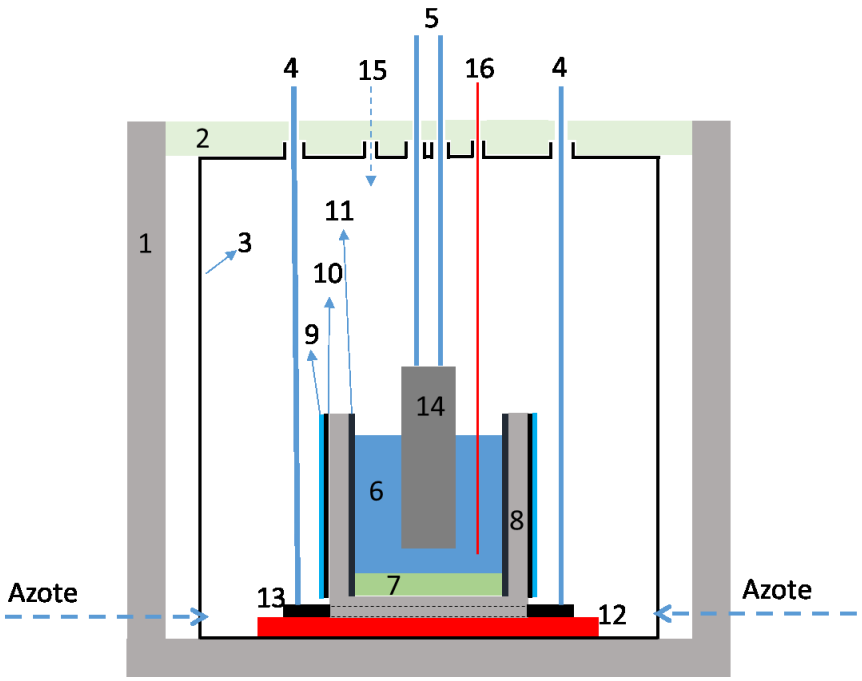

Figure 3-4. Schéma du montage expérimental; 1 : four, 2 : isolation en alumine, 3 : porte-creuset en Inconel^{TM}, 4 : tiges de cathode, 5 : tiges d'anode, 6 : bain, 7: aluminium, 8 : bloc cathodique, 9 : plaque en Inconel^{TM}, 10 : feutre de carbone, 11 : plaques de carbure de silicium, 12 : carreau de carbure de silicium, 13 : barre collectrice, 14 : anode, 15 : point d'échantillonnage, 16 : thermocouple

3.2 Plans d'expériences

3.2.1 L'impact de la nuance de bloc cathodique

Ayant pour but l'identification de propriétés importantes des blocs cathodiques qui influencent la formation ou la dissolution de boue dans le procédé Hall-Héroult, cinq différentes nuances industrielles de bloc cathodique sont étudiées d'après le Tableau 3-1. Dans le contexte de cette partie du projet, toutes les expériences s'effectuent à la température de 960 °C, à une intensité de courant électrique de 73 A tout en utilisant 1700 g d'un bain acide industriel (CR = 2.2, 10 % (massique) d'alumine et 5 % (massique) de fluorure de calcium) et un temps d'électrolyse de 8 heures. Dans ces expériences, les surfaces verticales à l'intérieur des blocs cathodiques sont protégées par quatre plaques en alumine. Après la durée d'électrolyse, le système se refroidit à la température de la pièce et la cellule est mise dans une boîte à gants sous atmosphère d'argon pour empêcher l'oxydation.

Tableau 3-1. Propriétés des blocs cathodiques

Propriété	Nuance de bloc cathodique				
	A	B	C	D	E
Conductivité thermique (W/m.K)	125* 112**	130* 115**	145* 135**	130* 105**	130* 105**
Résistivité électrique (μΩ.m)	12.0	10.5* 11.5**	8.0* 9.0**	10.5* 13.0**	10.5* 13.0**
Porosité ouverte (%)	18	14	15	20	14
Perméabilité à l'air (nPerm)	8	7	3	6	5

* : horizontale; ** : verticale

3.2.2 L'impact des paramètres d'opération

L'objectif de cette section du projet est de trouver le paramètre le plus important entre les trois facteurs, à savoir la température d'opération, la chimie du bain (CR) et la nuance de bloc cathodique. Un plan factoriel complet, ayant trois variables (chacune disposant de deux niveaux), est mis en œuvre, tel que présenté dans le Tableau 3-2. Grâce à un tel plan d'expériences, on peut déterminer les trois effets principaux ainsi que leurs interactions. Dans ces expériences, les surfaces verticales à l'intérieur des blocs cathodiques sont protégées par quatre plaques de carbure de silicium[1]. Ayant les mêmes intensités de courant électrique (73 A), on utilise 1000 g de bain (4 % (massique) d'alumine et 5 % (massique) de fluorure de calcium) avec deux CRs différents selon le Tableau 3-2. La durée des essais dans cette campagne d'expériences est déterminée par le début de l'effet d'anode (c'est-à-dire, l'essor soudain du voltage vers 10 V). Pendant les expériences, des échantillons de bain sont prélevés en utilisant un doigt froid.

3.3 Autopsies et méthodes d'analyse

Tout d'abord, après que les blocs sont refroidis à la température de la pièce, les plaques en Inconel™ sont enlevées. Ensuite, les blocs sont coupés au moyen d'une lame au diamant. Il existe deux façons de couper les blocs. La première présentée à la Figure 3-5, est mise en œuvre

[1] Saint-Gobain, ADVANCER® CN-703

quand on étudie l'impact de la nuance de bloc cathodique (section 3.2.1). Dans ce type d'autopsie, la cellule est coupée à travers les plaques en alumine et le métal d'aluminium afin d'observer l'interface carbone-aluminium moyennant le microscope optique (la Figure 3-5a). Après l'observation optique, des échantillons sont coupés de la surface du bloc afin qu'on puisse les analyser par microscopie électronique à balayage couplée à la spectroscopie par dispersion d'énergie (la Figure 3-5b). La deuxième, illustrée à la Figure 3-6, est mise en œuvre lorsque l'on étudie l'impact des paramètres d'opération (section 3.2.2). Étant donné la difficulté à couper des plaques de carbure de silicium, à cause de ses résistances mécaniques, les parois verticales des blocs cathodiques sont coupées, ce qui permet une séparation facile entre la partie inférieure du bloc cathodique et la nappe d'aluminium.

Tableau 3-2. Conditions expérimentales d'après le plan factoriel complet

Test-ID	Température d'opération moyenne (°C)	CR initial	Nuance de bloc cathodique
B-940-22	940	2.2	B
D-960-22	960	2.2	D
B-960-38	960	3.8	B
D-960-38	960	3.8	D
D-940-38	940	3.8	D
B-940-38	940	3.8	B
D-940-22	940	2.2	D
B-960-22	960	2.2	B

Après avoir séparé la nappe d'aluminium et la partie inférieure du bloc cathodique, les dimensions de la boue ont été mesurées selon la Figure 3-7.

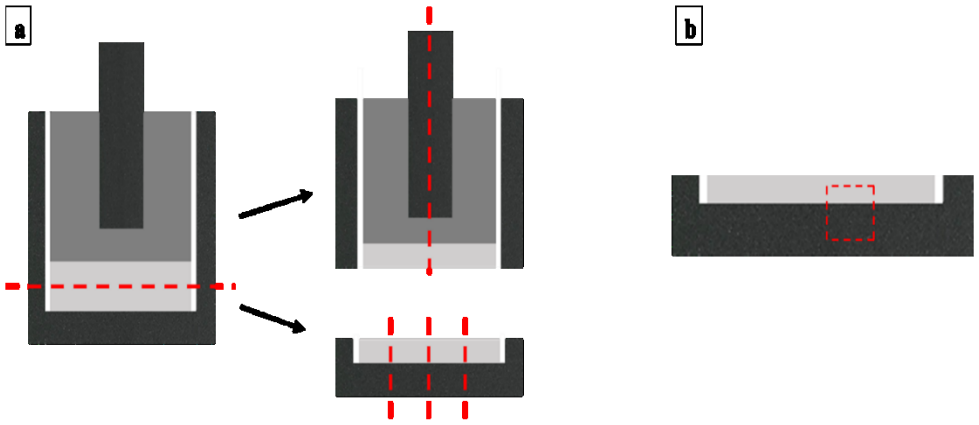

Figure 3-5. Première façon de coupage (lignes pointillées rouges) pour étudier l'impact de la nuance de bloc cathodique afin d'observer l'interface carbone-aluminium a) au microscope optique et b) au microscope électronique. [Landry et coll., 2019]

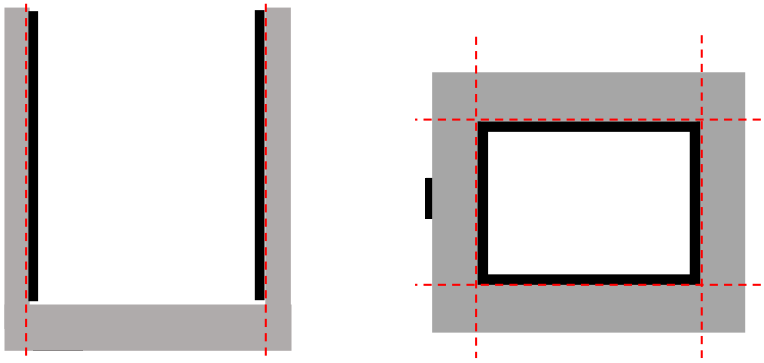

Figure 3-6. Deuxième façon de coupage (lignes pointillées rouges) pour étudier l'impact des paramètres d'opération; à gauche : vue de côté et à droite : vue de haut; les plaques de carbure de silicium sont illustrées en noir.

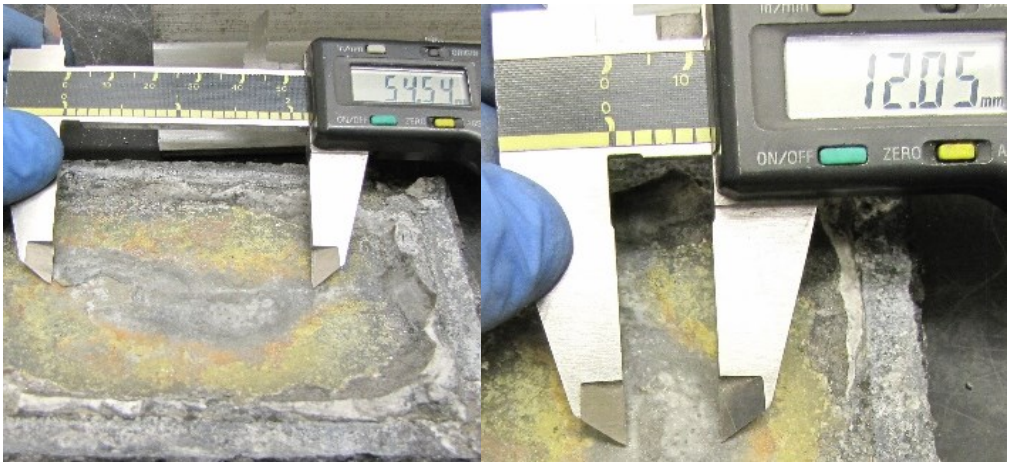

Figure 3-7. Mesure des dimensions d'une boue typique; toutes les dimensions sont en mm.

3.3.1 Microscopie optique

Les premières observations de l'interface carbone-aluminium ainsi que la photographie correspondante se font respectivement moyennant le stéréomicroscope Leica© MZ FLIII et la caméra numérique Leica© DC300. Le microscope ayant un grossissement de 8x à 100x possède une résolution maximale de 3,15 mégapixels. Une vue panoramique faite avec les photos numériques prises est utilisée pour distinguer l'interface carbone-aluminium.

3.3.2 Diffractométrie de rayons X (DRX), Fluorescence des rayons X (FRX)

Après avoir prélevé des échantillons de bain, ceux-ci sont concassés et transformés en poudre dans un broyeur à billes. Les échantillons sont tassés et chargés dans un porte-échantillons rotatif à 1 s^{-1}. L'analyse DRX est effectuée avec un diffractomètre X'Pert PRO MPD ayant un détecteur PIXcel^{1D} muni d'un filtre de nickel. La teneur de calcium totale est mesurée avec un détecteur XRF Potflux Channel (Figure 3-8). Une fente divergente de 1/4°, une fente convergente de 1/2°, un masque de 20 mm et une fente d'antidispersion de 7,5 mm dirigent le faisceau vers l'échantillon et vers le détecteur. Le voltage et l'intensité du générateur sont 40 kV et 40 mA.

La méthode Rietveld a été ensuite utilisée afin de quantifier les phases cristallines présentes dans les échantillons analysés par DRX [Feret, 2008]. Cette méthode peut quantifier: cryolite (Na_3AlF_6), chiolite ($Na_5Al_3F_{14}$), cryolites de calcium (dont $Na_2Ca_3Al_2F_{14}$, $NaCaAlF_6$, $Na_4Ca_4Al_7F_{33}$), fluorure de calcium (CaF_2), fluorure de sodium (NaF), fluorure d'aluminium (AlF_3), différentes phases d'alumine (dont α, γ, δ, θ, β), carbure d'aluminium (Al_4C_3), aluminium et carbone. L'identification de ces phases sert principalement à déterminer le ratio de cryolite (CR), en utilisant un bilan purement stœchiométrique, ce qui détermine l'acidité et la conduite thermochimique du bain cryolitique [Allard et coll., 2014b; 2015].

Pour la détection du calcium, avant chaque campagne d'analyse, 7 standards de calibrage[1] fournis par RioTinto, ont été analysés par le diffractomètre. Après le calibrage du détecteur XRF Potflux Channel, des échantillons ont été analysés.

[1] http://www.lgcstandards.com/FO/en/ARMI/Rio_Tinto_Alcan_CRMS_and_Non-Metalic_Standards

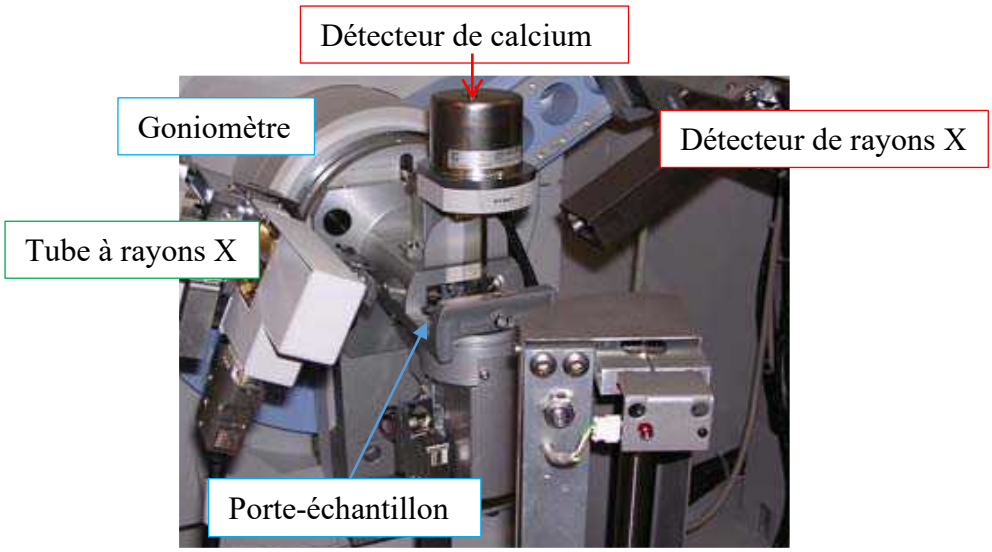

Figure 3-8. Configuration du diffractomètre et du détecteur XRF; adaptée de Feret [2008]

3.3.3 Microscopie électronique à balayage et spectroscopie par dispersion d'énergie

Le microscope Hitachi© modèle S-4700 et le module SDE Oxford Instruments modèle X-Max 50 mm^2 ont été utilisés dans ce projet. L'analyse est faite sous vide avec une tension d'accélération et une intensité du rayon respectivement de 20 kV et de 10 µA. Les éléments cartographiés sont principalement F, C, Al, Na, O et Ca. Des photos prises dans des régions possédant un certain intérêt (e.g. couche de bain, érosion, etc.) sont ensuite traitées avec le logiciel INCA[1](*Integrated Calibration and Application Tool*) afin de différencier les diverses phases présentes grâce à un code de couleur de manière à rendre visibles certains dépôts.

3.3.4 Analyse élémentaire de l'oxygène

La teneur en alumine a été obtenue par un TCH-600 (LECO). Des échantillons ont été analysés en cinq exemplaires avec des capsules en étain et des paniers de nickel. La moyenne de l'écart type des exemplaires était de 0,1%.

3.4 Calculs thermodynamiques

Le comportement des phases en équilibre et des propriétés thermophysiques du bain (c'est-à-dire la viscosité, la densité, la conductivité thermique, la capacité thermique spécifique et la conductivité électrique) ont été calculées à l'aide du logiciel FactSage (version 7.3). La base de

[1] https://www.etas.com/en/products/inca.php

données FThall a été utilisée pour modéliser le système NaF-AlF_3-CaF_2-Al_2O_3. Les équilibres de phase au sein d'une cellule d'électrolyse ont été calculés à la pression atmosphérique en sélectionnant FThall-BathA (l'électrolyte tenant compte des métaux dissous) et FThall-CryH (la cryolite non stœchiométrique à haute température).

CHAPITRE 4 IMPACT DE LA NUANCE DE CATHODE SUR LA FORMATION DE CARBURES

4.1 Avant-propos

Auteurs et affiliations :

Jean-René Landry : étudiant à la maîtrise, Département de génie chimique et génie biotechnologique, Université de Sherbrooke, Québec, Canada.

Mojtaba Fallah Fini : étudiant au doctorat, Département de génie chimique et génie biotechnologique, Université de Sherbrooke, Québec, Canada.

Gervais Soucy : professeur titulaire, Département de génie chimique et génie biotechnologique, Université de Sherbrooke, Québec, Canada.

Martin Désilets : professeur titulaire, Département de génie chimique et génie biotechnologique, Université de Sherbrooke, Québec, Canada.

Patrick Pelletier : scientifique de recherche brasquage, Solutions Technologiques Aluminium – CRDA, Rio Tinto, Québec, Canada.

Loig Rivoaland : responsable de projets transverses, Carbone Savoie, Vénissieux, France.

Didier Lombard : champion innovation & consultant matériaux / brasquage, Solutions Technologiques Aluminium – LRF, Rio Tinto, Saint Jean de Maurienne, France.

État de l'acceptation : Version finale publiée.

Revue : *The Minerals, Metals and Materials Society, Light Metals Division*

Référence : Landry et coll. [2018]

Lien d'accès : https://www.doi.org/10.1007/978-3-319-72284-9_161

Contributions à la thèse :

Étant donné l'interaction entre la boue et la couche de carbures au fond de la cellule, cet article de conférence se concentre sur les mesures effectuées au microscope optique et électronique de la boue et de la couche de carbures. En effet, la dissolution des carbures dans les boues et les réactions correspondantes qui changent les propriétés des boues; il faut donc étudier les comportements des blocs cathodiques concernant la formation des couches de carbures. Les résultats correspondants servent pour expliquer la tendance différente, par rapport à la formation ou la dissolution de boue, entre les nuances de cathode qui sont étudiées au Chapitre 5 et au Chapitre 6.

Contributions des auteurs[1, 2]:

Jean-René Landry : analyse formelle (50%), conceptualisation (50%), investigation (50%), méthodologie (50%), rédaction du premier brouillon (100%), révision (100%), validation (50%), visualization (100%); total (60%)

Mojtaba Fallah Fini : analyse formelle (50%), conceptualisation (50%), investigation (50%), méthodologie (50%), revue (100%), validation (50%); total (40%)

Gervais Soucy : ressources, revue, révision, surveillance, administration de projet, acquisition de financement

Martin Désilets : revue, révision, surveillance

Didier Lombard : ressources, revue, révision

Patrick Pelletier : ressources, revue, révision

Loig Rivoaland : ressources, revue, révision

Titre français :

Étude en laboratoire de l'impact de la nuance de cathode sur la formation de dépôts à la surface de la cathode des cellules Hall-Héroult

[1] Pourcentage approximatif just entre les premiers deux auteurs
[2] Trouver lexique des rôles des auteurs à la page xi.

Résumé :

Une étude concernant l'effet de la nuance de bloc cathodique sur la formation de dépôts à l'interface carbone-aluminium des cellules Hall-Héroult est effectuée, utilisant différentes nuances de cathode industrielle à l'échelle de banc d'essai, ayant les conditions d'opération suivantes : densité de courant de 0.9 A/cm^2, atmosphère inerte d'azote à 960 °C, durée d'électrolyse de 8 heures, teneur initiale en alumine du bain de 10 % (massique), ratio de cryolite initial du bain de 2,2, et enfin teneur initiale en CaF_2 du bain de 5 % (massique). Les analyses suivantes sont réalisées : la diffraction des rayons X sur les échantillons de pied de talus, de talus, de boue et de bain en plus de la microscopie électronique à balayage avec analyse dispersive en énergie et la microscopie optique de l'interface carbone-aluminium. Les premiers résultats font allusion au fait que l'épaisseur de la couche de carbures d'aluminium augmente à mesure que la porosité du matériau cathodique devient plus élevée.

4.2 Laboratory Study of the Impact of the Cathode Grade on the Formation of Deposits on the Cathode Surface in Hall-Héroult Cells

Keywords: Cathode grade; carbon-aluminum interface; aluminum carbide; sludge; graphitized; impregnated graphite

4.2.1 Abstract

This experimental study investigates the effect of the cathode grade on the formation of deposits at the carbon aluminum interface in Hall-Héroult electrolysis cells. Five different industrial cathode grades are tested on a bench scale aluminum electrolysis set-up with the following operational parameters: cathodic current density of 0.9 A/cm^2, under a nitrogen atmosphere at 960 °C for 8 hours with initial bath composition of 9 wt% alumina, cryolite ratio of 2.18 and 5% CaF_2. Postmortem analyses include X-ray diffraction on the ledge toe, ledge, sludge and bath samples as well as scanning electron microscopy and optical microscopy of the carbon aluminum interface. Early results suggest that the thickness of the aluminum carbide layer increases with the porosity of the carbon material.

4.2.2 Introduction

The formation of deposits on the surface of the cathode in Hall-Héroult cells is a phenomenon that disturbs the electrical current paths and accelerates the cathode wear [Keller, 2005; Geay et coll., 2013]. Nowadays, for high amperage cells, industrials are leaning towards graphitized types of cathode blocks because of their higher thermal conductivity and low electrical resistivity compared to semi-graphitic or graphitic types of cathode [Sørlie et Øye, 2010]. Although the physical properties have improved, the formation of deposits on the cathode surface is still an ongoing problem at the industrial level. Investigations on this problem often focus on the operating conditions of the cell and little on the equipment type such as cathode grade. Industrials have reported different behaviors among graphitized cathode types regarding deposit formation. This may be attributed to the differences in properties such as porosity, permeability or density. These differences may induce various behaviors in the electrolyte, thus potentially affecting the formation of deposits [Novak et coll., 2012]. Distinct types of deposits at the carbon-aluminum interface were observed:

(a) The formation of a layer of aluminum carbide (Al_4C_3) infiltrated in the carbon block has been established [Coulombe et coll., 2016]. Moreover, it is stipulated that the combined formation and dissolution of this layer wear off the carbon surface of the block and that the use of graphitized blocks results in a higher wear of the cathodic carbon block [Tschöpe et coll., 2013]. Aluminum carbides are formed by the contact of the metal with the carbon interface (reaction 4-1) or by the interaction of carbon with the intercalated bath components according to reaction 4-2 and reaction 4-3 [Zoukel et coll., 2009]. The subsequent dissolution of aluminum carbides is described by reaction 4-4.

$$Al_{(l)} + C_{(s)} \rightarrow Al_4C_{3\,(s,diss)} \qquad 4\text{-}1$$

$$8Al_2O_{3\,(s)} + 12Na_{(in\,C)} + 3C_{(s)} \rightarrow Al_4C_{3\,(s)} + 12NaAlO_{2\,(s)} \qquad 4\text{-}2$$

$$3C + 4AlF_{3\,(diss)} + 12e^- \rightarrow Al_4C_{3\,(s,diss)} + 12F^-_{(diss)} \qquad 4\text{-}3$$

$$Al_4C_{3\,(s)} + 5AlF_{3\,(diss)} + 9NaF_{(l)} \rightarrow 3Na_3Al_3CF_{8\,(diss)} \qquad 4\text{-}4$$

(b) In addition, the presence of sludge in the center of aluminum reduction cells is often found under alumina point feeders. It is often said to be caused by the cover material falling during anode changes. It is also thought to be attributed to an incomplete dissolution of alumina, leading to agglomerates, which may carry bath components through the metal pad down to the carbon interface [Keller, 2005; Dassylva-Raymond et coll., 2014]. Aluminum carbides may dissolve in the sludge found under the aluminum [James et coll., 1995].

(c) Furthermore, the heat losses through sidewalls and bottom of the cell may cause the side ledge to grow at the carbon-aluminum interface [Allard et coll., 2014b]. The impact of all these phenomena is the enhanced erosion of the block at the tip of the frozen ledge and disturbed current paths [Siew et coll., 2005; Einarsrud et coll., 2016], with an increase in cathode voltage drop.

The formation of these deposits is certainly affected by the cathode block properties. This experimental study will investigate the role of the cathode grade by making further links between specific properties of the block and the formation of deposits.

4.2.3 Methodology

Experimental set-up

Aluminum electrolysis tests are done using five industrial cathode grades (A, B, C, D and E) provided by a specialized Hall-Héroult cathode producer. Grades A to D are graphitized block grades and E is impregnated graphite (block graphitized then impregnated with pitch and rebaked). The properties of these grades are listed in Table 4-1.

Table 4-1. Cathode block properties at room temperature (*: horizontal; **: vertical)

Properties	A	B	C	D	E
Thermal conductivity (W/m.K)	125* 112**	130* 115**	120	135* 105**	130* 105**
Open porosity (%)	18	14	15	20	14
Air permeability	8	7	3	6	5

The propensity to form sludge by grade reported in industry is D = E > A > B > C, D and E being the grades that equally form the most sludge. This study aims to evaluate the behavior of the experimental cells for comparison with the real-life behavior reported.

Experimental rectangular blocks of the five grades have been machined for laboratory electrolysis tests. All dimensions of the cell components are shown in Figure 4-1.

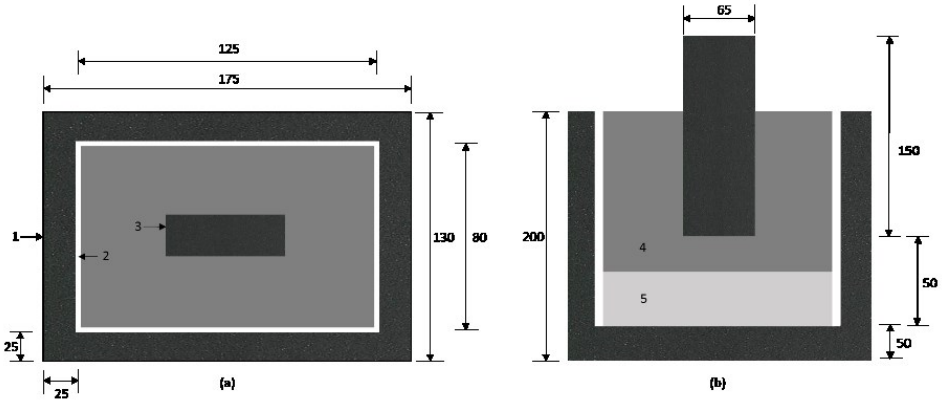

Figure 4-1. Sizing of experimental Hall-Héroult cells for this study, top view (a) and side view (b). All dimensions are in millimeters. 1: carbon crucible, 2: alumina plates, 3: anode, 4: bath, 5: aluminum pad

The cell is filled with 1700 g of industrial bath initially containing 9 wt% alumina with a cryolite ratio (CR) of 2.18. A block of approximately 500 g of aluminum is placed at the bottom of the cell prior to the electrolysis and 5 mm thick alumina plates cover all vertical walls of the carbon block to limit bath infiltration. The cell is positioned inside a crucible made of Inconel placed inside an oven. The temperature is measured in three locations: inside the bath, in the carbon side wall and outside the cell.

The electrolysis tests are done at a bath temperature of 960 °C, a current density of 0.9 A/cm^2 for 8 h under a N_2 atmosphere. The anode to cathode distance is set to 2 cm. In order to highlight the impact of the cathode grade, no feeding is used, and all parameters are kept constant during the cell operation for all cathode grades.

Autopsies and characterization

At the end of the electrolysis time, the electricity is cut off and the furnace is set to room temperature for cooling. In order to observe the deposits at the carbon-aluminum interface, the cooled cell is cut using a diamond blade saw. Cuts are made in the center of the cell and in the periphery. Each section of the carbon-aluminum interface is observed with a stereomicroscope. Pictures are taken to recreate panoramic views of the interface. For composition, harvested samples are powdered using a ball mill then put in the rotating sample holder of the X-ray diffraction (XRD). The chemical composition is provided by the Rietveld analysis of the sample. Scanning electron microscopy-energy dispersive spectroscopy (SEM-EDS) was used for surface analysis and elemental cartography. This method of analysis allows observation and easy measurements of the aluminum carbide layer in the carbon block.

4.2.4 Results

Aluminum carbide observation

Scanning electron microscopy was used to observe the carbon-aluminum interface. For each site of interest, the elemental cartography included mapping of carbon, aluminum, oxygen, fluoride, calcium and sodium. Figure 4-2 shows the observable carbide layer.

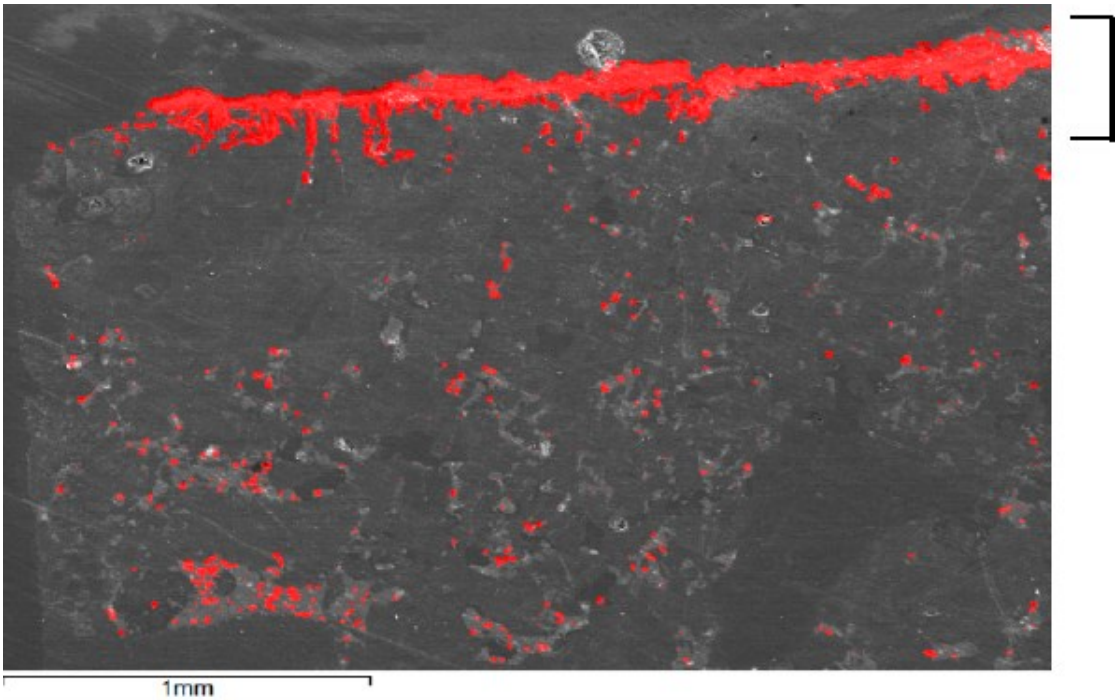

Figure 4-2. Scanning electron microscopy of the carbon-aluminum interface of experimental cell E (impregnated graphite). The position of the aluminum carbide layer is shown by the bracket symbol.

A noticeable distinct red layer containing atoms of aluminum was visible at the interface for every sample taken. The values of the measured thickness of the carbide layer for each cathode grade are summarized in Table 4-2. The following data were obtained by averaging all direct measurements of the layer. The samples were taken under the sludge, under the ledge toe and in the "cleaner" areas in between (direct contact of aluminum and carbon).

Table 4-2. Average aluminum carbide layer thickness is ± 4 μm. The average data for two tests of each grade is displayed.

Cathode type	Graphitized				Impregnated graphite
Cathode grade	A	B	C	D	E
Carbide layer thickness (μm)	54 | 55	65 | 66	41 | 48	89 | 96	65 | 72

The impregnated graphite grade had the sharpest and most distinct layer of aluminum carbide. Other graphitized grades had a dispersed carbide layer.

Ledge and sludge observations

Microscopic observations revealed the presence of sludge accumulated near the center of the carbon-aluminum interface under the anode tip. Typical profiles of sludge are exhibited in Figure 4-3.

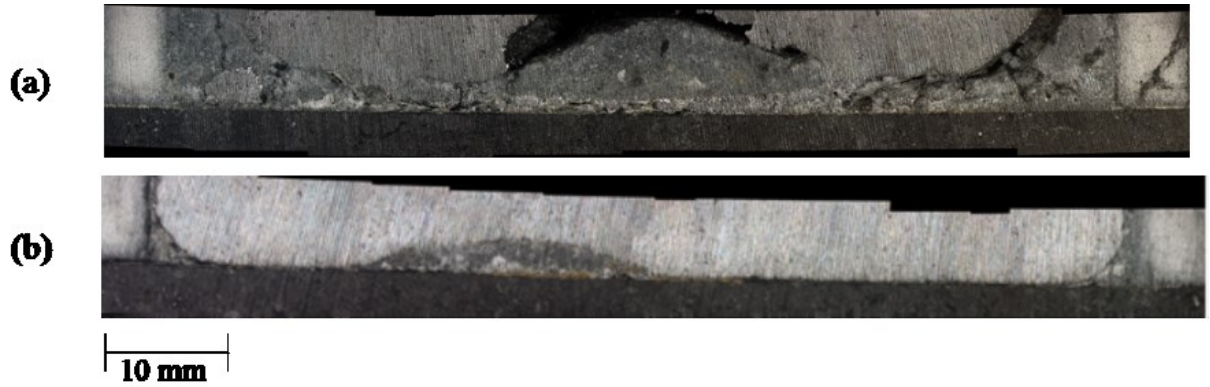

Figure 4-3. Sludge profiles for graphitized grade A (a), impregnated graphite grade E (b)

All grades displayed a central deposit of sludge. As indicated in Table 4-3, graphitized grade A had the thickest central sludge with a thick bath film covering the carbon-aluminum interface and thicker ledge. The experimental cell of grade A had the thicker layer of sludge and the four other grades showed thinner layer than grade A. At this stage, it is difficult to conclude a sludge propensity trend among the other grades. For each experiment, the central deposit was harvested along with a ledge toe sample from the same cell. The CR and alumina content of these samples are also summarized in Table 4-3.

Table 4-3. CR, total alumina content and height of ledge toe and central sludge deposits from XRD analysis

	Ledge toe		Central sludge		
	CR	Total Al_2O_3 (wt%)	CR	Total Al_2O_3 (wt%)	Height (± 0.5 mm)
A (graphitized)	2.87	25.0	2.09	10.2	8.1
B (graphitized)	2.87	23.3	2.92	9.8	3.4
C (graphitized)	2.73	27.4	2.95	11.4	4.7
D (graphitized)	2.85	21.4	2.79	13.5	3.2
E (imp. graphite)	2.12	28.8	2.08	19.1	5.1

4.2.5 Discussion

Aluminum carbide layer – effect of porosity

The data for the thickness of the aluminum carbide layer has been plotted in Figure 4-4.

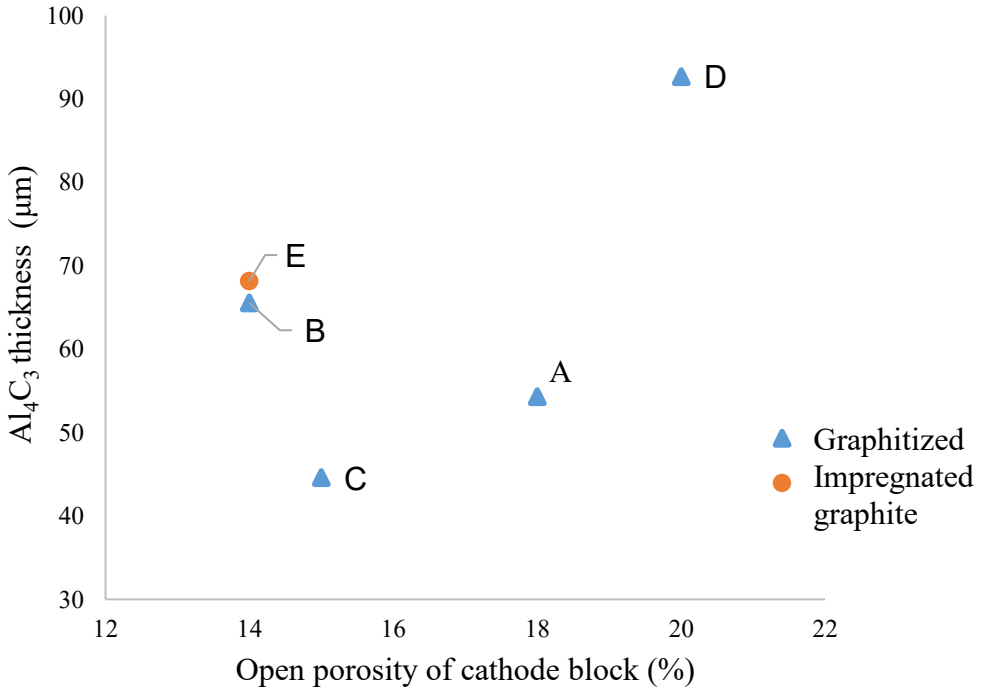

Figure 4-4. Thickness of the aluminum carbide layer at the carbon-aluminum interface of the five experimental cells (triangles: graphitized blocks; circle: impregnated graphite).

Measurements for graphitized cathode blocks A, C and D show a trend between the block's open porosity and the thickness of the aluminum carbide layer at the carbon-metal interface. The thicker layer of B may be explained by its permeability that is roughly 60 % higher than the one of grade C, thus allowing more bath species to infiltrate and further react according to reaction 4-2. In this way, the thickness of the aluminum carbide layer may be affected by the combination of both open porosity and air permeability of the cathode block. This is shown with the case of grades B and E that have similar porosity, permeability and carbide thickness. The high amount of sludge in grade A may explain the thinner than expected carbide layer. This could be attributed to a combination of two phenomena. The high presence of sludge reduces carbides formed by reaction 4-1. Moreover, sludge areas, corresponding to lower current density, lessens sodium intercalation and carbides formed by reaction 4-2. The second phenomenon being aluminum carbide dissolution in sludge.

Central sludge

The presence of a central sludge deposit at the carbon-aluminum interface was not foreseeable since there was no direct feeding of alumina during all experiments. The absence of point feeding or anode change in this study insinuates that sludge may come from other phenomena.

Considering that the cell dimensions are too short for considerable MHD forces, only the generated gas at the anode tip will agitate the layer of bath and the metal pad. The detachment of metal from the main pad may lead to the access of some bath to the carbon-aluminum interface. A proof of this agitation was obtained by running a test during which the electrolysis was maintained during cooling until the entire system was solid. The agitated metal may also cause the tip of the ledge toe to be dragged towards the center of the carbon-aluminum interface (under the anode), contributing to the accumulation of sludge. In this experimental study, the sludge may well come from the ledge by agitation since Table 4-3 shows that the composition of the sludge and ledge are close. Furthermore, for a grade with thick ledge such as A, there is a film of the bath connecting the central sludge to the ledge toe visible on Figure 4-3 (section a). Its CR and alumina content are respectively 2.49 and 24.3 wt%, very similar to the ledge toe but higher than the sludge (see Table 4-3). The lower alumina content and CR of the central sludge in cell A may be explained by back feeding of alumina into the film and acidification through sodium loses [Whitfield et coll., 2004].

Knowing that the side ledge and ledge toe are formed when their temperatures reached a value below the liquidus of the bath, in that regard the thermal conductivity of the block may affect the extent of the ledge toe elongation, thus the amount of sludge.

4.2.6 Conclusions

Aluminum carbide behavior

The higher porosity of graphite deepens the reacting zone of infiltrated bath components, thus enlarging the apparent thickness of the carbide layer. Furthermore, the permeability of the carbon block may enhance the effect of porosity. On the contrary, the presence of sludge at the carbon-aluminum interface reduces the thickness of the aluminum carbide layer by dissolution of the carbides in the sludge. For graphitized grades, a thinner carbide layer can be obtained with blocks that have a low porosity, a low permeability and a high tendency to form sludge.

Sludge formation

This study has shown that sludge may form even without alumina point feeding or any manipulation with the anode.

The behavior of the five grades was not the same in experimental tests as in industrial cells regarding sludge propensity. The comparison between the laboratory tests with the industrial cell behavior of these grades regarding sludge formation is still under investigation. It may be achieved by further investigating the impact of other operating conditions such as feeding strategy or electrolysis time.

Analyses of sludge deposits suggest that the thermal conductivity of the carbon block may influence the amount of ledge, which can be transported along the carbon-aluminum interface by metal agitation.

CHAPITRE 5 IMPACT DE LA NUANCE DE CATHODE SUR LA FORMATION DE BOUES

5.1 Avant-propos

Auteurs et affiliations :

Jean-René Landry : étudiant à la maîtrise, Département de génie chimique et génie biotechnologique, Université de Sherbrooke, Québec, Canada.

Mojtaba Fallah Fini : étudiant au doctorat, Département de génie chimique et génie biotechnologique, Université de Sherbrooke, Québec, Canada.

Gervais Soucy : professeur titulaire, Département de génie chimique et génie biotechnologique, Université de Sherbrooke, Québec, Canada.

Martin Désilets : professeur titulaire, Département de génie chimique et génie biotechnologique, Université de Sherbrooke, Québec, Canada.

Patrick Pelletier : scientifique de recherche brasquage, Solutions Technologiques Aluminium – CRDA, Rio Tinto, Québec, Canada.

Loig Rivoaland : responsable de projets transverses, Carbone Savoie, Vénissieux, France.

Didier Lombard : champion innovation & consultant matériaux / brasquage, Solutions Technologiques Aluminium – LRF, Rio Tinto, Saint Jean de Maurienne, France.

État de l'acceptation : Version finale publiée.

Revue : *Metallurgical and Materials Transactions B*

Référence : Landry et coll. [2019]

Lien d'accès : https://doi.org/10.1007/s11663-018-1435-0

Contributions à la thèse :

Cet article a pour but de trouver des mécanismes grâce auxquels les propriétés des cathodes affectent la formation ou la dissolution de boues ayant des teneurs en alumine élevées. Parmi les facteurs qui avaient été exhaustivement traitées au Chapitre 2, deux semblent plus susceptibles d'influencer la formation ou la dissolution de boue, à savoir la température d'opération (par exemple l'importance de la conductivité électrique du bloc), et les phénomènes d'interface (par exemple l'importance de la perméabilité du bloc). Une brève section porte sur l'érosion des blocs en faisant un lien avec les mesures de carbures d'aluminium présentées au Chapitre 4.

Contributions des auteurs[1, 2]:

Jean-René Landry : analyse formelle (50%), conceptualisation (50%), investigation (50%), méthodologie (50%), rédaction du premier brouillon (100%), révision (100%), validation (50%), visualization (100%); total (60%)

Mojtaba Fallah Fini : analyse formelle (50%), conceptualisation (50%), investigation (50%), méthodologie (50%), revue (100%), validation (50%); total (40%)

Gervais Soucy : validation, ressources, revue, révision, surveillance, administration de projet, acquisition de financement

Martin Désilets : validation, revue, révision, surveillance.

Didier Lombard : ressources, revue, révision

Patrick Pelletier : ressources, revue, révision

Loig Rivoaland : ressources, revue, révision

Titre français :

Étude expérimentale de la nuance de cathode sur la formation de boues dans les cellules Hall-Héroult

[1] Pourcentage approximatif just entre les premiers deux auteurs
[2] Trouver lexique des rôles des auteurs à la page xi.

Résumé :

L'essor des coûts de production d'aluminium et la chute de durée de vie anticipée des cellules Hall-Héroult sont les deux désavantages de la formation de boue. Les cathodes de nuances graphitisées utilisées dans les cellules modernes permettent d'une part, d'appliquer de forts courants électriques; mais d'autre part, ces derniers entraînent des complications, dont le taux de détérioration cathodique et la production excessive de dépôts. Les nuances graphitisées n'ont pas toutes la même tendance à former des boues et il existe une rareté de données disponibles portant sur l'interaction entre les nuances/propriétés des blocs cathodiques et les boues générées.

Dans cette étude, cinq nuances de blocs cathodiques industriels à l'échelle de banc d'essai sont utilisées en effectuant les tests d'électrolyse, ayant les conditions d'opération suivantes : densité de courant de 0.9 A/cm^2, atmosphère inerte d'azote à 960 °C, durée d'électrolyse de 8 heures, teneur initiale en alumine du bain de 10 % (massique), ratio de cryolite initial du bain de 2,2, et teneur initiale en CaF_2 du bain de 5 % (massique) sans alimentation d'alumine. Les analyses suivantes sont réalisées : l'analyse Rietveld des dépôts, les observations de l'interface carbone-aluminium aux microscopes optique et électronique avec analyse dispersive en énergie.

Des boues distinctes situées au centre des cellules ont été générées. Les profils variables des boues semblent être liés aux conductivités thermiques des blocs cathodiques. Cette étude a essayé d'identifier des mécanismes de la formation de boues, plus précisément, le rôle relatif de la nuance de cathode.

5.2 Experimental Investigation of the Impact of the Cathode Grade on Sludge Formation at the Cathode Block-Aluminum Interface of Hall-Héroult Cells

Keywords: Cathode grade; sludge; carbon-aluminum interface

5.2.1 Abstract

The presence of resistive sludge on the cathode surface in Hall-Héroult cells can increase the aluminum production costs and reduces cell lifetime. Modern cells with graphitized cathode block generally operate satisfactorily but some are exhibiting excessive deposit formation, thus lower performances. Little attention has ever been given to the role of the cathode grade and its properties on sludge formation. In this investigation, five graphitized industrial cathode grades with varying properties are tested on a bench scale aluminum electrolysis set-up with cathodic current density of 0.9 A/cm^2, under a nitrogen atmosphere at 1233 K (960 °C) for 8 hours with initial bath composition of 10 wt% alumina, cryolite ratio of 2.2, 5 wt% CaF_2 and no point feeding. Postmortem characterization includes Rietveld refinement of deposits, optical microscopy and SEM-EDS observations of the carbon-aluminum interface. Sludge located near the center of the cathode surface was generated during the experiments despite the absence of point feeding. The sludge profile was variable among grades and could be related to the thermal conductivities of the blocks. This study has pushed further the understanding of the mechanisms of sludge formation and dissolution concerning the cathode grade properties.

5.2.2 Introduction

The problem concerning sludge

The main drawback of the Hall-Héroult process is its high electrical energy consumption. The formation and accumulation of electrically resistive sludge (aka *muck*) at the cathode block surface increase the electrical resistance of the cell, which boosts cathode voltage drop (CVD). The net effect is the higher energy requirement and thereby, higher aluminum production costs. Due to high electrical resistance of the sludge compared to the metal, the presence of sludge at the carbon-aluminum interface redirects the electrical current and creates high current density spots, prompting cathode block electrochemical wear [Liao et Øye, 2013]. Another consequence of the presence of sludge on the cathode surface is the generation of horizontal currents, which increase metal pad movement [Allard et coll., 2014b]. The increased metal flow and resulting oscillation of the bath-metal interface greatly contribute to difficulty in reducing the ACD and

increases aluminum solubility, prompting current efficiency losses [Grjotheim et Kvande, 1993; Song et coll., 2017a]. The control over the formation of sludge in Hall-Héroult cells is a key factor in avoiding high CVD, current efficiency losses and excessive cathode wear.

Description of deposits

During the regular operation of a typical alumina reduction cell there is a variety of inevitable deposits that form within the process through time.

Figure 5-1 displays the deposits that occur in modern point feeding cells.

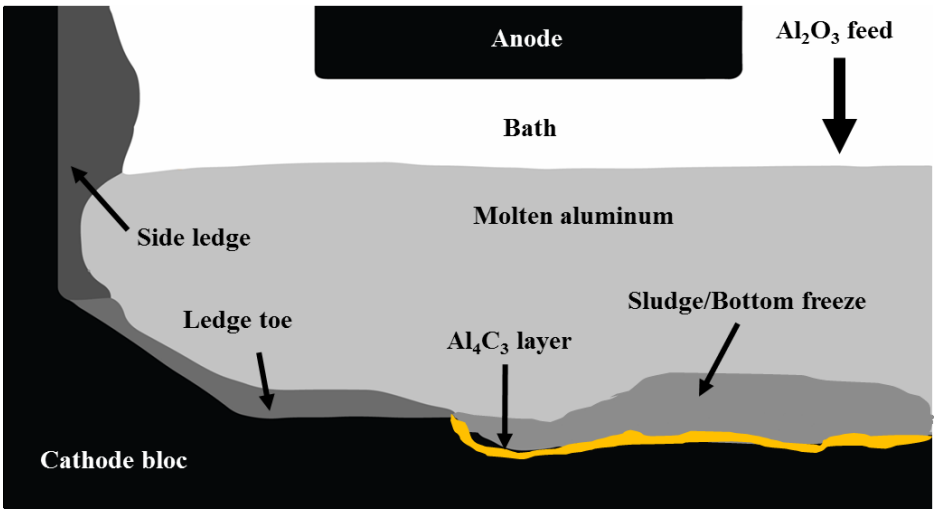

Figure 5-1. Deposits at the carbon-metal interface of Hall-Héroult cells

The protective side ledge is necessary in order to avoid molten metal and electrolyte attacks and infiltration in the sidewall that cause premature cell failures[Sørlie et Øye, 2010]. Ideally, this frozen layer of bath should cover the entire surface of the side lining. The ledge toe is a horizontal elongation of the side ledge formed on the cathode surface. In alumina point feeding cells, sludge mainly originates from alumina incomplete dissolution, collapse of top crust, anode change or failure in the heat balance of the cell [Utigard et Toguri, 1991]. A typical sludge is a mixture of undissolved solid alumina particles and saturated bath with density around 2400 kg/m^3, 20 - 50 wt% alumina, 2 – 10 wt% AlF_3 and 2 – 5 wt% CaF_2 [Grjotheim et Kvande, 1993; Allard et coll., 2015]. Bottom crust is caused by the complete solidification of sludge when its temperature reaches below the eutectic point of the sludge [Geay et coll., 2013]. According to Fallah Fini et coll. [2017], the most important factors that influence the sludge formation or dissolution are cell's hydrodynamics, operational temperature, electrolyte

chemistry, physicochemical properties of alumina and alumina feeding techniques. It must be underlined that sludge formation and solidification can be effectively reduced by keeping an appropriate superheat in the bath with respect to the acidity and alumina concentration in the cell.

Sludge back feeding mechanisms

Once sludge is formed at the cathode surface, several mechanisms are stipulated to contribute to its back feeding into the bulk. The presence of a bath film between the carbon block and the metal was said to be related to sludge formation and dissolution [Li et coll., 2015]. It was argued that sludge may be back fed through such a film wherein fluid flow is induced by interfacial tensions (IFT) differences [Utigard et Toguri, 1991; Utigard, 1999]. The bath film may also dissolve aluminum carbides formed at the carbon-aluminum interface, leading to net carbon losses of the block and cathode bottom wear [Zoukel et coll., 2009; Novak et coll., 2012; Liao et Øye, 2016]. A layer containing such aluminum carbides at the cathode block-aluminum interface was observed in both industrial and laboratory cells [Coulombe et coll., 2016; Novak et coll., 2018]. However, hardly any laboratory study has explicitly shown signs of erosion visibly related to aluminum carbide formation and dissolution. Sludge may also be back fed into the bulk by the means of hydrodynamics. Accordingly, sludge could be dragged along the cathode surface by saltation caused by the moving metal and eventually be transported through the metal and dissolve in the bulk [Kalgraf et Torklep, 1998].

Cathode grades in modern Hall-Héroult cells

The cathode material is of great importance, as it must endure several electrical, thermal and chemical phenomena during the lifetime of the cell. The optimal criteria for cathode lining material are: chemical inertness, low permeability towards the environment, sufficient thermal and mechanical strength, ability to distribute current evenly, allow low CVD, controlled heat losses and lowest possible cost [Grjotheim et Kvande, 1993]. Carbon in the allotropic form of graphite is the material that fulfills most of the latter requirements. With desired increased productivity, graphitized types of cathode blocks are attractive because of their higher thermal conductivity and lower electrical resistivity [Tschöpe et coll., 2012; Wang et coll., 2016]. However, graphitized cathode blocks in modern cells show higher wear rates because of increased amperage which has recently been correlated with high local current density and wear areas [Dreyfus et Joncourt, 1999; Skybakmoen et coll., 2011; Tschöpe et coll., 2013]. Cells with

graphitized cathode blocks of high thermal conductivity are more prone to bottom freeze, which increases the CVD [Rivoaland, 2016]. The thermal conductivity of the cathode block is also of major importance regarding the heat balance and the control of the thickness of the ledge and sludge formation. Controlled heat losses may also help to keep appropriate superheat, which disfavors sludge formation.

The impact of the cathode grade on sludge formation has not explicitly been investigated in literature. In fact, the industry has reported that distinctive cathode grades have shown variable propensities to form sludge. This experimental study will help to better understand the sludge formation phenomenon and to make further links between the graphitized cathode grade and the formation of deposits at the carbon-aluminum interface.

5.2.3 Methodology

Experimental set-up

Laboratory aluminum electrolysis tests were conducted using five industrial cathode grades (A, B, C, D and E) provided by a Hall-Héroult cathode producer. The grades A to D are graphitized and the grade E is impregnated graphite (i.e. graphitized then impregnated with pitch and rebaked). The properties of these grades were provided by the supplier and are listed in Table 5-1.

Table 5-1. Cathode block properties at room temperature (*: horizontal; **: vertical)

Properties	A	B	C	D	E
Thermal conductivity (W/m.K)	125*	130*	145*	130*	130*
	112**	115**	135**	105**	105**
Electrical resistivity (μΩ.m)	12.0	10.5*	8.0*	10.5*	10.5*
		11.5**	9.0**	13.0**	13.0**
Open porosity (%)	18	14	15	20	14
Air permeability (nPerm)	8	7	3	6	5

From experience with these types of blocks, the industry has noticed that the sludge formation tendency differed typically from one grade to another. The sludge formation tendency of cathode grades, that was observed and reported by the industry, is D = E > A > B > C; D and E being the grades that forms the most sludge. This study aims to evaluate the behavior of the

different grades of block in the experimental cells for comparison with the real-life behavior reported. Experimental rectangular blocks of the five grades have been machined for laboratory electrolysis tests. All dimensions of the cell components are shown in Figure 5-2.

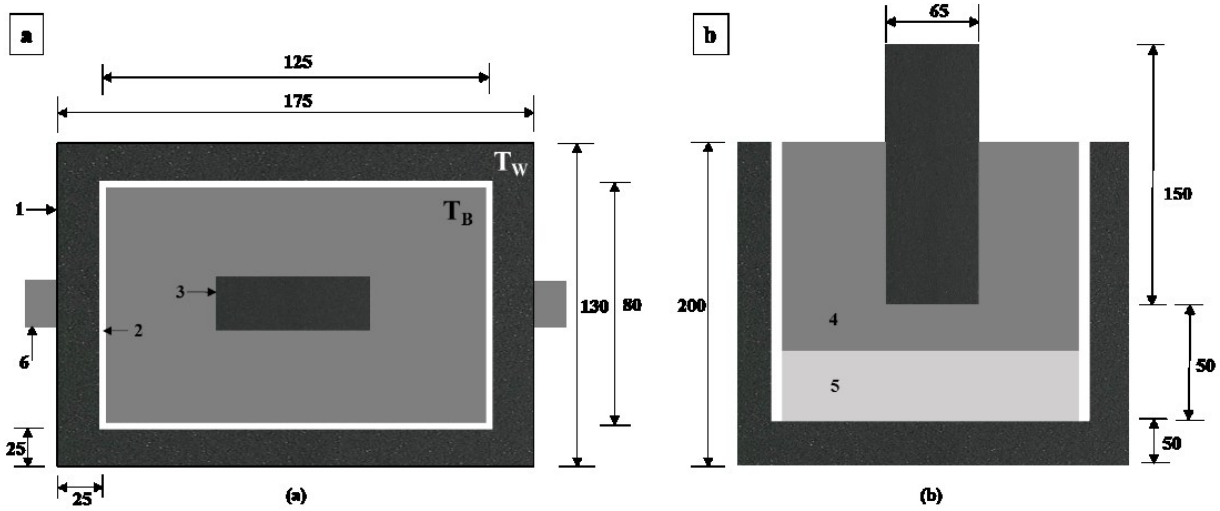

Figure 5-2. Sizing of experimental Hall-Héroult cells for this study, top view (a) and side view (b). All dimensions are in millimeters (mm). 1: carbon crucible, 2: alumina plates, 3: anode, 4: bath, 5: aluminum, 6: bus bar. T_W and T_B refer respectively to the positions of the thermocouples in the sidewall and in the bath

Alumina plates of 5 mm thickness are positioned on each cathode sidewall so that the current passes through the bottom. A plate of approximately 500 g of aluminum is placed at the bottom of the cell. The cell is then filled with 1700 g of industrial bath initially containing 10 wt% alumina with a cryolite ratio (CR) of 2.2. The anode is centered as the cryolite is being compacted in the cell. The cell is positioned inside a crucible made of Inconel placed inside a furnace. The temperature is measured in three locations: inside the bath, in the carbon sidewall and inside the crucible. The thermocouples are placed inside alumina sleeves in order to protect them from bath corrosion and to prevent short-circuiting the system. The bath thermocouple is left inside the bath until the electrolysis is stopped.

The electrolysis tests are done at a 0.9 A/cm^2 current density for 8 h under a N_2 atmosphere with a 2 cm ACD. The current is set to 73 A and is kept constant. The temperature and voltage are measured continuously during electrolysis. The bath is preheated between 1233 K and 1273 K (960 °C and 1000 °C) then the temperature is stabilized at 1233 K (960 °C) before the start of electrolysis. In order to highlight the impact of the cathode grade, no point feeding is used, and all parameters are kept constant during the cell operation for all cathode grades. At the end of

the electrolysis time, the electricity is cut off and the furnace is set to room temperature for cooling under nitrogen atmosphere. The time for the cell to reach room temperature is close to 30 hours in every case.

Autopsies

During its characterization, the cell is stored under argon atmosphere to avoid any oxidation reaction. In order to observe the deposits at the carbon-aluminum interface, the cell is cut using a diamond blade saw, as illustrated in Figure 5-3.

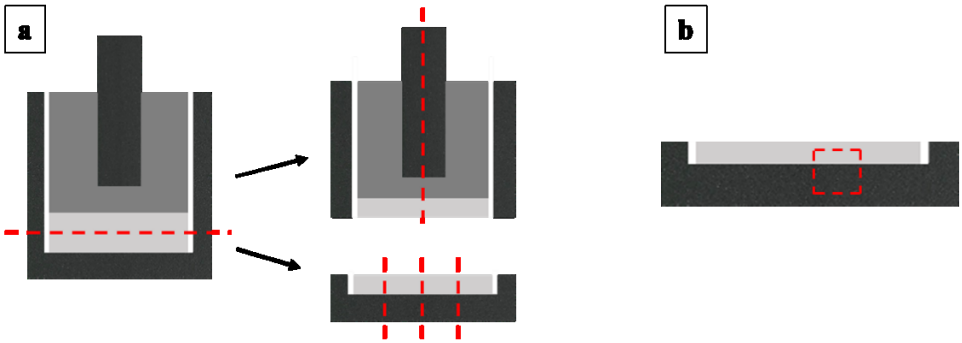

Figure 5-3. Positions of cuts for deposit observation (red dashed lines); a) cuts of the cell and cathode surface for microscopic sludge observations; b) cutting for SEM observations of the carbon-aluminum interface

The cathode surface is separated by first cutting through the metal pad. The top of the cell is cut in two in the middle of the anode and the cell bottom part is cut in three positions as shown in Figure 5-3 (section a). After microscopic observations of the obtained slices of the cathode floor, cubes of the carbon-aluminum interface are carved with a diamond blade as shown in Figure 5-3 (section b).

Optical microscopy

Microscopic observations of the carbon-aluminum interface are done with a stereomicroscope Leica MZ FLIII. Panoramic views of the interface are made in order to obtain size and position of deposits. The microscopic observation of the carbon-aluminum interface allows to measure the size of sludge, the extent of the ledge toe and the existence of erosion marks, if any.

X-ray diffraction (XRD) and quantification of chemical composition

For the top part of the cathode block, samples are harvested from various regions of the bulk for chemical composition quantification. All deposits found at the bottom part of the block are

harvested for quantification (sludge, ledge toe). The harvested samples are powdered using a ball mill, back loaded as pressed powder in a cavity and analyzed by XRD. The equipment used for XRD is a PANalytical X'Pert PRO MPD diffractometer and a PIXcel^{1D} detector with a nickel filter. An XRF Potflux Channel was used to determine the total calcium content of samples. The quantitative analysis of each sample is obtained by the Rietveld refinement [Feret, 2008]. The CR based on stoichiometry (moles of NaF/moles of AlF_3) calculation is similar to the one used in previous studies on sludge formation as described by Allard et coll. [2014b].

Scanning-electron microscopy (SEM)

The surface analysis for elemental cartography is done using the scanning electron microscope Hitachi S-4700 on samples of the carbon floor. The acceleration voltage is set to 20 kV. The intensity of the beam is 10 µA and the working distance 12 mm. The elemental analysis is done with an Oxford X-Mas 50 mm^2 energy-dispersive X-ray spectroscopy module (EDS). Electronic microscopy of the carbon-aluminum interface allows evaluating the topography of the interface and measuring the aluminum carbide layer typically formed under the metal.

5.2.4 Results

For each experiment, the temperature was recorded with thermocouples in the bath, in the carbon sidewall and inside the Inconel crucible. Figure 5-4 depicts the temperature profile in the bath for the first five runs done for each cathode grade. The temperature of the bath is raised between 1233 K and 1273 K (960 °C and 1000 °C) before the start of electrolysis in order to assure that the bath is completely molten. Afterwards, the temperature of the bath is brought down to 1233 K (960 °C) before electrolysis is initiated. Immediately after the start of the electrolysis, there is a sudden increase in bath temperature due to the Joule effect. After about a thirty-minute period, the bath temperature suddenly drops by approximately 6 to 8 degrees in a one-minute timeframe, as it is observed in Figure 5-4. Subsequently, the bath temperature stabilizes back to 1233 K (960 °C) before it steadily decreases afterwards.

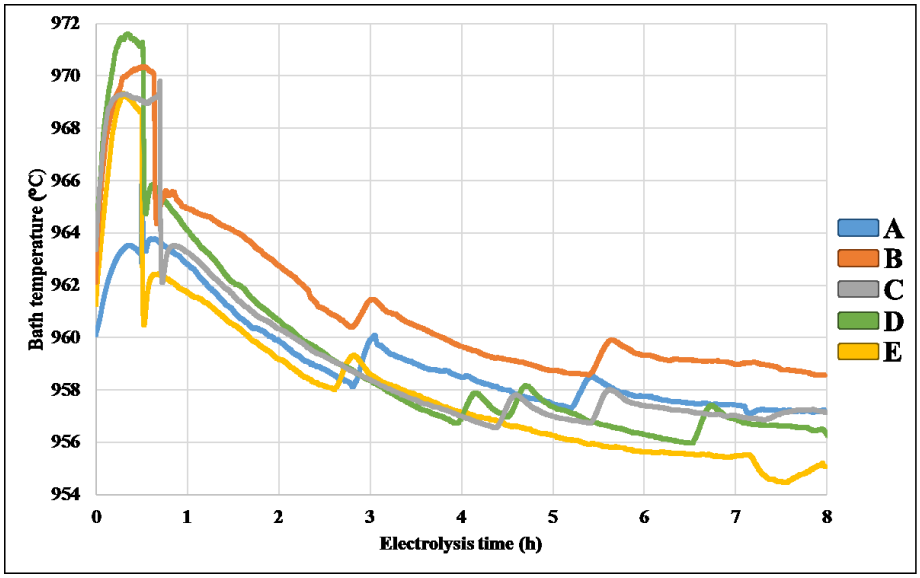

Figure 5-4. Temperature profile of the bath for the five experimental grades during electrolysis

The heat generated by the Joule effect in the cell is transferred to the carbon walls of the experimental cell. Due to the constant nitrogen flow inside the crucible, the heat generated in the cell is lost to the surroundings by different heat transfer mechanisms, including conduction through the walls, convection at the surface of the bath and evaporation of the bath. On the other hand, there is a considerable amount of radiative heat transfer between different elements, like the Inconel wall and the exterior of the cell. Consequently, the temperature of the bath is affected by a combination of the aforementioned heat transfer mechanisms. Nevertheless, the temperature recorded in the sidewall and in the crucible remained close to 1233 K (960 °C). Because of heat losses to the surroundings of the cathode block, the bath temperature tends to decrease during the operation. In order to keep the bath temperature as close as possible to 1233 K (960 °C), the temperature of the furnace is adjusted accordingly (in the range between 1223 K and 1228 K), causing the small bumps on the bath temperature profiles in Figure 5-4. As it can be seen, all five grades have a similar bath temperature profile during electrolysis with a roughly 5-degree margin. At the end of the 8-hour electrolysis period, the furnace is turned off and the cell is let to cool down under nitrogen atmosphere.

After electrolysis, the bottom part of the block is cut in four sections as described in Figure 5-3. Each cut may or may not show a vivid sludge formation at the carbon-aluminum interface. Accordingly, the states of the carbon-aluminum interface associated with the temperature profiles of Figure 5-4 are presented in Figure 5-5.

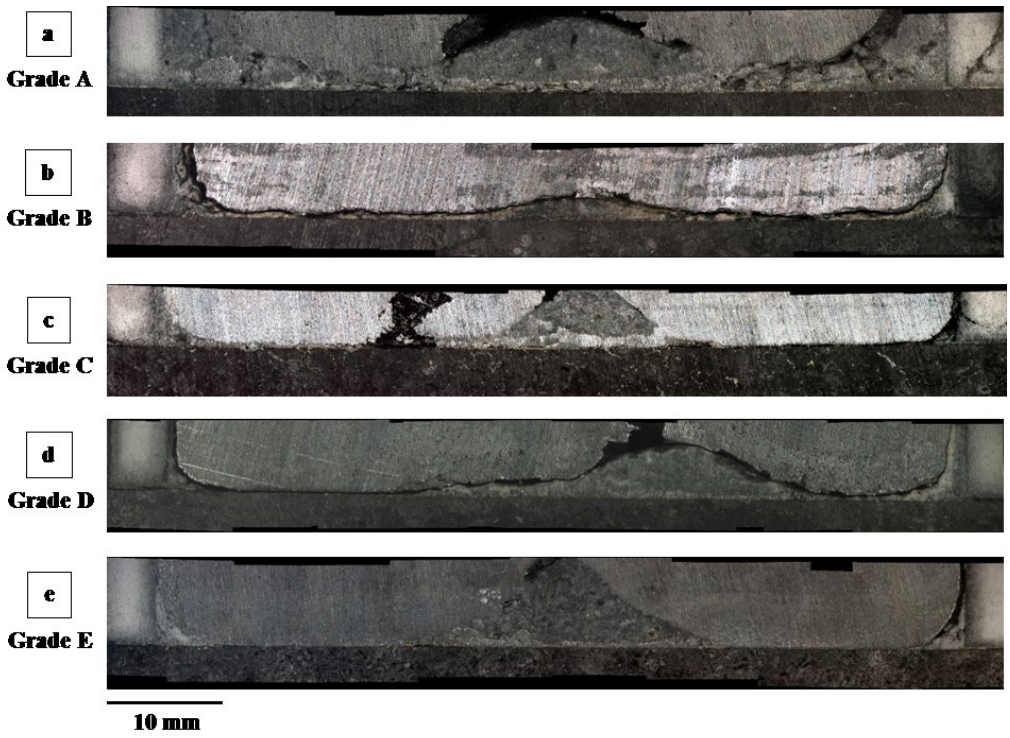

Figure 5-5. Microscopic observations of the carbon-aluminum interface profile in the center of the cell for the five cathode grades; grade A (a), grade B (b), grade C (c), grade D (d) and grade E (e)

As it is shown in Figure 5-5, the sludge profile is variable among the grades. An interesting cone shaped sludge deposit was found near the center of the cell. Moreover, a variable amount of bath fills the peripheral corners of the cell bottom, which represents the ledge toe in this experimental study. The ledge toe becomes thinner and thinner as it elongates towards the center of the cathode floor, leaving a bath layer between the carbon and the metal. However, during autopsies, it could be seen that this layer is not always covering the total surface of the cathode. The thin bath layer observable at the carbon-aluminum interface of grades B and C has a yellowish color and bright yellow marks appear clearly in the carbon of grade C. The thickness of the ledge toe is often variable within a single cell, making the carbon-metal interface profile asymmetrical. In Figure 5-5 (section c), there is an apparent empty space in the metal which can be explained by the contraction of the metal during cooling. For each run illustrated in Figure 5-5, the characterization of the visible central sludge deposit and the ledge toe is summarized in Table 5-2.

For the five runs shown in Figure 5-5/Table 5-2, the bulk of the electrolyte has an alumina content between 4 and 11 with a CR lower than 2 at the end of the electrolysis. The composition of the ledge toe has a higher alumina mass percentage and CR than the initial bath. Accordingly, it is a mixture of undissolved alumina and saturated bath. The central sludge deposits are also alumina-saturated bath and undissolved alumina with a CR less acidic than the initial composition of the bath (CR of 2.2 and 10 wt% alumina), which is also saturated bath. Besides, the sludge composition shown in Table 5-2 shows little variability; nevertheless, the sludge profiles from Figure 5-5 differ significantly. However, when comparing each run with close conditions, it is evident that the size, shape, location and composition of the sludge vary considerably from one run to the other (Figure 5-6).

Table 5-2. Total alumina content (from Rietveld refinement) and cryolite ratio of central and ledge toe sampled in cells from Figure 5-5

Cathode grade	Central sludge		Ledge toe	
	CR	Al_2O_3 (wt %)	CR	Al_2O_3 (wt %)
A (graphitized)	2.8	22	2.2	23
B (graphitized)	N/A	N/A	2.6	18
C (graphitized)	2.9	28	2.6	24
D (graphitized)	2.6	20	2.8	20
E (graphitized)	2.9	19	2.1	19

Nonetheless, in every case, the average CR of the ledge toe in impregnated graphite (grade E) is the lowest among all the grades. Moreover, grades B and C, which have high thermal/electrical conductivities, have the highest average CR while grade E has the lowest value. As sections c and d in Figure 5-6 reveal, the number of times that samples of central sludge were analyzed reflects the actual number of times that central sludge had formed. Evidently, grade A is the grade that contained the most sludge in this study although it was listed as the grade with second-highest sludge propensity by the industry. Moreover, a distinct central deposit was found only once for grade B.

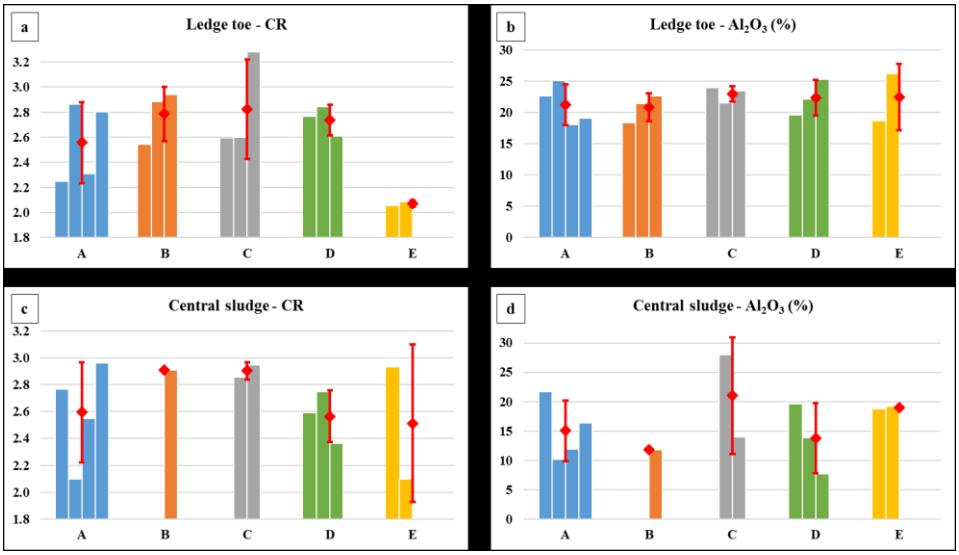

Figure 5-6. Characterization summary of all experiments; the red markers are the average values by grade with the standard deviation; CR of ledge toe (a), total alumina mass percentage of ledge toe (b), CR of central sludge (c) and total alumina mass percentage of central sludge (d)

Observations related to the post-mortem analysis of the bulk bath

The interior of the cell above the metal was also analyzed. It was found that the electrically insulating alumina plates were being dissolved during the experiments, implying an uncontrolled alumina feeding to the bath. The maximum point of erosion of the plates, shown on Figure 5-7, was at the bath-air interface, due to bubble-induced movement of the surface and the alumina dissolution in the low oxygen bath coming from the anode.

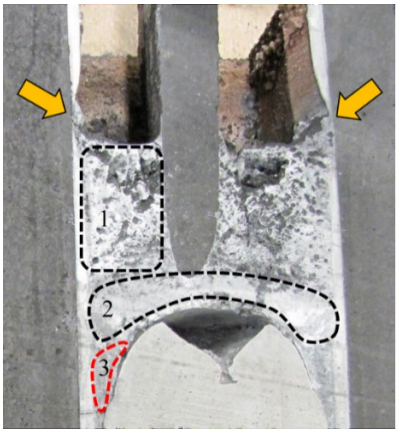

Zone	Al_2O_3 (%)	St. dev.	CR	St. dev.	Density (g/cm^3) at 1233 K (960 °C)
1	6	2	1.7	0.2	1.96
2	6	3	1.8	0.2	1.98
3	15	4	2.2	0.3	Bath: 2.04 + solid Al_2O_3
Central sludge	16	6	2.7	0.3	Bath: 2.09 + solid Al_2O_3
Ledge toe	21	4	2.6	0.3	Bath: 2.09 + solid Al_2O_3

Figure 5-7. Transversal cut of a typical experimental cell and the average alumina mass percentage and CR of the indicated zones; the yellow arrows indicate the typical region where the maximum erosion of alumina plates occurs. The region circled in red indicates that it is supersaturated in alumina

As it is shown in Figure 5-7, the darker electrolyte above the tip of the anode (i.e. zone 1) is quite porous, caused by the bubbling at the anode. The electrolyte below the anode (i.e. zone 2), is much more packed. The characterization of samples taken in the indicated zones reveals a gradient of alumina concentration, CR and density from the point of erosion to the cathode bottom. Samples from zone 2 have an average alumina concentration and acidity similar to zone 1. However, samples collected in zone 3 (gray bath between the metal and the alumina plate) have a higher average alumina content and CR, which is similar to the bottom deposits. Zone 3 is the farthest region from the anode tip, which is a highly agitated area; therefore, it may be the ideal location of alumina accumulation when it precipitates. The alumina concentration exceeds saturation in zone 3, in the central sludge and in the ledge toe. Other laboratory scale electrolysis experiments have shown the presence of sludge containing 25 wt% alumina and a CR of 2.2 (i.e. acidic) [Allard et coll., 2014a]. However, those experiments were done with alumina point feeding while the runs presented in this paper had no alumina point feeding. In this experimental study, the initial state of the electrolyte is a mixture of liquid bath and solid undissolved alumina. Considering the additional alumina is coming from the alumina plate erosion, it is not surprising to find considerable amounts of sludge at the bottom of each cell. This increase of alumina concentration to the system originates from the corrosion of the alumina plates caused by the low oxygen content of the bath surrounding the anode region. The XRD analysis of the samples shown in Figure 5-7 reveals that the composition of the electrolyte at the end of the run, above the metal, has on average 6 wt% Al_2O_3 with an average CR of 1.8. According to the phase diagram of the experimental system Al_2O_3-AlF_3-NaF-CaF_2, the onset of the experiment is within a two-phase region, requiring alumina precipitation enrichment of the bottom of the cell.

According to Figure 5-8, the acidification of the bulk has a stronger effect on the cryolite liquidus than on the alumina liquidus. Samples above the metal reached the liquid zone while deposits under the metal stayed in the alumina and bath mixture phase. The alumina concentration in the bulk at the end of the experiments suggests that the bath (initially supersaturated) reaches the saturation line during electrolysis. Upon alumina consumption from electrolysis, the alumina concentration in the bulk decreases. The bath depleted from alumina after electrolysis is circulated towards the top of the cell by the means of the bubble agitation, leading to more alumina from the plates getting dissolved, as observable in Figure 5-7. The undissolved alumina from the initial bath or the corrosion of the plates precipitates to the bottom.

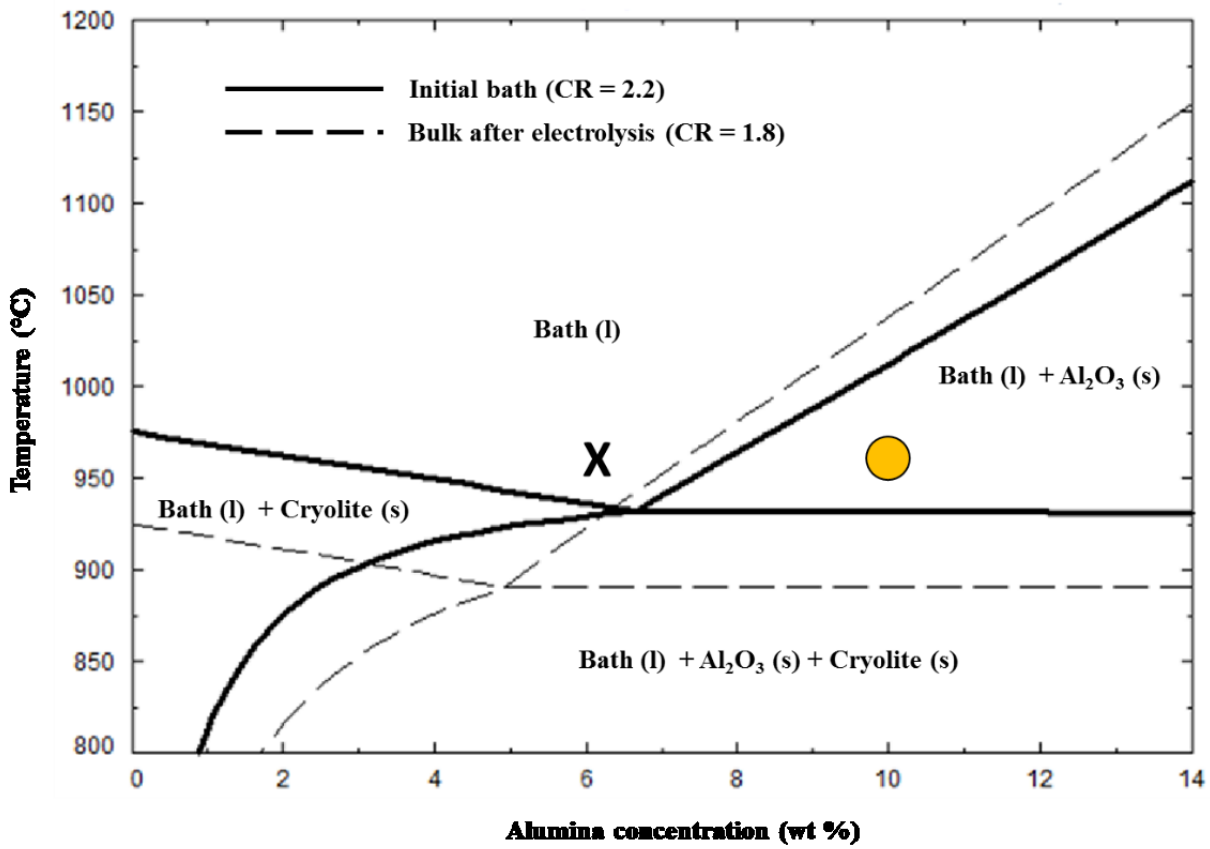

Figure 5-8. Thermodynamic phase diagram from FactSage of the system Al_2O_3-AlF_3-NaF-CaF_2; the yellow filled circle and X mark indicate respectively the initial condition of electrolysis and the composition of the bulk bath at the end of the run.

Observations on the profile characteristics of the bottom deposits

Although sludge profiles vary from one experiment to the other, some distinctive characteristics of each cathode grade with regard to sludge and other bottom deposits have been noted and summarized in Table 5-3.

Observations on the behavior of voltage during the electrolysis

The voltage for each run is measured continuously and the amperage is kept constant at 73 A. When current is launched, the voltage starts around 5.0 V, then decreases between 4.6 V and 4.9 V before it generally starts to rise. The tendency for highly electrically conductive grade C and impregnated graphite grade E is to start rising after roughly 3 hours of electrolysis. For grade B, the voltage typically starts to rise after 4 hours of electrolysis while graphitized grades

A and D present steadier voltage behaviors under 5 V during the 8-hour operation period. The average voltage for each grade is presented in Figure 5-9.

Table 5-3. Qualitative observations of carbon-aluminum interface for each cathode grade

Cathode grade	Observations
A (graphitized)	- High amount of ledge toe that stretches towards a continuous thick layer (>1 mm). - The thick layer always covers the entire area of the carbon-aluminum interface. - The ledge toe is evenly distributed around the perimeter of the cell.
B (graphitized)	- The ledge toe is not evenly distributed, it tends to be thicker in some areas, leaving other regions free of deposits or covered with a thin layer (<1 mm).
C (graphitized)	- Just like grade B, the ledge toe is not evenly distributed, but to a higher extent. - The bath layer is thin (<1 mm), non-continuous and with bright yellow marks. - Erosion of the carbon surface is observed.
D (graphitized)	- High amount of ledge toe is observed, not evenly distributed along the perimeter. - The thin layer (<1 mm), does not cover the total area of the cathode surface. - A small amount of central sludge is observed.
E (graphitized + impregnated)	- An uneven ledge toe distribution is noticed. - The thin layer (<1 mm), does not cover the total area of the cathode surface. - Variable amounts of central sludge is observed.

It does not seem likely that the voltage behavior in this study is directly correlated with the amount of sludge at the carbon-aluminum interface. On the other hand, as mentioned in Table 5-3, the cathode grade C also stood out for its visible erosion marks, which may explain the voltage rise. On the contrary, no visible signs of erosion were observed on impregnated graphite grade E.

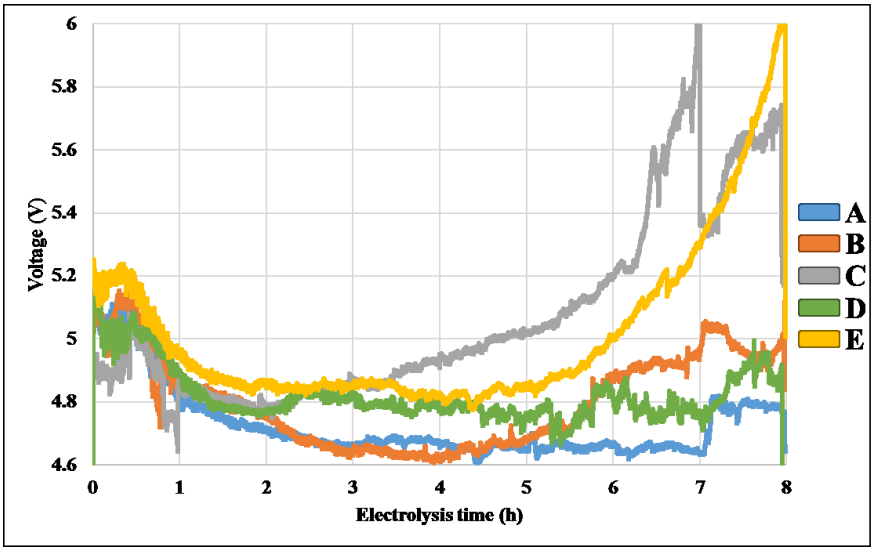

Figure 5-9. Average voltage by cathode grade

SEM-EDS observations of the carbon-aluminum interface

The highest erosion is located where the tip of the elongated ledge toe or thin layer disappeared. Moreover, SEM-EDS observations of the carbon-aluminum interface revealed the presence of a layer containing aluminum covering the carbon surface and going inside the wear pits (Figure 5-10).

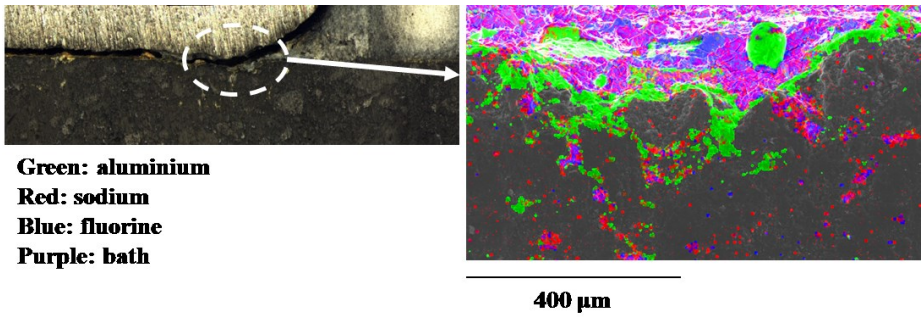

Figure 5-10. SEM-EDS observation of the indicated zone of the carbon-aluminum interface for grade C

The green layer containing aluminum in the SEM imaging appears to be aluminum carbide, which is nowadays thought to be highly responsible for cathode wear. This layer was observed with all five grades. The high wear, illustrated in Figure 5-10, suggests that the electrochemical formation of aluminum carbides and its subsequent dissolution in the bath (from ledge toe or thin layer) is faster for cathode grades with a film that does not cover the entire cathode surface. Moreover, it may explain the voltage rise observable for grade C. The eroded parts of the carbon

surface filled with bath may have prolonged the current paths around the pits, thus provoking voltage rise that is observed especially with grade C. The thickness of the aluminum carbide layer was measured for each block and an apparent correlation with the open porosity of the cathode grade has been previously established [Landry et coll., 2018]. In Figure 5-10, the aluminum carbide layer appears to be following the morphology of the carbon surface. Accordingly, erosion is taking place when aluminum carbides form around a small piece of carbon before dissolving inside the bath infiltrated in the pores. The detachment of the surrounded carbon piece accounts for the growing pit.

5.2.5 Discussion

Sludge formation is influenced by a myriad of phenomena that interact during the regular operation of a cell. The major factors are temperature of the bath, interfacial phenomena, hydrodynamics, bath chemistry and alumina feeding strategy [Fallah Fini et coll., 2017]. Since no point feeding was used in this study, the impact of feeding strategy on sludge formation will not be discussed and reader is encouraged to refer to Fallah Fini et coll. [2017]. Since the cathode block is an obligatory passage for heat, mass and electricity, consequently the aforementioned factors (i.e. temperature of the bath, interfacial phenomena, hydrodynamics, bath chemistry and alumina feeding strategy) should also be influenced by the thermal, electrical and structural properties of the cathode block.

Effect of temperature

The proper dissolution of alumina and avoidance of sludge formation call for an appropriate superheat of the bath. Since close to half of the heat losses go through the carbon walls of the cathode [Grjotheim et Kvande, 1993], the heat balance of the cell is partially controlled by the thermal conductivity of the cathode block. Expectantly, the cathode grade should have an impact on sludge formation through the cell heat balance. As it is seen in Table 5-1, the five cathode grades have different horizontal and vertical thermal conductivities, which suggests variable heat flows depending on the grade, thus variable sludge profiles. As mentioned earlier, the bath is heated by the Joule effect during electrolysis and cooled by several heat transfer modes. The heat generated inside the cell is transferred by conduction through the graphitized cathode block. The heat lost through the furnace walls and the nitrogen gas flow account for the convective cooling on the exterior of the cathode block. Moreover, the cell is subject to radiative heating

coming from the furnace. Due to the complex combination of heat transfer modes affecting the bath temperature, it is not obvious to clearly discern the impact of the thermal conductivity of the cathode block on the heat transferred by conduction through the carbon phase. Nevertheless, during the most stable period of electrolysis (after the sudden temperature increase and decrease seen in Figure 5-4), the experimental cooling rate of the bath was calculated for each run and is plotted in Figure 5-11.

Consequently, it was found that the grade with a significantly higher average thermal conductivity (i.e. grade C) had the fastest cooling rate during the electrolysis. This foreseeable result highlights the sensitivity of cathode grades to heat losses even though those grades have close thermal conductivities. The different thermal behaviors seen with the experimental cells yet again emphasize the fact that the heat balance of the cell is greatly influenced by the cathodic carbon block. Knowing that heat loss must be well controlled in order to keep an appropriate superheat and limit sludge formation, the choice of the cathode grade is important as it directly influences the rate and uniformity of heat losses. More uniform heat losses should help to control the position of the liquidus isotherm, thus keeping an appropriate uniform protective ledge. This may be easier to achieve by ensuring that the thermal conductivity of the carbon block is as uniform as possible in the whole block.

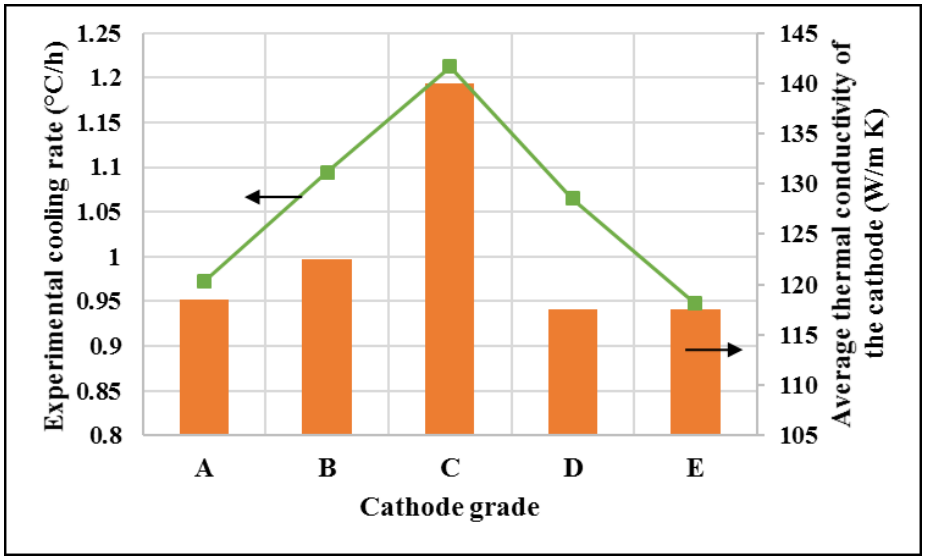

Figure 5-11. Average cooling rate per cathode grade and average thermal conductivity of the block: average conductivity was obtained by averaging the horizontal and vertical conductivities

However, it is known that the thermal conductivity of the cathode block changes during the lifetime of the cells and such changes are due to different phenomena that the cathode block endures [Yurkov, 2015]. Therefore, there must be a correlation between the cathode block raw microstructure (i.e. initial open porosity), infiltration depth of the bath and dynamic thermal conductivity during the operation. In fact, in a recent laboratory study, using similar cathode grades, the impregnated graphite with lower porosity had a lower bath penetration depth than non-impregnated graphite [Brassard et coll., 2016]. Consequently, in the current study, the impregnated grade E must have been filled with a smaller volume of bath. Despite its same raw thermal conductivity as grade E, grade D showed a significantly faster cooling rate than E during electrolysis. This could be due to a more intense change of thermal conductivity for grade D, resulting from a large bath infiltration enhanced by the higher open porosity of grade D. Although pitch impregnation of graphite blocks is typically used to decrease porosity and increase wear resistance, the pitch impregnation of grade E, while differentiating it from grade D, may also have helped to reduce the rate of heat losses.

Effect of interfacial tension (IFT)

At first, the formation of sludge was foreseeable because the initial bath composition was in the two-phase region (Figure 5-8). When central sludge was found, it was connected to the ledge toe by a bath layer more or less thin, as pictured in Figure 5-5. A similar bath layer was observed in previous experiments and was speculated to be resulting from the ledge toe/sludge displacement by MHD on the cathode block surface [Coulombe et coll., 2016]. Moreover, the existence of a bath film between the carbon and the aluminum was evoked and said to be related to the formation and dissolution of sludge [Li et coll., 2015]. Studies on IFT between cryolitic melts and aluminum showed that the IFT between the cryolitic melt and the molten aluminum increases with increasing AlF_3 because of the higher activity of sodium [Dewing et Desclaux, 1977; Utigard et Toguri, 1991; Korenko, 2008]. Accordingly, it was suggested that a movement in the liquid bath film can be induced if there is an IFT gradient between the bath at the aluminum-electrolyte interface and the film at the carbon-aluminum interface. Moreover, the direction of the movement of the film is from the region of lower IFT (i.e. low AlF_3) to the region of higher IFT (i.e. high AlF_3). The so-called Marangoni flow can back feed the sludge into the bulk if the direction is from the carbon-aluminum interface to the bulk. As it was mentioned previously, the thickness of the bath layer was variable among grades in this study.

For grade A, the bath layer was thicker and clearly distinguishable. In order to further discuss the influence of IFT and cathode grade, a schematic diagram is proposed in Figure 5-12.

The bath layer found below the aluminum seen in Figure 5-12 (section a) has a lower CR than the central sludge yet a similar alumina concentration. Also, a thin vertical bath film separating the aluminum pad and the alumina plate connects the bath layer and the bulk. Moreover, there is a gradient of CR from the bulk to the sludge, thus an IFT gradient. This suggests that central sludge may be back fed into the bulk through the bottom layer and the thin vertical film. As a result, alumina may back feed if fresh bath from the bulk can be circulated to the sludge through this film. Besides, the ability of the cathode block to pass sodium may tamper with the sodium depletion of the vertical bath film. As it is depicted in Figure 5-12 (section b), a high sodium diffusion through the cathode block and alumina plate may shift the CR of the bath film to more acidic, thus promoting sludge back feeding through this vertical film.

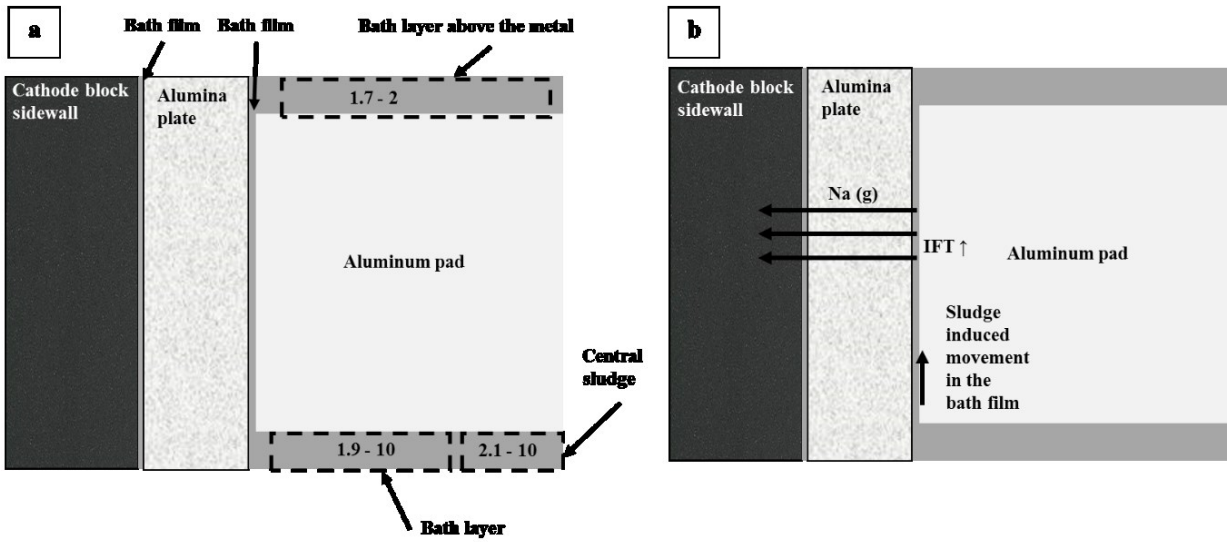

Figure 5-12. a) Bath film connecting the bottom bath layer and the bulk (CR – alumina wt%) for one run with cathode grade A, b) film movement induced by sodium losses in cathode block

The effective diffusion of sodium gas through the carbon may depend on its porosity, tortuosity and air permeability [Wang et coll., 2009]. Therefore, cathode grades with high sodium diffusivity may tend to have a lower CR in the bath between the sidewall and the metal, thus drawing mass transfer towards the bulk and promoting sludge back feeding. In this study, grade A was the grade with the highest air permeability, which may further explain the thicker bath layer observed. Other than the fact that grade A had a thick bath layer, no correlation was found

between the cathode properties and the acidity of the bath in the bulk or in any other deposit. Nevertheless, if the cathode block has the potential to alter the acidity of the bath, it may well lead to IFT gradients between the bottom deposits and the bulk, thus inducing Marangoni flows that affect sludge accumulation or back feeding. Furthermore, the Rietveld refinement of the bath samples at the aluminum-bath interface has shown too much variability to prove the presence of a consistent layer of bath rich in alumina that could sink through the metal pad. The agitation in the bath from the anode gas release, seen in Figure 5-7, may have caused such variability of concentration in the bath above the metal. With considerable agitation due to bubble movement and the small size of the cell, it is perceivable that hydrodynamics also plays a major role in formation or dissolution of sludge.

Effect of hydrodynamics

Irrespective to IFT induced movement, bubble movement and magneto-hydrodynamics are the most effective forces in the cell. In industrial cells, proper bubble agitation contributes to dissolution of fed alumina particles while oscillations of the bath-metal interface leads to losses in current efficiency [Thonstad et coll., 2001]. Also, the large molten metal pad is constantly in movement due to MHD forces. In this study, it would take a considerable movement of the metal pad in order to lift the bottom sludge deposits right up into the bulk. With regard to this fact, Kalgraf et Torklep [1998] have argued that the sludge back feeding process may be governed by the laws of sediment transport. Considering the fact that the sludge is a mixture of crystallized alumina particles and a saturated bath, sufficient turbulence of the metal pad movement could allow the sludge to be lifted (i.e. back-fed) into the bulk through the metal pad. In the present study, there is no obvious reason to believe that there was a sufficient metal pad movement from MHD near the cathode surface to transport sludge in such a manner. The agitation inside the cell is more likely to originate from bubble movement at the anode. Signs of agitation in the metal pad were only observed during the autopsy of a cell cooled during electrolysis. However, agitation signs were only observed in the ACD, which may be attributed to bubble induced movement or aluminum forming during cooling. Nevertheless, it is not clear at this point how the cathode grade can impact the sludge dissolution process through sediment transport-like movement.

5.2.6 Conclusions

Laboratory electrolysis tests with five different graphitized cathode grades were performed to study the formation of sludge at the cathode surface. This study has revealed the formation of a distinct conical sludge deposit near the center of the carbon-aluminum interface for each grade, despite the absence of point feeding during electrolysis. The central sludge and ledge toe deposits had an alumina mass percentage ranging from 10 to 25 wt% and a CR from 2.4 to 2.9. No correlation was found between the composition of the bottom deposits and the cathode grade in this study.

The profile of sludge was variable among cathode grades, which further suggests that the cathode grade has an impact on sludge formation. However, no clear correlation between the thermal conductivity of the cathode block and the temperature profiles was found, due to the complex array of heat transfers involved during the experiments. The observable temperature profile variations testify of the sensibility of the experimental set-up used in this study. Nevertheless, a certain amount of sludge was always found at the carbon-metal interface in each experiment. The phenomenon of sludge formation may be repeatable, granted that conditions inside the cells (especially temperature profiles) are replicated.

The higher CR of the central sludge versus the CR of the bulk suggested an induced movement in the vertical bath film, resulting from IFT difference between the bulk and the bottom of the cell, while enhancing the back feeding of the sludge. Therefore, the propensity of a cathode block to alter the acidity of the vertical bath film between the metal and the sidewall may then contribute to induce sludge back feeding. Cathode grades with high permeability may be more prone to sludge back feeding by IFT driven movement.

The wear of the carbon-aluminum interface may be faster for the cathode grades with a film that partially covers the cathode surface. A layer of aluminum carbide is observed with SEM-EDS inside the erosion pits. The erosion pits in the cathode surface may contribute to the voltage rise. In order to alleviate the problem of pit formation (i.e. erosion of cathode surface), other methods such as copper inserts can be used to lower the CVD, reduce the MHD forces and make current paths more uniform. The use of such inserts in combination with graphitic cathode grade was recently predicted to have an increased interest in a near future [Rivoaland, 2016]. Furthermore, the use of such cathode grades with lower electrical and thermal conductivities may help to keep

a better control over the heat balance, hence reduce sludge formation and its detrimental drawbacks.

CHAPITRE 6 IMPACT DES PARAMÈTRES D'OPÉRATION SUR LA FORMATION DE BOUES

6.1 Avant-propos

Auteurs et affiliations :

Mojtaba Fallah Fini : étudiant au doctorat, Département de génie chimique et génie biotechnologique, Université de Sherbrooke, Québec, Canada.

Gervais Soucy : professeur titulaire, Département de génie chimique et génie biotechnologique, Université de Sherbrooke, Québec, Canada.

Martin Désilets : professeur titulaire, Département de génie chimique et génie biotechnologique, Université de Sherbrooke, Québec, Canada.

Didier Lombard : champion innovation & consultant matériaux / brasquage, Solutions Technologiques Aluminium – LRF, Rio Tinto, Saint Jean de Maurienne, France.

Patrick Pelletier : scientifique de recherche brasquage, Solutions Technologiques Aluminium – CRDA, Rio Tinto, Québec, Canada.

Regis Paulus : Recherche et Développement Directeur, Carbone Savoie, Vénissieux, France.

État de l'acceptation : En révision (soumis le 10 janvier 2020, révisé le 1er mai 2020).

Revue : *Minerals Engineering*

Référence : Fallah Fini et coll. [2020b]

Contributions à la thèse :

Après avoir revu de nombreuses recherches effectuées sur les paramètres affectant la formation des boues et ses désavantages, trois concepts semblent absents, à savoir l'importance relative des paramètres d'opération, l'influence de la nuance cathodique et la formation expérimentale de boues induites chimiquement (c'est-à-dire précipitation des espèces cryolitiques). Ce chapitre comble cette lacune tout en réalisant un plan d'expériences qui se compose de la température d'opération, le ratio de cryolite (CR) et la nuance de cathode. Parmi les trois paramètres inclus

dans le plan expérimental (c'est-à-dire la température opérationnelle, le ratio de cryolite et la nuance de cathode), la température, représentant le niveau de surchauffe, était le seul paramètre statistiquement important. L'importance du taux de consommation en alumine (c'est-à-dire la cinétique) doit être prise en compte lorsque l'on regarde le taux de précipitation des espèces cryolitiques et ses transferts possibles vers le fond de la cellule. Enfin, d'après la différence entre les porosités ouvertes de deux nuances de bloc cathodique, une couche isolante de carbure et de bain solide couvre la surface de la cathode ayant une porosité supérieure.

Titre français :

Formation de boues induites chimiquement dans le procédé Hall-Héroult

Résumé :

Les résultats d'un plan d'expérience montrent que le paramètre le plus statistiquement significatif, entre la température d'opération moyenne, le ratio de cryolite (CR) et la nuance de cathode, est la température d'opération. Cependant, la précipitation d'espèces cryolitiques sous la nappe métallique (c'est-à-dire les boues induites chimiquement) dépende également de la polarisation de la concentration et du taux d'épuisement de l'alumine. Les interactions entre la couche de carbures et la boue peuvent expliquer l'augmentation du temps de réalimentation des boues pour des blocs cathodique. Le résultat de l'interaction entre la boue induite chimiquement et la boue riche en alumine est un mélange de faible densité qui peut être réalimenté.

6.2 Chemically Induced Sludge Formation in Hall-Héroult Process

Keywords: Hall-Héroult Process, Superheat, Sludge, Carbide, Cathode, Cryolite ratio

6.2.1 Abstract

Results of an experimental plan design show that the most statistically significant parameter, among average operational temperature, cryolite ratio (CR) and cathode grade, regarding the formation of chemically induced sludge, is operational temperature. However, the precipitation of cryolitic species under the metal pad (i.e. chemically induced sludge) is also a function of concentration polarization and alumina depletion rate. The interactions between the carbide layers and the sludge can explain the increased time of back-feeding for some cathode linings. The result of interaction between chemically induced sludge and alumina-rich sludge, is a low-density mixture that is back-fed into the bulk of the bath.

6.2.2 Introduction

In Hall-Héroult process, which is the main industrial process to produce primary aluminum, any accumulation of solid cryolitic bath under the aluminum metal pool is called sludge, as presented in recent literature reviews [Fallah Fini et coll., 2017; 2020a]. There are numerous mechanisms for the formation of sludge, including the fall of ACM or top crust into the cell, the fall of anode freeze during the anode change procedure, extension of ledge toe on the surface of the cathode due to excessive heat loss, agglomeration of fed alumina particles and finally chemically induced sludge formation. The latter may occur when the sodium concentration polarization increases the liquidus temperature of the interfacial layer between bulk of the bath and aluminum pool [Solheim, 2002]. Moreover, the depletion of alumina accompanied by concentration polarization increases the liquidus temperature even further [Coursol et coll., 2012].

Sludge formation in the cell is governed by several factors, namely the feeding strategy, physicochemical characteristics of the alumina, bath chemistry, interfacial phenomena, superheat level of the bath, hydrodynamics of the cell's fluids and finally the type of the cathode [Fallah Fini et coll., 2017; 2020a]. The presence of sludge, more specifically its extensive and uneven distribution, can reduce the current efficiency and increase the energy consumption of the Hall-Héroult process, which is one of the most energy intensive metallurgical processes in the world [Haraldsson et Johansson, 2018]. Accordingly, the behavior (i.e. formation or

dissolution) of the sludge is one of the main concerns of the primary aluminum producers and it must be revisited, especially in the case of reduced metal flow velocities and squeezed ACDs [Liu et coll., 2019]. Looking at the numerous researches done on the parameters affecting the sludge formation and its drawbacks, three concepts seem to be missing, namely the relative significance of the most important parameters, the influence of cathode grade and the experimental formation of chemically induced sludge even though there are speculations for formation of such deposits [Haupin, 1997; Solheim, 2002; Coursol et coll., 2012]. In order to accommodate these three missing concepts, it was decided to plan an experimental procedure to find out important operational parameters, study possible influence of cathode grade and show experimental evidences for the formation of chemically induced sludge. In fact, the importance of chemically induced sludge is due to its possible role in easing the dissolution of alumina-rich sludge. In other words, the cryolitic precipitates dissolve the alumina, lower the liquidus temperature and consequently increase the dissolution rate of alumina-rich sludge.

6.2.3 Materials and methods

Cell preparation

For each test, one kilogram of synthetic cryolitic bath was prepared by mixing Na_3AlF_6, AlF_3, NaF, Al_2O_3 and CaF_2. The chemical composition of the two baths (one acidic and one basic) are presented in Table 6-1. In order to show the effect of alumina diminution on the corresponding liquidus temperature, initial ($T_{liq.-in.}$) and final ($T_{liq.-fin.}$) liquidus temperatures are given considering the total consumption of alumina content.

Table 6-1. Chemical composition (wt%), CR, initial liquidus temperature (Tliq.-in. ºC) and final liquidus temperature (Tliq.-fin. ºC) of the two synthetic baths

Bath type	Na_3AlF_6	AlF_3	NaF	Al_2O_3	CaF_2	CR	$T_{liq.-in.}$ (ºC)	$T_{liq.-fin.}$ (ºC)
Bath 1	79.4	11.6	0	4.0	5.0	2.2	949	975
Bath 2	78.5	0	12.5	4.0	5.0	3.8	954	981

Two cathode grades (Table 6-2), manufactured by the same supplier from different raw materials, were used in the experiments. All dimensions of the cell components including the cathodic block, anode and collector bar are shown in Figure 6-1.

Table 6-2. Properties of the cathodic blocks at room temperature

Properties	Grade B	Grade D
Thermal conductivity (W/m.K)	$130^{=}$	$130^{=}$
	115^{Π}	105^{Π}
Electrical resistivity (μΩ.m)	$10.5^{=}$	$10.5^{=}$
	11.5^{Π}	13.0^{Π}
Open porosity (%)	14	20
Air permeability (nPerm)	7	6

$^{=}$: horizontal; $^{\Pi}$: vertical

Prior to each test, the external surface of each cathodic block is covered with carbon felt and later Inconel plates are welded on top of carbon felts surrounding the block. Moreover, in order to protect the vertical walls of the cathodic blocks, four plates of silicon carbide (Saint-Gobain, ADVANCER® CN-703, thickness = 7.9 mm) were placed inside the cells according to Figure 6-1. Next, a rectangular piece of aluminum block with the average weight of 474 ± 8 g was placed at the bottom of the cell. The cell was later filled with one kilogram of cryolitic bath having the composition given in Table 6-1. The anode was positioned as the bath was gradually being compacted into the cell according to Figure 6-1.

Operation procedure

Figure 6-2 schematically depicts the experimental set-up. When the cell assembly was ready, it was placed within an Inconel^{TM} cylindrical container, which was placed inside a cylindrical Pyradia electrical furnace. The electrolysis tests were conducted under a nitrogen atmosphere at 940-960 °C, according to the experimental plan design. The nitrogen flowrate was adjusted to 10 l/min during the tests. The electrical current of 73 A, giving a current density of 1 A/cm^2, was kept constant during the whole duration of the tests, which were stopped when an anode effect was detected. In the experimental set-up, the anode effect was noticed when the average operational voltage suddenly raised from around 5 V to 10 V. During the tests, samples were taken using a cold finger, an operation done after having previously stopped the electricity on the set-up.

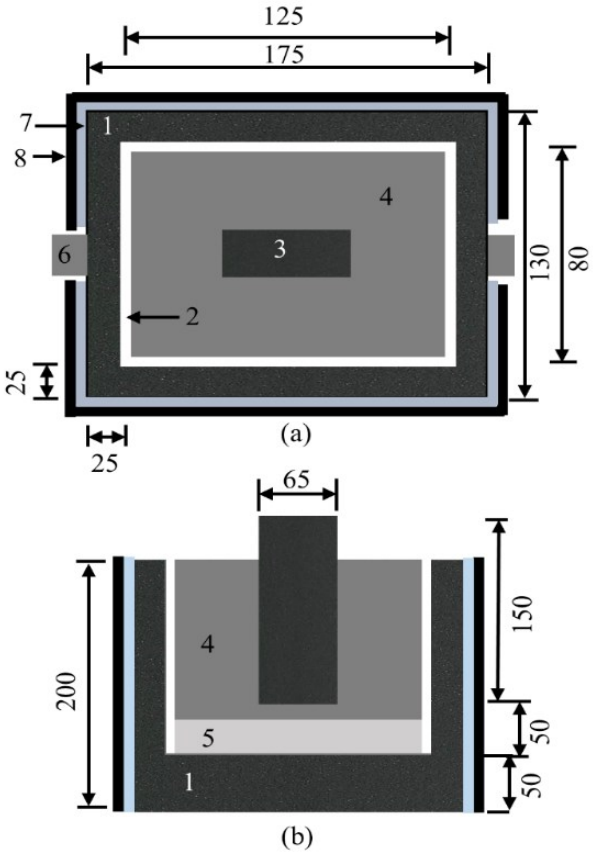

Figure 6-1. Experimental cell components and dimensions; top view (a) and side view (b). All dimensions are in millimeters (mm). 1: carbon crucible, 2: silicon carbide plates, 3: anode, 4: bath, 5: aluminum, 6: collector bar, 7: carbon felt, 8: InconelTM plate.

Experimental plan

A full factorial design plan having three variables and two levels was implemented according to Table 6-3. Two average operational temperatures, 940 °C and 960 °C, were selected considering the two initial CRs: one acidic (CR = 2.2) and the other basic (CR = 3.8). Due to operational problems, two tests were performed at average temperature of 950 °C instead of 940 °C. These two tests at average operational temperatures of 950 °C did not change the purpose and outcome of the experimental plan design. On the other hand, two cathodic grades (B and D) were used as the third parameter of the experimental plan design.

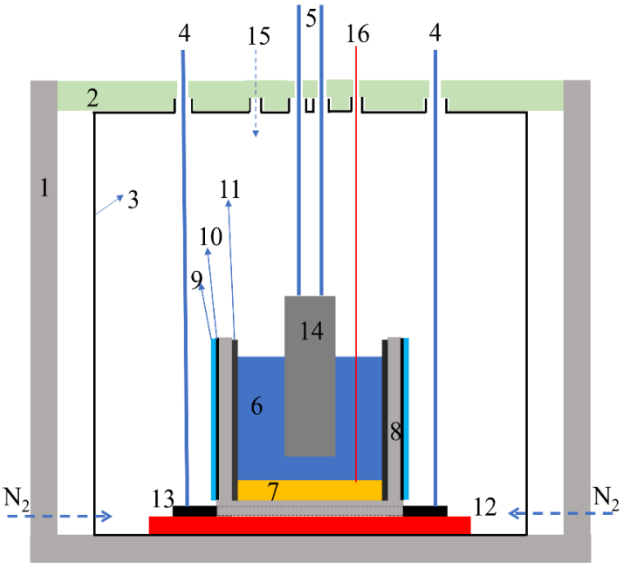

Figure 6-2. Schematic of the experimental set-up; 1: furnace, 2: alumina insulation, 3: cylindrical InconelTM container, 4: cathodic rod, 5: anodic rods, 6: bath, 7: aluminum metal pad, 8: cathodic block, 9: InconelTM plate, 10: carbon felt layer, 11: silicon carbide plates, 12: silicon carbide tile, 13: collector bar, 14: anode, 15: cold finger entrance, 16: thermocouple

Table 6-3. Experimental plan

Test-ID	Average bath temperature (°C)	Initial CR	Cathode grade
B-940-22	941	2.2	B
D-940-38	952	3.8	D
B-940-38	950	3.8	B
D-940-22	939	2.2	D
B-960-22	960	2.2	B
D-960-22	961	2.2	D
B-960-38	960	3.8	B
D-960-38	961	3.8	D

Autopsy

After stopping each experiment, the cell is let to cool down to the room temperature under nitrogen atmosphere. During the autopsy procedure, the cells are stored under argon in a glove box, to avoid further oxidation. Later the cell walls were cut (Figure 6-3) using a diamond blade,

which easily allows for the separation of the silicon carbide plates, metal pad and the bottom of the cathodic block. Later, samples were taken from the solidified bath.

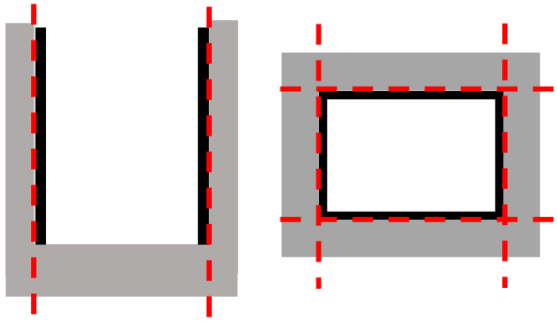

Figure 6-3. The cutting positions during the autopsy procedure;
the dashed lines show the cutting positions.

X-Ray diffraction (XRD), X-Ray fluorescence (XRF) and Rietveld quantification

The harvested samples were ground using a ball mill, back-fed into the appropriate cavities and analyzed by PANalytical X'pert PRO MPD diffractometer and a PIXcel^{1D} detector using a nickel filter. An X-Ray Fluorescence (XRF) Potflux Channel was used to determine the total calcium content of the samples (i.e. CaF_2 content). The quantitative analyses of the samples were done using Rietveld refinement by means of PANalytical HighScore Plus software. Finally, the CR of each sample is calculated by stoichiometry calculations according to Allard et coll. [2014b].

Oxygen determination

The powdered samples were analysed using a TCH-600 (LECO) equipment. Each sample was analyzed in quintuplicate using tin capsules and nickel baskets. The average of the standard deviation in the samples was 0.1%.

Thermodynamic equilibria modeling

The thermodynamic phase equilibria were calculated using FactSage software (version 7.3). The FThall database was used for modeling the NaF-AlF_3-CaF_2-Al_2O_3 system. The phase equilibria were calculated at atmospheric pressure selecting FThall-BathA (fluoride-oxide melt considering metal dissolution) and FThall-CryH (non-stoichiometric high-temperature cryolite). The thermophysical properties of the bath were calculated using FactSage software. The

calculated thermophysical properties include viscosity, density, thermal conductivity, specific heat capacity and electrical conductivity.

6.2.4 Results

Amount of the sludge formed

After having performed the autopsy for each test, an approximate volume (L×W×H/300) was calculated for each deposit formed at the bottom of the cell by measuring the length (L), the width (W) and the height (H) of each deposit (Figure 6-4). The factor (3x100) is representing a geometric and conversion factor to obtain the volume of the pyramidic sludge sample in mm^3x10^{-2} (Figure 6-5).

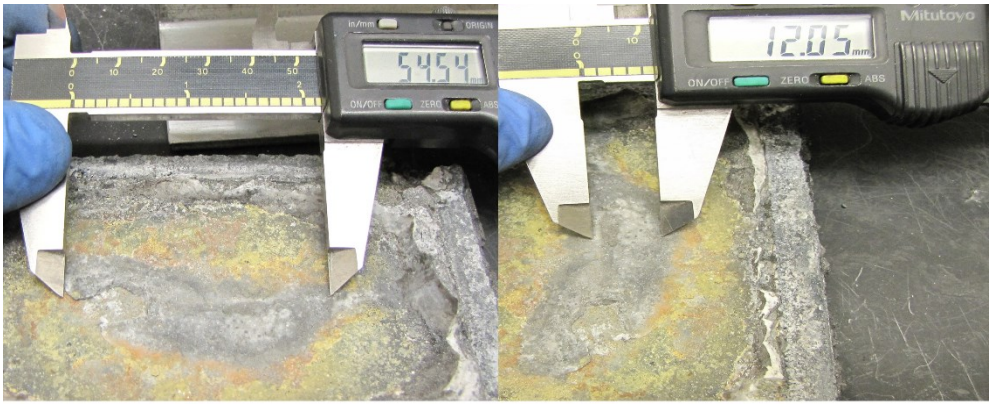

Figure 6-4. Measurement of dimensions of a typical sludge; all the dimensions are in mm.

Among the three parameters (i.e. the average operational temperature, initial CR and type of the cathode), the only statistically important parameter is the average operational temperature (Figure 6-5). In fact, considering the dominating effect of operational temperature, the average values for the volume of sludge formed accompanied by the corresponding standard deviations, show that there is no statistical difference between the tests done at different CRs or with different cathode types.

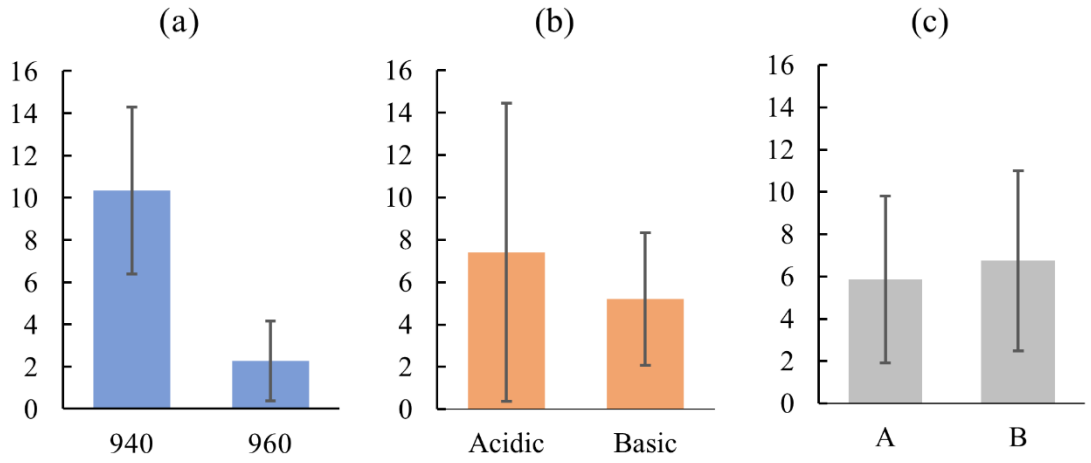

Figure 6-5. The influence of each parameter on the volume of the sludge ($mm^3 \times 10^{-2}$); a) average operational temperature (ºC); b) initial CR; c) cathode grade

Thermophysical properties of the sludge

In order to investigate the effect of temperature on the thermophysical properties of the sludges, several properties were determined from chemical analyses (i.e. CR, CaF_2 and Al_2O_3 contents) using FactSage software (Table 6-4).

Table 6-4. Chemical composition and thermophysical properties of the sludges

Test-ID	CR	Al_2O_3 (wt%)	CaF_2 (wt%)	Density (g/cm^3)	Viscosity* (Pa.s) $\times 10^{-3}$	Thermal conductivity* (W/m.K) $\times 10$	Specific heat capacity (J/g.K)
A-940-22	2.76	2.6	4.4	2.78	3.64	7.52	16.08
B-940-38	2.85	4.0	6.1	2.55	3.78	7.52	23.29
A-940-38	2.90	2.9	6.2	2.52	3.83	7.52	21.92
B-940-22	2.39	3.2	5.2	2.33	2.82	7.52	5.94
A-960-22	2.78	1.8	3.5	2.57	3.09	7.47	6.41
A-960-38	2.68	2.9	3.9	2.39	2.97	7.47	8.51
B-960-38	2.77	2.1	4.3	2.49	3.08	7.47	7.63

* Just considering the liquid fraction of the sludge

Among the thermophysical properties, only the thermal conductivity of the liquid fraction of the sludge and its specific heat capacity showed statistically significant correlations with the operational temperature.

Cold finger sampling results

Some complementary tests were done to get a deeper analysis of the influence of heat transfer rate and alumina consumption kinetics in the cells. These tests were done at the highest average operational temperature (i.e. 960 °C) with an initial acidic CR of 2.2. The tests were divided into two groups. Group 1 had a slightly smaller mass of aluminum pad (467 g), which given that the position of anode does not change, leads to a slightly higher ACD, causing a stronger Joule effect and increasing the heat generation inside the cell. Group 2 had a slightly larger mass of aluminum (478 g) which eventually leads to less heat generation in the bath and creates a much longer transient temperature in the cell. At certain intervals during these tests, samples were taken using a cold finger, and analysed to observe the depletion rate of the alumina during the electrolysis. The temperature profiles of these tests for Group 1 and Group 2 are illustrated in Figure 6-6 and Figure 6-7, respectively.

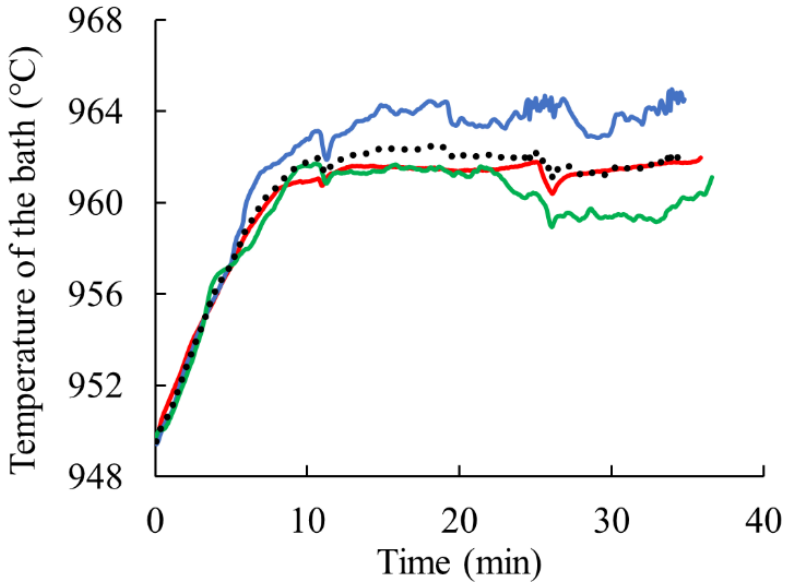

Figure 6-6. Triplicate of a test at average operational temperature of 960 °C, initial CR of 2.2 (Group 1); solid lines are the three replicas and the dotted line shows the average value.

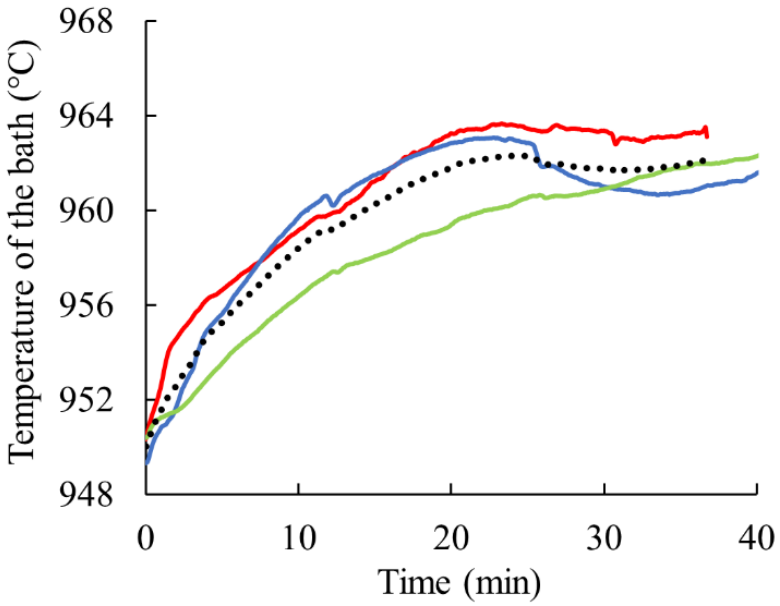

Figure 6-7. Triplicate of a test at average operational temperature of 960 °C, initial CR of 2.2 (Group 2); solid lines are the three replicas and the dotted line shows the average value.

The results of the tests also showed that Group 1 is more favorable to sludge formation than Group 2 while the rate of alumina depletion for the tests of Group 1 is higher than tests of Group 2 (Figure 6-8). The CRs of the samples during the tests remains almost constant, having the value of 2.3 ± 0.05.

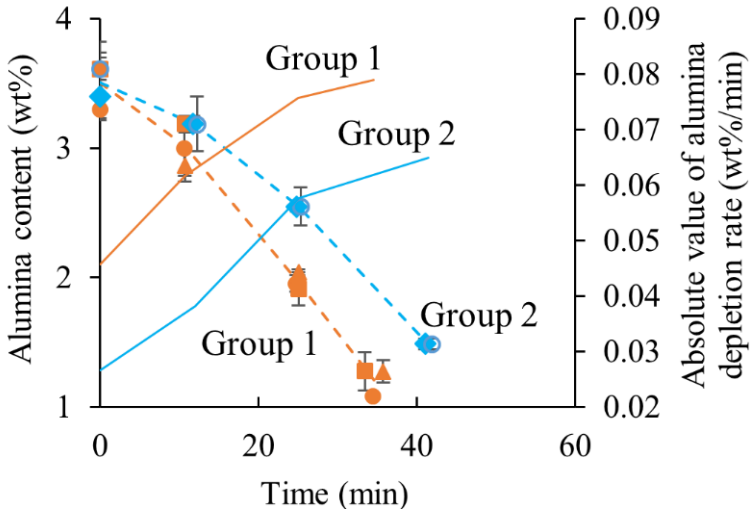

Figure 6-8. Depletion of alumina for two sets of experiments; Group 1 (■, ▲, ●); Group 2 (○, ♦); the dashed lines show the average values for the replicas; the solid lines show the absolute value of alumina depletion rate.

6.2.5 Discussion

Importance of superheat level

According to the comparative statistical analysis (see section 3.1), the most significant parameter among the three variables is the operational temperature (i.e. superheat level). The influence of superheat on the precipitation of solid species and the consequent formation of sludge is demonstrated in Figure 6-9. This figure shows that precipitation of solid species for a cell operating at an average superheat level of 9.5°C starts much later than a cell operating at a superheat level of 2.5°C.

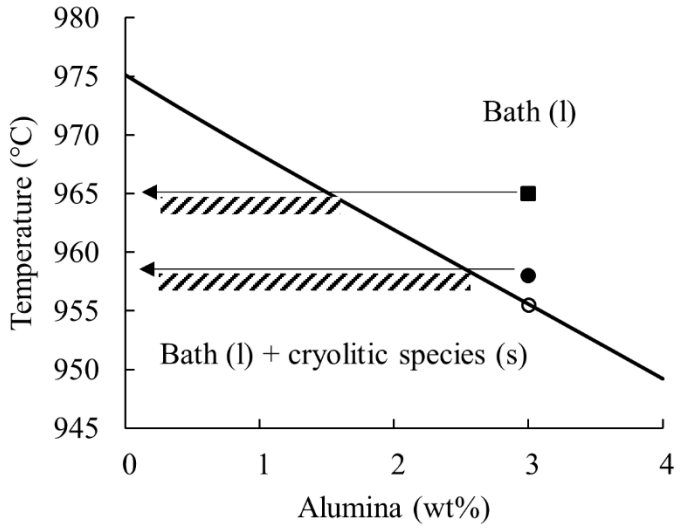

Figure 6-9. Influence of superheat level on the extent of sludge formation; ● shows a cell having superheat level of 9.5°C; ■ shows a cell having a superheat level of 2.5°C; ○ shows the liquidus temperature of the system being 955.5°C; the dashed areas show the precipitation regions.

Furthermore, the sludge tends to get higher values of CR, due to a) contact with a metal saturated in sodium, b) a cathodic block having significant amount of sodium, and c) concentration polarization on the surface of the metal. Such effects are depicted in Figure 6-10. The initial point (■) has a superheat level of ***A*** ºC. As the alumina is depleted, the system passes through the precipitation region (i.e. region ***B***) during which the solid cryolitic species precipitate. Finally, after depletion of alumina, the system reaches to the end point of the electrolysis (♦) having a final negative superheat level of ***C*** ºC. The accumulated solid cryolitic species in contact with a metal saturated in sodium as well as a cathodic block having significant amount

of sodium solidify even further ending up with a liquidus temperature about 990 ºC and a negative superheat level of ***D*** ºC.

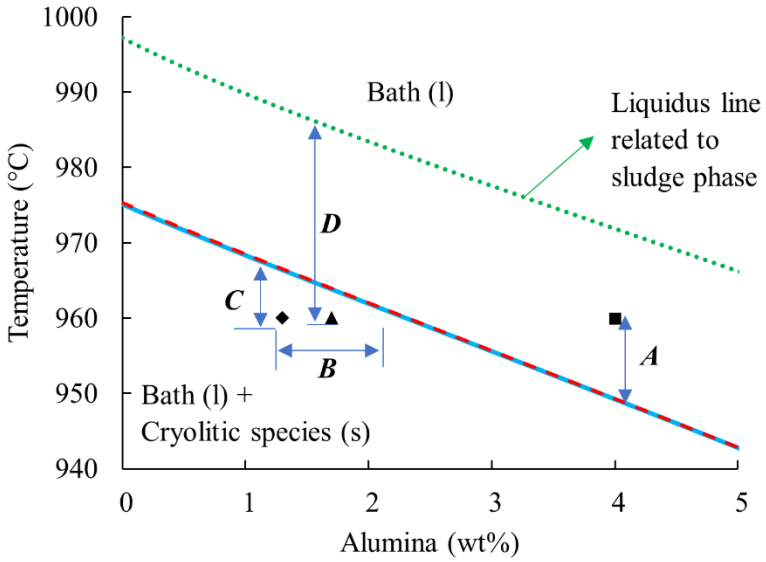

Figure 6-10. A thermodynamic system having CR = 2.2 and 5 wt% of CaF_2; initial point (■), bulk of the bath at the end of the electrolysis (♦) and sludge (▲); The solid line and dashed line show different liquidus lines at initial point and end of the electrolysis, respectively. ***A***) positive initial superheat level, ***B***) precipitation region, ***C***) negative final superheat level, ***D***) negative superheat level of the sludge

Moreover, given that at lower superheat level the percentage of the solid fraction of the bath above the metal surface is higher than tests with higher superheat, the former tests have more tendency towards sludge formation. In fact, after the start of electrolysis and reduction of interfacial tension between the metal and bath, such solid materials accumulated on the surface of the metal are more prone to sink and form sludge in comparison to the tests with higher superheat levels. Such solid particles are prone to entrain various quantities of liquid bath during their downward movement, which could explain why such deposits have different alumina contents or CRs.

Importance of CR

Comparing the volumes of sludge in each test, it was noticed that more sludge was formed during the tests with lower superheat and acidic bath chemistry. Such synergistic effect was expected given the sharp change of liquidus temperature versus the excess AlF_3 in the acidic range. Furthermore, it has been shown that in the case of acidic bath chemistry, the density of

the bath at the bath-metal interface is higher than the density of the bulk of the bath, while it is the opposite for the basic baths [Thonstad et coll., 2001]. The combination of such interfacial density difference and faster change of liquidus temperature tend to create more possibility for formation of sludge in case of acidic bath chemistry. On top of that, in case of lower superheat level, the higher amount of solid fraction in the bath above the metal pad is more prone to sediment at the bottom of the cell.

Importance of thermochemistry

According to the thermodynamic calculations obtained by using FactSage software, the only physicochemical parameters, which are statistically correlated with the superheat levels at the bottom of the cells, were the specific heat capacity and thermal conductivity of the deposits. According to Figure 6-11, as the solid fraction of the sludge increases (i.e. the sludge freezes), the specific heat capacity tends to increase, while the electrical conductivity of the solid cryolitic precipitates simultaneously decreases. The change of physicochemical properties of the sludge depends on heat loss, sodium infiltration, carbide dissolution and phase change [Utigard, 1993; James et coll., 1995; Allard et coll., 2015]. For example, given that the alumina saturation temperature for the typical sludge shown in Figure 6-11 occurs at 940.6 °C, the crystallization of alumina particles out of the bath at 940°C dramatically increases the specific heat capacity of the sludge. In addition, as the typical sludge starts to solidify, the thermal conductivity of its liquid fraction tends to increase according to Figure 6-11, considering the relevant change of mass, composition and temperature. However, given that the liquid fraction of the sludge tends to diminish during the freezing, the effect of corresponding increased thermal conductivity seems to be negligible. Moreover, the relationship between the specific heat capacity and the thermal conductivity allude to the importance of heat diffusivity of the sludge, an important parameter that requires further attention for future works by performing autopsies on the industrial samples, measuring the corresponding thermal conductivities and specific heat capacities.

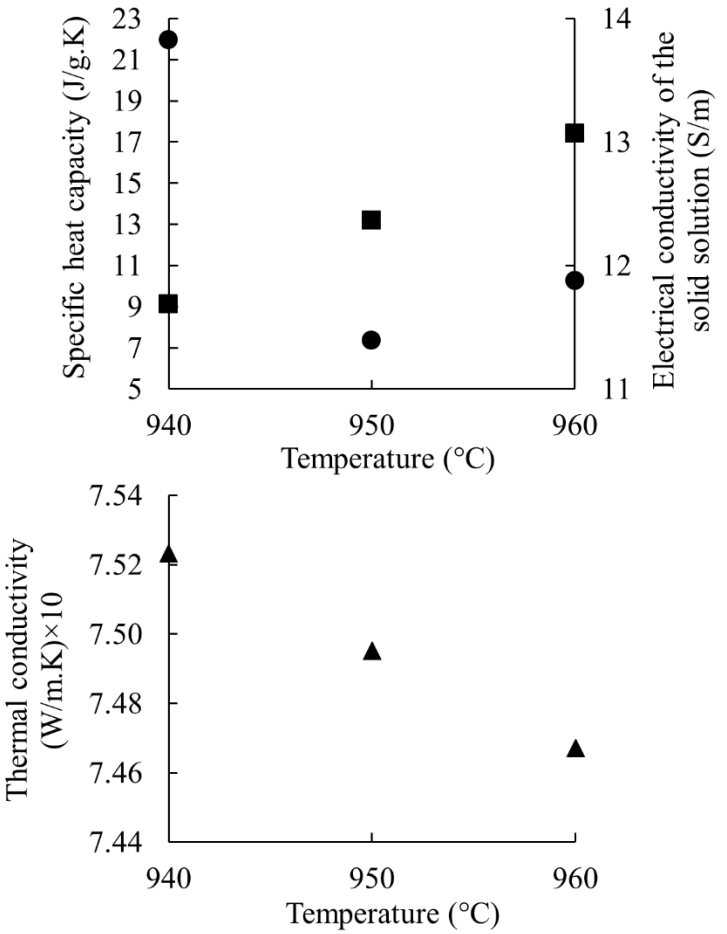

Figure 6-11. Electrical conductivity of the solid solution (■), specific heat capacity (●) and thermal conductivity of the liquid fraction at three temperatures for a typical bath containing 6.2 wt% of CaF_2, 2.9 wt% of Al_2O_3 and a CR = 2.9; the data are calculated using FactSage software.

Importance of alumina depletion rate

Comparing the average temperature profile during electrolysis at a temperature around 962 °C for the tests in Group 1, shown in Figure 6-12, it is evident that longer periods of stable electrolysis temperature lead to faster alumina depletion, which leads to faster precipitation of solid cryolitic species (i.e. faster change of liquidus temperature). The higher average voltage for tests in Group 1 compared to tests in Group 2 (i.e. 5.3 V versus 5.1 V) also leads to more heat generation. The higher amount of heat generation during the transitory period increase the liquid fraction of the bath which in return triggers a faster alumina depletion rate, hence higher rate of precipitation of bath species. Furthermore, as the electrolysis goes on, the reduction of alumina concentration increases the electrical conductivity of the bath which can increase the

alumina depletion rate even more. In addition, it must be emphasized that the anodic overvoltage, as the alumina is being depleted, can be considerable sources of heat generation inside the laboratory scale cells. Furthermore, the more stable and higher temperature in case of tests in Group 1 can lead to lower viscosity and interfacial tension which can help the submergence of precipitated solid species.

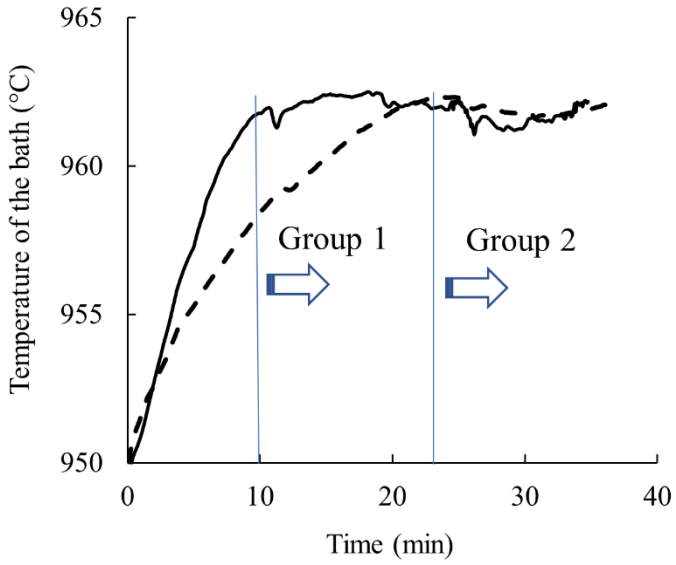

Figure 6-12. Comparison of average operational temperatures for tests in Group 1 (solid line) and tests in Group 2 (dashed line)

As for tests in Group 2, the amount of sludge for these tests is so little that makes the sampling impossible without contamination of the samples with high amount of carbide, carbon and aluminum (Figure 6-13). In this case, the overall lower superheat level during the electrolysis lead to slower consumption of alumina, hence slower crystallization rate of the bath components due to decrease of liquidus temperature. Another important factor in slower temperature profile for tests in Group 2 can be the cooling effect of the liquid aluminum. The 10 grams difference between the amounts of aluminum in two sets of tests can increase the heat transfer through the metal pad and decrease the rate of temperature evolution.

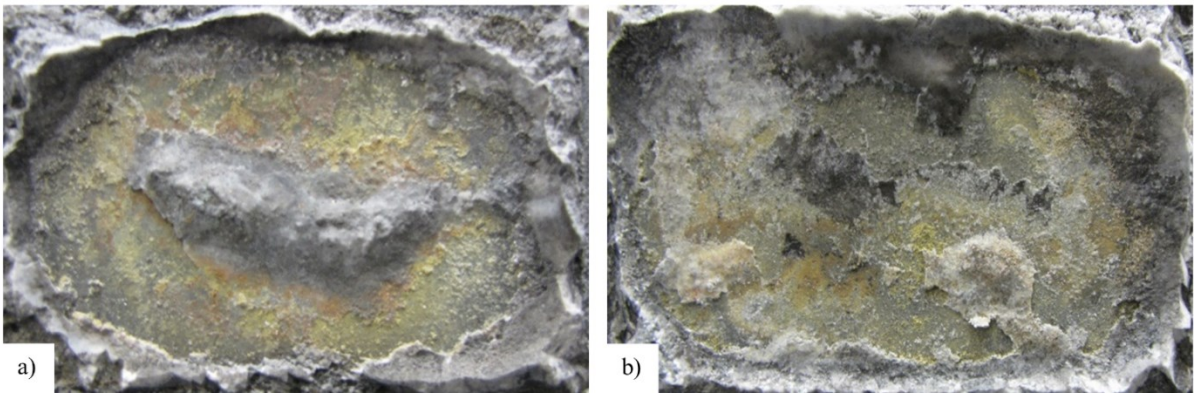

Figure 6-13. Comparison of sludge formation for two tests at average operational temperature of 960 °C and an initial CR of 2.2; a) Group 1; b) Group 2

Importance of cathode grade

The cathode grade might have un influence on solidification of the sludge depending on the position of its formation and its interactions with the carbonaceous materials. First, given the negligible temperature gradient in cathode linings of the industrial cells, the cathode lining can not have a significant impact on the solidification of the sludge through heat loss. However, if the sludge is formed close to the side walls the considerable local heat loss may freeze the sludge before being back-fed. Of course, in the latter case, the interactions of the ledge toe and the sludge must be considered. Accordingly, the cathode grade may have more influence on hardening/dissolution of sludge upon meeting sludge and not during the formation of sludge.

Secondly, looking at the industrial trends, it is evident that cells using cathode grade B have more sludge formation tendency in comparison to cells operating with cathode grade A. On top of that, industrial data also reveal that cathode B has 7-12 % more operational cathodic resistance than cathode A. Such data are consistent with the laboratory tests results that confirm cathode B, having a higher open porosity than cathode A, demonstrates a thicker layer of aluminum carbide [Landry et coll., 2018; Gheribi et coll., 2020]. Accordingly, the higher open porosity of the cathode B may provide more opportunity for interaction of the more acidic bath of the sludge and the carbonaceous species at the bottom of the cell. Moreover, the carbide layer upon interaction with the sludge is partially dissolved, which can enhance the diffusion of bath towards the carbon surface and formation of more carbide [James et coll., 1995]. The reaction of carbonaceous species with the bath and formation of more carbide, increases the CR and liquidus temperature of the bath even further [Senanu et coll., 2019]. Consequently, a thicker

frozen layer of carbide and bath will cover the bottom layer of the cathode B. The solidification of a thicker layer of the sludge creates an insulating layer, which not only hinders its dissolution, but also by decreasing the local current density decreases the local aluminum production under the sludge [Liu, 1995; Taylor, 1997; Keller, 2005]. According to Herstad et coll. [1983a; 1983b], at higher current densities, the produced aluminum droplets under the sludge can have a wedging effect and partially remove the sludge. Finally, looking at the whole picture, the sludge at the bottom of the cells using cathode B requires much longer time to be dissolved through the combination of thermal and interfacial phenomena at the bottom of the cell.

Implications for industry

Formation of unevenly distributed sludge is a major concern for the aluminum smelters due to its detrimental role in several phenomena including the cathode wear, the energy consumption, the ACD control, etc. Consequently, either the formation of sludge should be reduced or methods to dissolve the formed sludge should be developed. Irrespective of the control mechanisms such as reducing the AlF_3 addition frequency, reducing the metal pad level and increasing the superheat level, other chemical processes within the cell can also lead to partial dissolution of sludge. Such processes include the changes in the chemistry of the bath caused by changes in local CR or depletion of alumina. In an industrial cell, a sodium concentration polarization occurs due to sodium migration towards the bath-metal interface. Consequently, the local liquidus temperature increases and solid cryolitic species precipitate on the surface of the metal. What's more, a low alumina content can increase the liquidus temperature even further and enhance the solidification of the species. Coursol et coll. [2012] claim that the interfacial presence of such precipitates can hinder the transfer of oxidizing metallic species towards the bath and hence increase the current efficiency. Moreover, Solheim [2002] suggests that these cryolitic precipitates may fall to the bottom of the cell and help the dissolution of the hard muck on the surface of the cathode.

This research showed for the first time that such cryolitic solid species could precipitate and accumulate under the metal pad. The interaction of such solid cryolitic species with the alumina-rich sludge can cause the formation of a mixture with lower density than the density of the molten aluminum. Consequently, the low-density bath can be back-fed either through the metal pad or through the thin bath film that separates the metal from the side ledge. An example for

such phenomenon, let's look at the interaction of an industrial alumina rich sludge, having a CR = 2.6 with an alumina content ≈ 26% and a CaF_2 content ≈ 5%, with one of the deposits formed in this research, having a CR = 2.7 with an alumina content ≈ 2% and a CaF_2 content ≈ 5%. The latter mixture, assuming no change in CR of the mixture, can lead to the formation of a mixture having a density of 2.1 g/cm^3 which can be easily back-fed into the bulk of the bath above the metal pad. However, precipitation of such low alumina content precipitates at the bottom of the cell could also lead to the formation of solid deposits on the surface of the cathode lining if the back-feeding process is not fast enough and heat loss occurs at the bottom of the cell [Gerlach et Winkhaus, 1985].

Frankly, the important questions for industry are when and at what conditions such cryolitic precipitates can overcome the interfacial barrier between the aluminum and bath. Two factors can enhance the precipitation of solid cryolitic species on the surface of the metal pad, namely the alumina depletion rate and secondly the concentration polarization. The concentration polarization in the industry depends on the cell design, operating condition and on the convection pattern in the cell, which means the cells with more interfacial instability will have less concentration polarization [Thonstad et coll., 2001]. On the other hand, the alumina depletion rate is also a function of numerous parameters such as percentage of alumina dissolving, back-feeding of alumina and current efficiency, which are all dependent on temperature [Whitfield et coll., 2004]. On top of that, the accumulation of solid species on the surface of the metal pad creates local heat, which will eventually dissolve all or a portion of such precipitates which will in return affect the alumina depletion rate [Haupin, 1997]. In fact, the resulting fluctuation of voltage caused by accumulation and melting of such precipitates can be interpreted as rise and fall of alumina concentration in the cell [Haupin, 1997]. Moreover, Whitfield et coll. [2004] have shown that the alumina depletion rate is also a function of alumina concentration gradient (i.e. difference between the electrolyte and saturation) in the cell. The homogeneity of the alumina content in the cell is also dependent on the hydrodynamics and interfacial phenomena that occur in the system. Accordingly and considering all the above-mentioned factors, during the underfeeding period of smelters, the alumina depletion rate accompanied by the concentration polarization may cause a critical precipitation rate of cryolitic species, fast enough not only to be able to avoid melting but also to be able to surpass the local bath-metal interfacial barrier.

6.2.6 Conclusions

Among the three parameters that were included in the experimental plan design (i.e. operational temperature, CR and cathode grade), operational temperature was the only statistically significant parameter regarding the formation of sludge. The precipitation rate of the cryolitic species (i.e. chemically induced sludge) depends on sodium concentration polarization, alumina depletion rate and superheat level. The interactions between the carbide layers and the sludge can explain the increased time of back-feeding for certain cathode linings. The dissolution of alumina-rich sludge in cryolitic precipitates (i.e. chemically induced sludge) creates a mixture with lower density than the density of the molten aluminum, hence its faster back-feeding. It is most likely that synergistic effect of sodium concentration polarization and alumina consumption rate during the underfeeding period of smelters cause the precipitation of cryolitic species.

CHAPITRE 7 CONCLUSION

7.1 Sommaire

7.1.1 Importance des propriétés des blocs cathodiques

Parmi les propriétés des blocs cathodiques, deux sont les plus importantes, à savoir la conductivité thermique et la porosité ouverte. La conductivité thermique influence les différents comportements thermiques observés par rapport aux cellules expérimentales, ce qui souligne encore une fois le fait que l'équilibre thermique de la cellule est fortement influencé par le bloc cathodique. Sachant que les pertes de chaleur doivent être bien contrôlées afin de maintenir une surchauffe appropriée et limiter la formation de boues, le choix de la nuance de cathode est important car il influence directement la perte de chaleur. Cette dernière entraîne la solidification de boue au fond de la cellule, ce qui agit comme une couche d'isolation. À mesure que les boues se forment soit par agglomération d'alumine, soit par précipitation d'espèces cryolitiques, celles-ci doivent être éliminées avant que la perte de chaleur au fond de la cellule les transforme définitivement en couches solides difficiles à solubiliser et qui forment une isolation thermique.

Cependant, la conductivité thermique des blocs cathodiques n'est pas toujours constante pendant la durée de vie des cellules d'électrolyse. Celle-ci change à cause de plusieurs phénomènes, dont la pénétration du bain, la formation de couches de carbures, etc. Ces deux phénomènes sont aussi affectés, entre autres, par les porosités ouvertes des cellules. En fait, étant donné que la cathode se trouve loin de la position d'alimentation de l'alumine dans les cellules, la nuance de cathode peut exercer plus d'influence sur la solidification ou sur la dissolution de la boue après que la boue a été formée sur la cathode. Cette solidification/dissolution se produit grâce aux phénomènes d'interface, ou d'interaction avec les boues. Des boues exposées aux blocs cathodiques ont des teneurs élevées de sodium, ce qui peut induire des mouvements interfaciaux entre elles et du bain dans la cellule. D'ailleurs, des cathodes ayant des porosités ouvertes plus élevées peuvent fournir plus de possibilités d'interaction entre le bain de la boue et les espèces carbonées au fond de la cellule.

De plus, la couche de carbures lors de l'interaction avec la boue est partiellement dissoute, ce qui peut accélérer la diffusion du bain vers la surface du carbone et la formation additionnelle de carbures. La réaction des espèces carbonées avec le bain et la formation de carbure augmente

encore le ratio de cryolite et la température de liquidus du bain. Par conséquent, une couche de carbure et de bain gelé plus épaisse risque alors de couvrir la surface de la cathode. La solidification d'une couche isolante des boues non seulement entrave la dissolution de boues, mais réduit aussi la production locale d'aluminium en dessous des boues en diminuant l'intensité de courant locale. La production locale d'aluminium en dessous des boues a un effet de fendage[1] tout en enlevant partiellement les boues (Figure 7-1). Enfin, en regardant tous les faits susmentionnés, des boues formées au fond des cellules utilisant des cathodes avec des porosités ouvertes plus élevées ont besoin de plus de temps pour être dissoutes par une combinaison de phénomènes chimiques et interfaciaux.

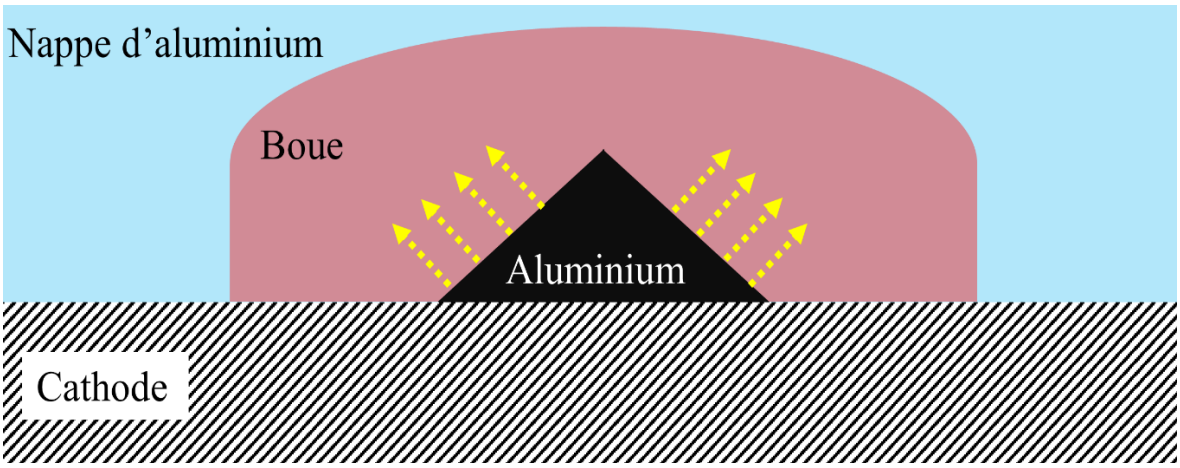

Figure 7-1. Effet de fendage à cause de la production locale d'aluminium en dessous d'une couche de boue; l'aluminium produit se comporte comme une cale (coin). Les flèches jaunes illustrent la force déployée en raison de la formation et de l'accumulation d'aluminium, ce qui enlève partiellement la boue.

7.1.2 Importance relative des paramètres d'opération

Entre les trois paramètres d'opération principaux (c'est-à-dire, la température d'opération (ou la surchauffe), le ratio de cryolite (CR) et la nuance de cathode), le plus important, par rapport à la formation ou la dissolution de boue, est la température d'opération. D'après les équilibres de phase au sein d'une cellule, la précipitation d'espèces cryolitique pour une cellule fonctionnant à un niveau de surchauffe de X commence beaucoup plus tard qu'une cellule fonctionnant à un niveau de surchauffe de Y, si X > Y.

[1] En anglais « *wedging effect* »

Également, étant donné qu'à un niveau de surchauffe inférieur, le pourcentage de la fraction solide du bain au-dessus de la surface métallique est plus élevé que les tests avec une surchauffe plus élevée, les premiers ont plus tendance à former plus de boues. En fait, après le début de l'électrolyse et la réduction de la tension interfaciale entre le métal et le bain, ces matériaux solides sont plus enclins à couler jusqu'au fond de la cellule et à former des boues. Ces particules solides sont sujettes à entraîner différentes quantités de bain liquide pendant leur chute vers le bas, ce qui pourrait expliquer pourquoi ces dépôts ont des teneurs en alumine ou CR différentes.

En comparant les volumes de boues dans chaque essai, il a été remarqué que de plus grandes quantités de boues se sont formées pendant les essais possédant une surchauffe plus faible et un bain acide (C'est-à-dire CR < 3). Un tel effet synergique était attendu compte tenu de la forte variation de la température du liquidus par rapport à l'excès d'AlF_3 dans la région acide. Par ailleurs, en cas de niveau de surchauffe inférieur, la quantité plus élevée de fraction solide dans le bain au-dessus de l'aluminium est plus sujette à précipiter au fond de la cellule. Enfin, le taux de précipitation des cryolites augmente considérablement en cas de niveaux de surchauffe inférieurs et d'excès plus élevé d'AlF_3.

7.1.3 Précipitation des espèces cryolitiques

Deux facteurs peuvent augmenter la précipitation d'espèces cryolitiques solides à la surface du métal, à savoir le taux d'épuisement de l'alumine et la polarisation de concentration. La polarisation de concentration dans l'industrie dépend de la conception de la cellule, des conditions de fonctionnement et de la convection dans la cellule. D'autre part, le taux d'épuisement de l'alumine est également fonction de nombreux paramètres, dont le pourcentage de dissolution d'alumine, le retour de l'alumine et l'efficacité de courant. De plus, le taux d'épuisement de l'alumine est également fonction du gradient de concentration d'alumine (c'est-à-dire la différence entre l'électrolyte et la saturation). L'homogénéité de la teneur en alumine dans la cellule dépend également de l'hydrodynamique et des phénomènes interfaciaux. En conséquence, pendant la période de sous-alimentation, le taux d'épuisement de l'alumine assorti de la polarisation de concentration entraîne un taux de précipitation critique des espèces cryolitiques de manière à dépasser la barrière interfaciale bain-métal.

7.2 Contributions

7.2.1 Revue sur la formation de boue concernant le procédé Hall-Héroult

Ce projet a fourni un article de journal publié dans le journal *Mineral Processing and Extractive Metallurgy Review*, ce qui servira de seule référence sur la formation de boue concernant le procédé Hall-Héroult. Il s'agit d'une revue exhaustive incluant les différents paramètres qui sont liés à la formation et à la dissolution de boue, à savoir la température d'opération (c'est-à-dire surchauffe du bain), la chimie du bain, la nuance de cathode, l'alimentation d'alumine, les propriétés de l'alumine, l'hydrodynamique et les phénomènes d'interface.

7.2.2 Nuance de cathode et formation/dissolution de boues

La nuance de cathode peut avoir une influence sur la solidification de la boue selon la position de sa formation et ses interactions avec les matériaux carbonés. Tout d'abord, vu le gradient de température négligeable des cathodes des cellules industrielles, la cathode ne peut pas affecter la solidification des boues par la perte de chaleur. Cependant, si la boue se forme près des parois latérales, la perte de chaleur locale considérable solidifie la boue. Conséquemment, au cas où la perte de chaleur cause un gradient de température considérable, la conductivité thermique de la nuance cathodique aide la perte de chaleur à travers le bloc et augmente la possibilité de solidification de la boue.

En deuxième lieu, une porosité ouverte élevée facilite l'accès du bain des boues aux espèces carbonées au fond de la cellule. En outre, la réaction des espèces carbonées avec le bain et la formation de carbure augmente encore le ratio de cryolite et la température de liquidus du bain. Par conséquent, une couche isolante de carbure et de bain solide couvre la surface de la cathode. Cette dernière, non seulement ralentit la dissolution de boues, mais en diminuant la densité de courant locale, diminue également la production locale d'aluminium en dessous de la boue qui peut montrer un effet de fendage et enlever partiellement les boues.

7.2.3 Il s'agit de surchauffe et de cinétique

Un plan d'expériences qui a été complété, a comme résultats, entre autres, le rôle significatif de la température d'opération, c'est-à-dire le niveau de surchauffe, parmi les trois variables, soit la température d'opération, le ratio de cryolite (CR) et la nuance de cathode. En outre, le taux de la précipitation d'espèces cryolitiques est lié au taux de l'épuisement de l'alumine. Dans une cellule industrielle, une polarisation de concentration et la faiblesse de la teneur en alumine

peuvent accroître la température du liquidus. Cette étude, pour la première fois, présente l'observation de ce type de matériaux solides ainsi que ses propriétés thermophysiques calculées grâce au logiciel FactSage.

7.3 Travaux à l'avenir

Les travaux suivants pourraient être entrepris :

a) Faire des autopsies en milieu industriel, afin d'observer la différence entre les couches de carbures en dessous des boues ainsi que la différence entre la production d'aluminium.

b) Réaliser des tests à l'aide des cellules transparentes « *see through* » afin d'observer des phénomènes qui arrivent à l'intérieur, dont la précipitation.

c) Mesurer en ligne la concentration de l'alumine dans le but d'avoir des tendances de l'épuisement de l'alumine plus continues.

d) Déterminer expérimentalement les propriétés thermiques des boues faute de données thermiques correspondantes.

ANNEXE A

A.1 Exposé de conférence ICSOBA 2017

A.1.1 Avant-propos

Auteurs et affiliation :

Mojtaba Fallah Fini : étudiant au doctorat, Département de génie chimique et génie biotechnologique, Université de Sherbrooke, Québec, Canada.

Gervais Soucy : professeur titulaire, Département de génie chimique et génie biotechnologique, Université de Sherbrooke, Québec, Canada.

Martin Désilets : professeur titulaire, Département de génie chimique et génie biotechnologique, Université de Sherbrooke, Québec, Canada.

Patrick Pelletier : scientifique de recherche brasquage, Solutions Technologiques Aluminium – CRDA, Rio Tinto, Québec, Canada.

Didier Lombard : champion innovation & consultant matériaux / brasquage, Solutions Technologiques Aluminium – LRF, Rio Tinto, Saint Jean de Maurienne, France.

Loig Rivoaland : responsable de projets transverses, Carbone Savoie, Vénissieux, France.

État de l'acceptation : Version finale publiée.

Revue : *Proceedings of ICSOBA Conference 2017.*

Référence : Fallah Fini et coll. [2017]

Lien d'accès : https://icsoba.org

Contributions à la thèse :

Étant un exposé concis qui traite plutôt de l'existence de problème de la boue, sa thermochimie, etc., cet article de conférence est la première revue de la littérature sur la formation de boues.

Titre français :

La formation de boues dans le procédé Hall-Héroult : un problème actuel.

Résumé :

Une revue de la littérature concise sur l'investigation de la formation de boues dans les procédés Hall-Héroult est réalisée. La formation de boues et sa transformation en dépôt cathodique résistif est l'une des préoccupations majeures des industriels. Cependant, de nos jours, en raison de l'abondance de la production, en particulier de la Chine, tous les producteurs d'aluminium doivent comprendre les phénomènes concernant ces types de dépôts. Dans cet article de conférence, le phénomène de formation de boues et son effet néfaste sur le procédé Hall-Héroult sont présentés. La thermochimie de la boue est ensuite présentée. En outre, quatre facteurs les plus importants par rapport à la formation de boues, à savoir l'hydrodynamique, la température d'opération (c'est-à-dire, le niveau de surchauffe), l'alimentation d'alumine et la chimie du bain sont présentés.

A.1.2 Sludge Formation in Hall-Héroult Process: An Existing Problem

Keywords: Hall Héroult process; hydrodynamics; sludge formation; alumina feeding strategy; bath chemistry; operational temperature

Abstract

A concise literature review is done on the industrial and laboratory scale investigations of sludge formation in the Hall Héroult Process. Formation of sludge and consequently its transformation into resistive cathodic deposits has been one of the focal concerns of the aluminum producers. However, nowadays due to the profusion of production, especially by China, all the major producers of aluminum have increased their efforts towards sludge minimization and better understanding of the phenomena that lead to formation of such deposits. In this review article, first the sludge formation phenomenon and its detrimental effect in Hall-Héroult process is introduced. Later, the thermochemistry of the sludge is presented. Furthermore, four of the most important factors in sludge formation namely hydrodynamics, operational temperature (i.e. superheat level), alumina feeding, and bath chemistry are reviewed.

Introduction

Aluminum is a strategic metal in transportation, packaging, construction, electrical industry, consumer durables and machinery [Bray, 2019]. Furthermore, recent developments in the production of aluminum batteries has created yet another potential market for the consumption of aluminum in the future [Zhang et coll., 2016]. According to the world's annual production of aluminum and its trend in recent years, China has become a formidable producer of aluminum in the last 6 years [Bray, 2018] and this has forced other producers of aluminum to try to reduce their production cost more and more by investing in research and development (R&D).

In an ideal aluminum electrolysis process and according to Faraday's law for 1 kAh of electrical current 0.3356 kg of aluminum must be produced. However, in reality, an efficiency of ≈ 95-96 % is observed [Tabereaux et Peterson, 2014]. Two major phenomena account for such a loss of efficiency. The first reason is the back reaction of solubilized aluminum ions with CO_2 gas and production of CO gas and dissolved Al_2O_3. The second major phenomenon is the formation of resistive deposits on the surface of the cathode. Such deposits not only create more resistivity against the electrical current and increase the required electrical energy, but also as it is

mentioned in the following paragraphs, contributes to the four significant factors reducing the current efficiency.

Sludge Formation and Its Drawbacks

In an ideal scenario, upon the introduction of alumina onto the cryolitic bath surface, alumina particles easily dissolve and disperse evenly at interelectrode space (i.e. distance between anode and upper surface of metal pad). Unfortunately, just like most of engineering cases, such ideal situation is hardly possible and when undissolved clumps of alumina sink to the bottom of the cell, beneath the metal pad, a dense and viscous phase called sludge is formed. According to Tabereaux et Peterson [2014], the following steps are followed upon addition of 1–2 kg of alumina particles onto the surface of bath by point feeders. At first, the particles get wetted by the bath. Later the alumina particles absorb the sensible heat and their temperature increases from 100 °C to 960 °C. At this stage, the wetted undissolved particles form agglomerates and subsequent dissolution occurs around the alumina particles creating a supersaturated local bath. Gradually most of the alumina particles dissolve into the bath and distribute in the cell by the turbulence flow. Sludge is a paste-like viscous combination of alumina particles and alumina-saturated bath. The average properties of a typical sludge sample is as follows: density of ~2 400 kg/m^3, alumina content of 20-50 wt%, AlF_3 2-10 wt%, CaF_2 2-5 wt% [Grjotheim et Kvande, 1993; Allard et coll., 2015].

Formation of sludge is not a favorable phenomenon since, it contributes to the four significant factors reducing the current efficiency, namely operational temperature, bath chemistry, current density and the stability of the metal-bath interface. A typical sludge phase with the aforementioned characteristics has an electrical conductivity of 1.0 S/cm ± 0.2, which is about twice when compared to bath and 30 000 times when compared to molten aluminum [Keller, 2005; Geay et coll., 2013]. Such electrical resistivity diverts the local current density and creates areas with higher current density and consequently higher cathode wear [Liao et Øye, 2013]. The sludge formation also consequently influences the carbide content, carbon particles dispersion, bath superheat and loss of current efficiency. Extensive sludge formation increases the occurrence of anode effect, during which the anode is poorly wetted by the electrolyte resulting in extensive carbon dusting. Presence of dispersed carbon particles in the bath not only increases the electrical resistivity of the bath (i.e. higher energy consumption) [Bugnion et

Fischer, 2016], but also by reaction with dissolved aluminum and formation of aluminum carbide, causes higher solubility of aluminum and loss of current efficiency [Wang et coll., 1994; Ødegård et coll., 2013b].

Besides, the sludge also tampers with the hydrodynamics of the cell. The higher electrical resistivity of the sludge-covered cathode area diverts the local current to flow horizontally towards the edges of the sludge. Such horizontal current flows perturb the dominant vertical current flows leading to additional instability of the metal-bath interface [Tarapore, 2013]. The oscillation of metal-bath interface has a dramatic effect on the optimum operation of the cell considering the large aspect ratio of the cell and higher resistivity of the bath compared to metal pad [Davidson et Lindsay, 1998]. Moreover, the shear amount of metal-bath interfacial stress leads to higher aluminum solubility (i.e. fogging effect), which consecutively accounts for higher back reaction and loss of current efficiency [Thonstad et coll., 2001]. In addition, such metal/bath instabilities results in change of anode-cathode distance (i.e. increasing ACD), cell voltage drop (CVD) and heat balance which dramatically affect the current efficiency and energy consumption [Welch et Kuschel, 2007].

Thermochemistry of Sludge Phase

Thermodynamics of the metallurgical systems is of great importance since it can guide the scientists to not only find the optimum pressure, temperature and compositions but also it provides an in-depth study of the interactions that happen between the cell's fluids, linings, cathode materials and impurities. The review of such systems is way out of the scope of this concise review article but avid readers are referred to references such as Thonstad et coll. [2001] and Sørlie et Øye [2010]. To our best of knowledge, the most exhaustive and specific thermodynamic study of the sludge in the aluminum electrolysis cells has been done partially by Liu [1995] and more comprehensively by Allard et coll. [2015].

The main points according to Liu [1995] could be summarized as follows: first, the dissolution of the bottom crust also known as ridge is hindered due to its insulating effect. As it is mentioned, when the cell is heated up to dissolve the cathodic deposits, this process may take few days. The reason for the delay can be partly attributed to the high temperature gradient within the cathodic deposits (5 – 10 ºC), called insulating effect of the cathodic deposits. Second,

the difference in liquidus temperatures of various sludge samples (950-964 °C) is mostly due to the CaF_2 content since excess AlF_3 has little impact on liquidus curve in the range of 0-7 wt%.

According to Allard et coll. [2015], the main chemical species of sludge samples found in industrial cells are Na_3AlF_6, $Na_5Al_3F_{14}$, $Na_2Ca_3Al_2F_{14}$ and α-alumina. If the bath is not supersaturated with alumina, addition of alumina decreases the liquidus temperature. However, as the concentration of alumina goes beyond 7 wt%, the liquidus temperature starts to rise. The melting temperature of the solid solution phase (cryolite + CaF_2 + AlF_3) is highly influenced by alumina content if it is less than 7 wt%, while at higher alumina content, an isothermal melting point of 933 °C is noticed.

The typical concentration of CaF_2 in deposits is 2-5 wt%. Based on experimental results, most of the calcium content within the deposits comes from $Na_2Ca_3Al_2F_{14}$ and $NaCaAlF_6$. $NaCaAlF_6$ can form a solid solution in α/β-cryolite. High CaF_2 content decreases the sludge solubility. Other solid calcium containing phases include $Na_2Ca_3Al_2F_{14}$ (formed at CaF_2 wt% > 10) and $Na_4Ca_4Al_7F_{33}$ (formed at high acidity). The sludge (typically containing 40 wt% alumina), may behave as a mixture of solid alumina in a liquid (at T > 933 °C) or, if heat losses are high enough as a solid phase (at T < 933 °C). In conclusion, the temperature of the cell's bottom must be kept well above 951 °C in order to keep the liquid fraction of the sludge around 70 wt% and enhance the possibility of the sludge dissolution [Allard et coll., 2015].

Important Factors in Sludge Formation/Dissolution

Formation/dissolution of sludge or central resistive cathodic deposits in aluminum electrolysis cells is correlated to several parameters such as cell's hydrodynamics, operational temperature, bath chemistry, physicochemical characteristics of alumina and feeding strategies.

a) Hydrodynamics

One of the strongest sources of agitation in the electrolysis cells is the magneto-hydrodynamics (MHD) force. Such a force is the result of the interaction between the high-amperage DC electrical current and the magnetic field created by this current. It has to be emphasized that the shearing stress at the interface of metal/bath leads to excessive dissolution of aluminum (i.e. fogging effect) and such aluminum species leads to excessive formation of carbide within the cells and further loss of current efficiency [Thonstad et coll., 2001]. In order to minimize the

detrimental effect of MHD forces, a typical layer of 25 cm of molten aluminum is maintained during the operation [Tabereaux et Peterson, 2014].

However, since the metal pad moves mostly under the influence of hydromagnetic force field, such movements may also help the back-feeding of sludge. Sludge dissolution is a long and time-consuming process since it is not in direct contact with the bulk bath. Thonstad et coll. [1980] mention that dissolution rate of sludge is approximately independent of agitation rate and diffusion controlled. On the other hand, comparing the dissolution rate of alumina particles in the industrial cells, it has been revealed that bubble induced agitation of the bath is also of great importance [Thonstad et coll., 2001]. As it is introduced in the alumina feeding strategies (section c), the diversion of anodic bubbles towards the feeding channel has enhanced the alumina dissolution.

b) Temperature

Due to the multicomponent nature of the bath and its consequences on the phase diagram, operational temperature is also related to the superheat level of the bath. The operating temperature of the modern aluminum smelters depends on the acidity of the bath and superheat level (Figure A- 1). The dissolution reaction of alumina is an endothermic process, moreover the alumina feed is at room temperature. The summation of the dissolution energy and sensible heat is enough to decrease the temperature of the melt by 15˚C if 1 wt% of alumina (with respect to total mass of the bath) is introduced into the cell [Welch et Kuschel, 2007]. Such calculations show that heat transfer within the cell is crucial for proper dissolution of the alumina and further prevention of sludge formation. Moreover, Hove et Kvande [1982] have shown that higher temperatures enhance the back-feeding of sludge. It has been well established that proper heat transfer to the alumina particles in the feeding zone is crucial for avoiding sludge formation. The preheating of the alumina particles (600 °C) for compensation of the sensible heat, has been quite effective in increasing the dissolution rate of the alumina particles (+ 80 %) but, it has shown negative effect on the dissolution rate of alumina agglomerates (- 30 %) [Kobbeltvedt, 1997]. It is claimed that the negative or negligible effect of preheating on dissolution rate of alumina agglomerates is related to the loss of moisture content [Kobbeltvedt, 1997]. The most effective parameter for the dissolution of the alumina agglomerates is the superheat level. It has been shown that a 20 °C increase of superheat level from 10 °C to 30 °C may enhance the

dissolution rate of the alumina agglomerates up to 50 % [Kobbeltvedt, 1997]. On the other side, lower superheat level can reduce the dissolution rate of the alumina agglomerates up to 35-50 % [Kuschel et Welch, 2013].

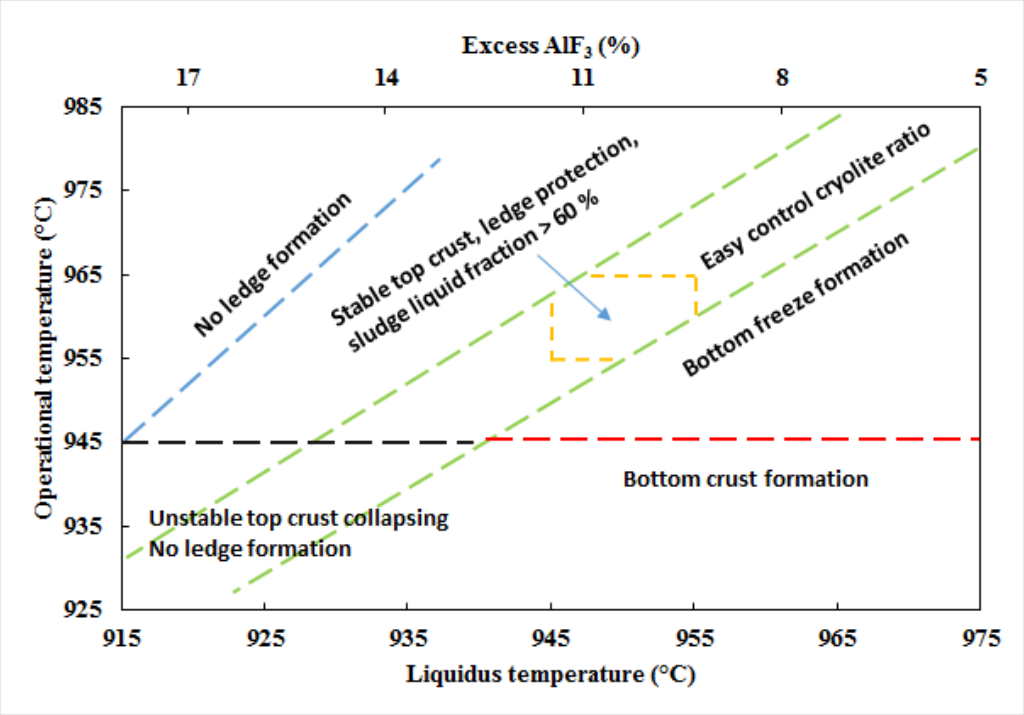

Figure A- 1. The schematic influence of temperature and bath acidity on operation of the cells; adapted from Taylor et Welch [2004] and Allard et coll. [2015].

Coulombe et coll. [2016] have investigated the influence of the heat transfer rate on sludge formation in laboratory scale set-up. It has been shown that more sludge is formed at lower heat transfer rate from the walls of an experimental cell when compared to tests with higher heat transfer rate. They justify such results by claiming that for tests with higher heat transfer rate, more cryolite is precipitated and an extended ledge toe is formed. Such ledge toe extension links to the sludge and creates a less dense liquid (compared to aluminum) with lower liquidus temperature, which in turn helps the dissolution of the sludge. The influence of proper heat transfer in avoiding the formation of alumina agglomerate/sludge or enhancing its dissolution is linked to proper turbulence of the bath at feeding zone.

c) Physico-chemical characteristics of alumina and alumina feeding strategy

Tabereaux et Peterson [2014] have summarized some of the most important characteristics of alumina feed. Such factors include angle of repose of 33-35 °C, attrition index of 10–15 %, fines

(≤ 45 μm) in fraction of 6-8 wt%, superfines (≤ 20 μm) in fraction of 0.5-3 wt%, α-alumina content of 2-15 wt%, moisture content of 0.65-0.90, surface area (BET) 60–80 m^2/g, loose density of 0.96 g/cm^3 and a vibrated bulk density of 1.1 g/cm^3. Besides, the saturation concentration of alumina in the bath (i.e. NaF-AlF_3-CaF_2-alumina system) is around 7-8 wt% depending on the acidity of the bath in the range of 6-16 wt% of AlF_3.

As Grjotheim et Kvande [1993] indicate, the normal grain size of the alumina feed is 20-150 μm. Big particles do not dissolve properly within bath while fine particles create fume emission and difficulty in mechanical handling. Coarse particles (≥ 100 μm) fraction is usually < 15 wt% (preferably 2-7 %) whereas fine particles (≤ 45 μm) fraction is usually < 20 % (preferably 3-8 wt%). Superfine particles (≤ 20 μm) fraction is also very important and its preferential content is circa 0.5 wt%. The finer particles create top crusts with shorter lifetime yet the density of the crusts will be higher than the ones made from coarse particles [Gerlach et Winkhaus, 1985]. Fine particles dissolve individually faster than coarse particles but the poor wetting properties of fine particles as a bulk lead to a slower dissolution [Isaeva et coll., 2009]. Due to such poor wetting properties, electrolyte cannot penetrate within the intergranular voids and instead, finer particles fill the voids between the coarser particles and the rafts float for a much longer time before dissolving [Isaeva et coll., 2009]. Moreover, fine particles contain larger amount of α-alumina compared to the bulk of the feed alumina which also causes a hard-to-dissolve top crust/raft/agglomerates [Metson et coll., 2005]. On the other hand, it has been claimed that there is no correlation between the size of the alumina particles (or median size) and dissolution rate [Maeda et coll., 1985; Bagshaw et Welch, 2013]. Wang [2009] has categorized some of the different results on the influence of alumina particle size on the dissolution rate.

The porosity of primary alumina is in general around 75 % and it does not have any significant influence on the dissolution behaviour [Grjotheim et Kvande, 1993]. As it is mentioned in section b), the preheating of alumina to low temperatures (100 – 300 ºC) has a detrimental effect on the dissolution rate of alumina. This phenomenon is related to the loss on ignition (LOI) [Kobbeltvedt, 1997]. The volatile content of the alumina not only causes more turbulence by eruptive behaviour of evolved gases, but also reduces the flow funnel time of the alumina particles, leading to better dispersion and enhanced mass/heat transfer [Welch et Kuschel, 2007]. According to Wang [2009], there are different research results pertaining to the effect of the surface area on alumina particles' dissolution rate. Some results indicate that higher surface area

enhances the dissolution rate [Bagshaw et Welch, 2013] whereas some other mention that surface area has negligible effect on the dissolution rate [Jain et coll., 1983b]. Nevertheless, there is a strong relationship between the LOI and the specific surface area of alumina particles [McGeer et Zwicker, 1982]. Some of the research show that higher α-alumina content and coarser particles tend to increase the dissolution rate while some other researches show that there is no correlation between the particle size distribution and the dissolution rate [Wang, 2009]. Such contradictory results may be due to the numerous factors that affect the alumina dissolution such as the physical, chemical, morphological and microstructural traits of fed alumina, as well as the dynamics of the feeding process, the chemistry of the electrolyte, and the superheat level of the bath [Tabereaux et Peterson, 2014].

Smelting grade alumina (SGA) typically consists mostly of γ-alumina (also known as sandy alumina) with a 2 – 15 wt% of α-alumina (also known as floury alumina) [Tabereaux et Peterson, 2014]. The type pf alumina is important since γ-alumina has a lower flow funnel time, higher surface area and higher dissolution rate which makes it more ideal for aluminum electrolysis cells. Upon addition to the melt, γ-alumina exothermally transforms into α-alumina, which is less soluble, and later, endothermally dissolves within the bath. γ-alumina transformation into α-alumina creates thin plates (*ca.* 0.5 µm) while thicker alumina plates (*ca.* 1.5 µm) are the initial feed α-alumina content that has precipitated without dissolution and act as building blocks of the agglomerates [Thonstad et coll., 2001]. Also it has to be emphasized that as time goes on and with the aid of heat loss, the alumina platelets within the sludge start to grow by crystallization of alumina-saturated interstitial bath of the agglomerates [Kachanovskaya et Arakelyan, 1976].

According to Hove et Kvande [1982], there is a direct relationship between the feeding strategy, anode effect and sludge formation. It means that the state of sludge formation is related to the volume of the batch of fed alumina, rate of the feeding and duration of feeding time. For example, in the worst-case scenario, a huge volume of alumina fed at a high rate and short duration of time may increase the sludge formation and leads to anode effect.

One of the most significant inventions in the Hall-Héroult process was the introduction of point feeders in the 1960s in the USA [Tarcy et coll., 2011]. Point feeders use 2-6 holes (punched by 6-10 cm rods) through the top crust to administer approximately 1-5 kg of alumina per each

feeder pipe per one minute or so [Tarcy et coll., 2011; Lavoie et coll., 2016]. Such an approach simultaneously minimizes the sludge formation and dusts/fluorides emission and has led to anode effect frequency of less than 0.02 per pot per day [Taylor et Welch, 2004].

Nevertheless, point feeders have their own drawbacks. One of the drawbacks of push-feeding is the fluctuation of the alumina content as the crust breaker can't introduce all the feed that hopper has added [Kobbeltvedt, 1997]. The crust breaker is used to push-feed the alumina into the bath when the feeding holes are closed by piled-up alumina [Lavoie et coll., 2016]. The piled-up alumina is prone to get sintered into α-alumina and particles' clotting [Kobbeltvedt, 1997], which not only hinder the alumina dissolution process but also increase the possibility of sludge formation. So, one of the most important factors in avoiding the formation of sludge is to keep the feeding holes open.

In order to do so, one approach is to increase the bath turbulence and dissolution rate of the fed alumina by diverting the anodic gases towards the feeding zone [Moxnes et coll., 1998]. Finally, some improvement of feeding pipe design and increasing the delivery height of the feed release has been practiced to not only reduce the feeding rate of the alumina but also increase the penetration depth of the alumina particles into the bath [Bagshaw et coll., 1985; Tessier et coll., 2013].

d) Bath chemistry

The chemistry of the bath is a significant parameter in the normal operation of the electrolysis cells and as it is well established it is interlinked with the current efficiency and environmental issues [Welch, 2007]. Among the 10 most important breakthroughs and developments in industrial aluminum process, three distinct parameters are directly related to the chemistry of the bath, namely point feeding technology, computer controlling of the cell and higher AlF_3 bath chemistry [Tarcy et coll., 2011]. The point feeding technology tries to create a low level of alumina content (1-5 wt%) while using the line amperage and cell's resistivity as a method to monitor alumina content. Higher acidity of the bath was first tried in 1950s and when it showed potential for improvement of current efficiency, it became a cornerstone of next generations of cells [Holmes, 1995].

A typical electrolysis cell uses 9-11 wt% AlF_3, 4-6 wt% CaF_2, 1.5-4 wt% Al_2O_3 and in some cases 2-4 wt% MgF_2/LiF [Tabereaux et Peterson, 2014]. The application of LiF and MgF_2 is to

reduce the aluminum solubility in the bath and hence increase the current efficiency [Bosshard et coll., 1983]. It has been shown that with the addition of LiF (2-4 wt%) or AlF_3 (10 wt%), no significant change in the pattern of bottom crust formation is noticed; however, industrial tests have shown that the usage of lithium fluoride or low cryolite ratios exacerbates the bottom crust formation [Thonstad et coll., 1982]. A summary of the effects of various additives on the physicochemical properties of the bath has been presented by Habashi [2003]. Moreover, the influence of impurities such as silica and iron oxide is reviewed by other references [Grjotheim et coll., 1982; Thonstad et coll., 2001].

All of the common additives (i.e. LiF, NaF, CaF_2, MgF_2 and AlF_3) reduce the liquidus temperature of the bath [Haupin, 1991]. The reduction of liquidus temperature is a beneficial phenomenon since it reduces the operating temperature and enhances the current efficiency [Bosshard et coll., 1983]. This is also beneficial since at constant operating temperature, lower liquidus temperature (i.e. higher superheat level), reduces the chance of sludge solidification. On the other hand, almost all the aforementioned common additives reduce the solubility of alumina which enhances the possibility of sludge formation.

The chemistry of the bath also defines the viscosity and density of the bath which are among the parameters that affect the current efficiency [Grjotheim et coll., 1985]. Lower density of the bath consequently reduces the density of the alumina-bath agglomerates, hence hindering the sludge formation [Keller, 1984]. Since the density of aluminum pad (2.3 kg/L) does not change significantly with temperature within the range of 940-970 ˚C, most of the density difference is accounted for by the cryolitic melt. Preferably a density difference > 0.2 kg/L provides a proper immiscibility between the metallic and cryolitic melts [Grjotheim et Kvande, 1993: p. 53]. Besides, lower bath densities specially in the case of lithium containing systems can create carbon particles accumulation at the metal-bath interface (also known as carbonation) [Coursol et coll., 2012]. Presence of carbon particles in the system may lead to increased bath electrical resistivity and loss of current efficiency [Grjotheim et coll., 1982]. In addition to density, viscosity of the electrolyte also affects the hydrodynamics of fluids influencing phenomena such as gas bubble detachment and precipitation of undissolved alumina agglomerates [Haupin, 1991]. A high viscosity not only can reduce the transfer rate of dissolved aluminum leading to less back reaction and higher current efficiency [Robelin et Chartrand, 2011], but also can reduce the terminal velocity of the alumina agglomerates.

After alumina particles agglomerate and sink through the bath, there is yet another barrier (i.e. interface of metal/melt) to cross before they reach the surface of the cathode block. All common additives increase the metal/melt interfacial tension. Lower cryolite ratios and higher alumina contents also increase the interfacial tension while the bath is not saturated with alumina [Thonstad et coll., 2001]. In addition to the aforementioned factors, evaporation of volatile species also affects the chemistry of the bath. The most volatile species are the sodium and aluminum fluoride or the combination of these species as $NaAlF_4$ [Grjotheim et Kvande, 1993]. Evaporation of such chemicals changes the cryolite ratio and it is required to control the bath chemistry by introduction of fresh materials. High cryolite ratio increases the liquidus temperature and consequently the sludge finds more opportunities to transform into solid deposit [Allard et coll., 2014a].

Conclusion

Hall-Héroult process has gone through numerous adjustments since its commercialization at the end of 19^{th} century. Such adjustments include modification of the bath chemistry, sophisticated control and feeding systems, application of novel refractory materials, development of new cathode materials, magnetic field compensation, optimization of anode effect frequency, etc. Such adjustments all had one aim and it was to increase the current efficiency. According to Welch [2007], each of the former adjustments have increased the current efficiency up to 2 % and nowadays a typical current efficiency of ~ 96 % is practical [Taylor et Welch, 2004]. But if the aim of the aluminum industry is to reach a current efficiency of 97 % by 2020 [Kvande, 2011], a better understanding of the phenomena that cause loss of current efficiency is necessary. Maybe one of the oldest and still existing problems of the aluminum smelters is the sludge formation. Presence of sludge dramatically reduces the current efficiency by tampering with operational temperature, bath chemistry, current density and stability of the metal-bath interface. This concise review article tries to provide a reminder on the existing problem of sludge formation (a.k.a muck) and hopes to motivate young scientists and engineers to pull the aluminum industry out of sludge.

LISTE DES RÉFÉRENCES

Abd El All, S., Gerlach, J. & Hennig, U. 1980. Interactions between powdered alumina and fluoride melts with regard to the properties of the reaction products. *Erzmetall,* 33(10), pp. 504-509.

Allard, F., Coulombe, M.-A., Soucy, G. & Rivoaland, L. 2014a. Cartography and chemical composition of the different deposits in the hall-heroult process. *In:* Grandfield, J., (éd.) Light Metals 2014. Hoboken, NJ, É.-U.: John Wiley & Sons, Inc., pp. 1233-1238, https://doi.org/10.1002/9781118888438.ch206.

Allard, F., Soucy, G. & Rivoaland, L. 2014b. Formation of deposits on the cathode surface of aluminum electrolysis cells. *Metallurgical and Materials Transactions B,* 45(6), pp. 2475-2485, https://doi.org/10.1007/s11663-014-0118-8.

Allard, F., Soucy, G., Rivoaland, L. & Désilets, M. 2015. Thermodynamic and thermochemical investigation of the deposits formed on the cathode surface of aluminum electrolysis cells. *Journal of Thermal Analysis and Calorimetry,* 119(2), pp. 1303-1314, https://doi.org/10.1007/s10973-014-4288.

AluQuébec. 2019. *Primary production* [En ligne]. : The Quebec Aluminium industrial cluster. Disponible : https://www.aluquebec.com/en/aluminium-cluster/primary-production [Page consultée le 2019-07-15].

Archer, A. M. 1983. Considerations in the selection of alumina for smelter operation. *JOM,* 35(9), pp. 43-46, https://doi.org/10.1007/BF03338364.

Archer, A. M. 2013. Considerations in the selection of alumina for smelter operation. *In:* Bearne, G., Dupuis, M. & Tarcy, G. (éds.) *Essential Readings in Light Metals.* Vol. 2, Hoboken, NJ, É.-U.: John Wiley & Sons, Inc., pp. 569-573, https://doi.org/10.1002/9781118647851.ch84.

Bagshaw, A. N., Kuschel, G., Taylor, M. P., Tricklebank, S. B. & Welch, B. J. 1985. Effect of operating conditions in the dissolution of primary and secondary (reacted) alumina powders in electrolytes. *In:* Bohner, H. O., (éd.) Light Metals 1985. Warrendale, PA, É.-U.: The Metallurgical Society of AIME, pp. 649-659.

Bagshaw, A. N. & Welch, B. J. 2013. The Influence of alumina properties on Its dissolution in smelting electrolyte. *In:* Donaldson, D. & Raahauge, B. E. (éds.) *Essential Readings in Light Metals.* Vol. 1, Hoboken, NJ, É.-U.: John Wiley & Sons, Inc., pp. 783-787, https://doi.org/10.1002/9781118647868.ch107.

Bosshard, E., Knaisch, O., Schmidt-Hatting, W. & Blanc, J. M. 1983. EPT 18: the new 180-ka-pot of alusuisse. *In:* Adkins, E. M., (éd.) Light Metals 1983. Warrendale, PA, É.-U.: The Metallurgical Society of AIME, pp. 595-605.

Brand, A., Allen, L., Altman, M., Hlava, M. & Scott, J. 2015. Beyond authorship: attribution, contribution, collaboration, and credit. *Learned Publishing,* 28(2), pp. 151-155, https://doi.org/10.1087/20150211.

Brassard, M., Soucy, G., Désilets, M. & Lombard, D. 2016. Impact of aluminium pad and operation parameters on graphitised and graphitic cathodes expansion and bath penetration. *Canadian Metallurgical Quarterly,* 55(3), pp. 356-364, https://doi.org/10.1080/00084433.2016.1195052.

Bray, E. L. 2018. *Aluminum Statistics and Information* [En ligne]. : U.S. Geological Survey. Disponible : https://www.usgs.gov/centers/nmic/aluminum-statistics-and-information [Page consultée le 2018-05-13].

Bray, E. L. 2019. Aluminum. *Mineral Commodity Summaries 2019.* É.-U.: U.S. Geological Survey, pp. 20-21, https://doi.org/10.3133/70202434.

Bugnion, L. & Fischer, J. C. 2016. Effect of carbon dust on the electrical resistivity of cryolite bath. *In:* Williams, E., (éd.) Light Metals 2016. Hoboken, NJ, É.-U.: John Wiley & Sons, Inc., pp. 587-591, https://doi.org/10.1002/9781119274780.ch99.

Charette, A. & Kocaefe, Y. S. 2012. *Le carbone dans l'industrie de l'aluminium,* Chicoutimi, QC, Canada: Les Presses de l'aluminium, 325 p.

Coulombe, M.-A., Soucy, G., Rivoaland, L. & Davies, L. 2016. Factors leading to the formation of a resistive thin film at the bottom of aluminum electrolysis cells. *Metallurgical and Materials Transactions B,* 47(2), pp. 1280-1295, https://doi.org/10.1007/s11663-015-0567-8.

Coursol, P., Dufour, G., Coté, J., Chartrand, P. & Mackey, P. 2012. Application of Thermodynamic Models for Better Understanding and Optimizing the Hall-Heroult Process. *JOM,* 64(11), pp. 1326-1333, https://doi.org/10.1007/s11837-012-0426-x.

Dando, N., Wang, X., Sorensen, J. & Xu, W. 2010. Impact of thermal pretreatment on alumina dissolution rate and HF evolution. *In:* Johnson, J. A., (éd.) Light Metals 2010. Warrendale, PA, É.-U.: Minerals, Metals and Materials Society, pp. 541-546.

Dassylva-Raymond, V., Kiss, L. I., Poncsak, S., Chartrand, P., Bilodeau, J. F. & Guérard, S. 2014. Modeling the Behavior of Alumina Agglomerate in the Hall-Héroult Process. *In:* Grandfield, J., (éd.) Light Metals 2014. Hoboken, NJ, É.-U.: John Wiley & Sons, Inc., pp. 603-608, https://doi.org/10.1002/9781118888438.ch102.

Davidson, P. A. & Lindsay, R. I. 1998. Stability of interfacial waves in aluminium reduction cells. *Journal of Fluid Mechanics,* 362, pp. 273-295, https://doi.org/10.1017/S0022112098001025.

Dewing, E. W. & Desclaux, P. 1977. The interfacial tension between aluminum and cryolite melts saturated with alumina. *Metallurgical Transactions B,* 8(3), pp. 555-561, https://doi.org/10.1007/bf02658622.

Djukanovic, G. 2018. *Aluminium: Year in Review and What to Expect in 2019* [En ligne]. : . Disponible : https://aluminiuminsider.com/aluminium-year-in-review-and-what-to-expect-in-2019/ [Page consultée le 2019-06-19].

Dreyfus, J.-M. & Joncourt, L. 1999. Erosion mechanisms in smelters equipped with graphite blocks. A mathematical modeling approach. *In:* Eckert, C. E., (éd.) Light Metals 1999. Warrendale, PA, É.-U.: Minerals, Metals & Materials Society, pp. 199-206.

Einarsrud, K. E., Skybakmoen, E. & Solheim, A. 2016. On the Influence of MHD Driven Convection on Cathode Wear. *In:* Grandfield, J., (éd.) Light Metals 2014. Cham, Suisse: Springer International Publishing, pp. 485-490, https://doi.org/10.1007/978-3-319-48144-9_82.

Fallah Fini, M., Landry, J.-R., Soucy, G., Désilets, M., Pelletier, P., Rivoaland, L. & Lombard, D. 2020a. Sludge Formation in Hall–Héroult Cells: Drawbacks and Significant Parameters. *Mineral Processing and Extractive Metallurgy Review,* 41(1), pp. 59-74, https://doi.org/10.1080/08827508.2018.1536658.

Fallah Fini, M., Soucy, G., Désilets, M., Lombard, D., Pelletier, P. & Paulus, R. 2020b. On the problem of sludge formation in Hall-Héroult process. *Minerals Engineering,* en révision.

Fallah Fini, M., Soucy, G., Désilets, M., Pelletier, P., Lombard, D. & Rivoaland, L. 2017. Sludge formation in Hall-Héroult Process: an existing problem. Proceedings of ICSOBA 2017 Conference. Hamburg, Germany: ICSOBA, pp. 987-996.

Feret, F. R. 2008. Breakthrough in analysis of electrolytic bath using Rietveld-XRD method. *In:* Deyoung, D. H., (éd.) Light Metals 2008, Warrendale, PA, USA. : The Minerals, Metals & Materials Society, pp. 343-346.

Gasik, M. M. & Gasik, M. I. 2003. Smelting of aluminum. *In:* Totten, G. E. & MacKenzie, D. S. (éds.) *Handbook of Aluminum.* Vol. 2, NY, É.-U.: Marcel Dekker, pp. 47-79, https://doi.org/10.1201/9780203912607.

Geay, P.-Y., Welch, B. J. & Homsi, P. 2013. Sludge in operating aluminum smelting cells. *In:* Bearne, G., Dupuis, M. & Tarcy, G. (éds.) *Essential Readings in Light Metals.* Vol. 2, Hoboken, NJ, É.-U.: John Wiley & Sons, Inc., pp. 222-228, https://doi.org/10.1002/9781118647851.ch32.

Gerlach, J., Hennig, U. & Kern, K. 1975. The dissolution of aluminum oxide in cryolite melts. *Metallurgical and Materials Transactions B,* 6(1), pp. 83-86, https://doi.org/10.1007/bf02825681.

Gerlach, J. & Winkhaus, G. 1985. Interactions of alumina with cryolite-based melts. *In:* Bohner, H. O., (éd.) Light Metals 1985, Warrendale, PA, USA. : The Metallurgical Society of AIME, pp. 301-313.

Gheribi, A. E., Fallah Fini, M., Rivoaland, L., Lombard, D., Soucy, G. & Chartrand, P. 2020. Cathodic Wear by Delamination of the Al4C3 Layer During Aluminium Electrolysis.

Metallurgical and Materials Transactions B, 51(1), pp. 161–172, https://doi.org/10.1007/s11663-019-01731-9.

Grjotheim, K., Haupin, W. E. & Welch, B. J. 1985. Current efficiency - relating fundamental studies to practice. *In:* Bohner, H. O., (éd.) Light Metals 1985. Warrendale, PA, É.-U.: The Metallurgical Society of AIME, pp. 679-694.

Grjotheim, K., Krohn, C., Malinovský, K., Matiašovský, J. & Thonstad, J. 1982. *Aluminium Electrolysis: Fundamentals of the Hall-Héroult Process,* Düsseldorf, Allemagne: Aluminium-Verlag, 443 p.

Grjotheim, K. & Kvande, H. (éds.) 1993. *Introduction to Aluminium Electrolysis: Understanding the Hall-Héroult Process,* Düsseldorf, Allemagne: Aluminium-Verlag GmbH, 260 p.

Grjotheim, K. & Welch, B. J. 1989. Technological developments for aluminum smeltinq as the industry enters the 21st century. *JOM,* 41(11), pp. 12-16, https://doi.org/10.1007/bf03220378.

Grjotheim, K., Welch, B. J. & Taylor, M. P. 1989. Relating operating strategy and performance in aluminium smelting cells - an overview. *In:* Campbell, P. G., (éd.) Light Metals 1989. Warrendale, PA, É.-U.: The Metallurgical Society of AIME, pp. 255-260.

Habashi, F. 2002. Hall, Heroult and the production of aluminum. *CIM Bulletin,* 95(1062), pp. 109-113.

Habashi, F. 2003. Extractive metallurgy of aluminum. *In:* Totten, G. E. & MacKenzie, D. S. (éds.) *Handbook of Aluminum.* Vol. 2, NY, É.-U.: Marcel Dekker, pp. 1-45, https://doi.org/10.1201/9780203912607.

Haraldsson, J. & Johansson, M. T. 2018. Review of measures for improved energy efficiency in production-related processes in the aluminium industry – From electrolysis to recycling. *Renewable and Sustainable Energy Reviews,* 93, pp. 525-548, https://doi.org/10.1016/j.rser.2018.05.043.

Haupin, W. 1991. The influence of additives on Hall-Héroult bath properties. *JOM,* 43(11), pp. 28-34, https://doi.org/10.1007/BF03222717.

Haupin, W. 1997. Understanding boundary layers. *In:* Huglen, R., (éd.) Light Metals 1997. Warrendale, PA, É.-U.: The Minerals, Metals & Materials Society, pp. 319-323.

Herstad, O., Krohn, C. H., Sørlie, M. & Øye, H. A. 1983a. Precipitation of alumina and aluminum carbide during electrolysis of cryolite-alumina melts. *In:* Adkins, E. M., (éd.) Light Metals 1983. Warrendale, PA, É.-U.: The Metallurgical Society of AIME, pp. 347-356.

Herstad, O., Krohn, C. H., Sørlie, M. & Øye, H. A. 1983b. Precipitation of solid components during electrolysis of cryolite-alumina melts. *Aluminium,* 59(3), pp. 200-206.

Holmes, G. T. 1995. Hall cell ampere efficiency up 12% in 3 decades. *In:* Evans, J. W., (éd.) Light Metals 1995. Warrendale, PA, É.-U.: The Minerals, Metals & Materials Society, pp. 371-373.

Hove, S. J. & Kvande, H. 1982. Center-break alumina feeding and sludge control of prebaked cells. *In:* Andersen, J. E., (éd.) Light Metals 1982. Warrendale, PA, É.-U.: The Metallurgical Society of AIME, pp. 513-529.

International-Aluminium-Institute. 2019. *Primary aluminium smelting energy intensity* [En ligne]. : The International Aluminium Institute. Disponible : http://www.world-aluminium.org/ [Page consultée le 2019-07-15].

Isaeva, L. A., Braslavskii, A. B. & Polyakov, P. V. 2009. Effect of the content of the α-phase and granulometric composition on the dissolution rate of alumina in cryolite-alumina melts. *Russian Journal of Non-Ferrous Metals,* 50(6), pp. 600-605, https://doi.org/10.3103/S1067821209060078.

Jain, R. K., Taylor, M. P., Tricklebank, S. B. & Welch, B. J. 1983a. A study of the relationship between the properties of alumina. Its interaction with aluminium smelting electrolytes. Proceedings of the 1st International Symposium on Molten Salt Chemistry and Technology. Kyoto, Japon: Electrochemical Society of Japan, pp. 59-64.

Jain, R. K., Tricklebank, S. B., Welch, B. J. & Williams, D. J. 1983b. Interaction of aluminas with aluminium smelting electrolytes. *In:* Adkins, E. M., (éd.) Light Metals 1983. Warrendale, PA, É.-U.: The Metallurgical Society of AIME, pp. 609-622.

James, B. J., Welch, B. J., Hyland, M. M., Metson, J. B. & Morrison, C. D. 1995. Interfacial processes and the performance of cathode linings in aluminum smelters. *JOM,* 47(2), pp. 22-25, https://doi.org/10.1007/BF03221401.

Kachanovskaya, I. S. & Arakelyan, O. I. 1976. Behavior of alumina in the deposits and crust of an aluminum electrolytic cell. *Tsvetnye Metally,* (4), pp. 37-40.

Kalgraf, K. & Torklep, K. 1998. Sediment transport and dissolution in Hall-Heroult Cells. *In:* Welch, B., (éd.) Light Metals 1998. Warrendale, PA, É.-U.: Minerals, Metals & Materials Society, pp. 455-464.

Keller, R. 1984. Alumina dissolution and sludge formation. *In:* McGeer, J. P., (éd.) Light Metals 1984. Warrendale, PA, É.-U.: The Metallurgical Society of AIME, pp. 513-518.

Keller, R. 2005. Alumina dissolution and sludge formation revisited. *In:* Kvande, H., (éd.) Light Metals 2005. Warrendale, PA, É.-U.: The Minerals, Metals & Materials Society, pp. 147-150.

Keller, R., Burgman, J. W. & Sides, P. J. 1988. Electrochemical reactions in the Hall-Heroult cathode. *In:* Boxal, L. G., (éd.) Light Metals 1988. Warrendale, PA, É.-U.: The Metallurgical Society of AIME, pp. 629-631.

Kheiri, M., Gerlach, J., Hennig, U. & Kammel, R. 1987. Formation and behavior of crusts and bottom sludge in alumina reduction electrolysis. *Erzmetall,* 40(3), pp. 127-131.

Kobbeltvedt, O. 1997. Dissolution Kinetics for Alumina in Cryolite Melts. Distribution of Alumina in the Electrolyte of Industrial Aluminium Cells. PhD Thesis, Norwegian University of Science and Technology. Trondheim, Norvège, 191 p.

Kobbeltvedt, O. & Moxnes, B. P. 2013. On the bath flow, alumina distribution and anode gas release in aluminium cells. *In:* Bearne, G., Dupuis, M. & Tarcy, G. (éds.) *Essential Readings in Light Metals.* Vol. 2, Hoboken, NJ, É.-U.: John Wiley & Sons, Inc., pp. 257-264, https://doi.org/10.1002/9781118647851.ch37.

Kobbeltvedt, O., Rolseth, S. & Thonstad, J. 1996. On the mechanisms of alumina dissolution with relevance to point feeding aluminium cells. *In:* Hale, W., (éd.) Light Metals 1996. Warrendale, PA, É.-U.: The Minerals, Metals & Materials Society, pp. 421-427.

Korenko, M. 2008. Interfacial Tension between Aluminum and Cryolite Alumina Melts. *Journal of Chemical & Engineering Data,* 53(3), pp. 794-797, https://doi.org/10.1021/je700652x.

Kuschel, G. I. & Welch, B. J. 2013. Further studies of alumina dissolution under conditions similar to cell operation. *In:* Bearne, G., Dupuis, M. & Tarcy, G. (éds.) *Essential Readings in Light Metals.* Vol. 2, Hoboken, NJ, É.-U.: John Wiley & Sons, Inc., pp. 112-118, https://doi.org/10.1002/9781118647851.ch15.

Kvande, H. 2011. Production of primary aluminium. *In:* Lumley, R. (éd.) *Fundamentals of Aluminium Metallurgy: Production, processing and applications.* Cambridge, R.-U.: Woodhead Publishing, pp. 49-69, https://doi.org/10.1533/9780857090256.1.49.

Kvande, H., Chen, J. & Haupin, W. E. 1994. Minimizing energy consumption through optimizing alumina concentration in the bath of Hall-Heroult Cells. *In:* Mannweiler, U., (éd.) Light Metals 1994. Warrendale, PA, É.-U.: The Minerals, Metals & Materials Society, pp. 429-440.

Landi, M. F., Bacchiega, R. & Battaglia, A. 1968. Oriented recrystallization of alumina from cryolite baths for the production of aluminum by electrolysis of the separated ore. *La Metallurgia Italiana,* 60(11), pp. 939-44.

Landry, J.-R., Fallah Fini, M., Soucy, G., Désilets, M., Pelletier, P., Rivoaland, L. & Lombard, D. 2018. Laboratory study of the impact of the cathode grade on the formation of deposits on the cathode surface in Hall-Héroult Cells. *In:* Martin, O., (éd.) Light Metals 2018. Cham, Suisse: Springer International Publishing, pp. 1229-1233, https://doi.org/10.1007/978-3-319-72284-9_161.

Landry, J.-R., Fallah Fini, M., Soucy, G., Désilets, M., Pelletier, P., Rivoaland, L. & Lombard, D. 2019. Experimental Investigation of the Impact of Cathode Grade on Sludge Formation at the Cathode Block-Aluminum Interface of Hall–Héroult Cells.

Metallurgical and Materials Transactions B, 50(1), pp. 416-428, https://doi.org/10.1007/s11663-018-1435-0.

Lavoie, P., Taylor, M. P. & Metson, J. B. 2016. A review of alumina feeding and dissolution factors in aluminum reduction cells. *Metallurgical and Materials Transactions B,* 47(4), pp. 2690-2696, https://doi.org/10.1007/s11663-016-0680-3.

Leitner, M., Leitner, T., Schmon, A., Aziz, K. & Pottlacher, G. 2017. Thermophysical properties of liquid aluminum. *Metallurgical and Materials Transactions A,* 48(6), pp. 3036-3045, https://doi.org/10.1007/s11661-017-4053-6.

Li, T., Johansen, S. T. & Solheim, A. 2015. Detailed Model of Electrochemical Cathode Wear in Hall-Héroult Cells. *In:* Hyland, M., (éd.) Light Metals 2015. Cham, Suisse: Springer International Publishing, pp. 831-836, https://doi.org/10.1007/978-3-319-48248-4_140.

Liao, X.-a. & Øye, H. A. 2016. Physical and Chemical Wear of Carbon Cathode Materials. *In:* Tomsett, A. & Johnson, J. (éds.) *Essential Readings in Light Metals.* Vol. 4, Cham, Switzerland: Springer International Publishing, pp. 992-998, https://doi.org/10.1007/978-3-319-48200-2_131.

Liao, X. & Øye, H. A. 2013. Carbon cathode corrosion by aluminium carbide formation in cryolitic melts. *In:* Tomsett, A. & Johnson, J. (éds.) *Essential Readings in Light Metals.* Vol. 4, Hoboken, NJ, É.-U.: John Wiley & Sons, Inc., pp. 984-991, https://doi.org/10.1002/9781118647745.ch132.

Liu, W., Zhou, D. & Zhao, Z. 2019. Progress in Application of Energy-Saving Measures in Aluminum Reduction Cells. *JOM,* 71(7), pp. 2420-2429, https://doi.org/10.1007/s11837-019-03487-8.

Liu, X. 1995. Thermochemistry of electrolyte, sludge/ridge, ledge and cell cover. Proceedings of the 5th Australasian Aluminum Smelter Technology Workshop. Queenstown, New Zealand: Royal Australian Chemical Institute and University of South Wales, pp. 619-627.

Lorentsen, O. A. 2014. 125 years of the Hall-Héroult Process—What Made It a Success? *In:* Gaune-Escard, M. & Haarberg, G. M. (éds.) *Molten Salts Chemistry and Technology.* Chichester, R.-U.: John Wiley & Sons, Inc., pp. 103-112, https://doi.org/10.1002/9781118448847.ch1k.

Maeda, H., Matsui, S. & Era, A. 1985. Measurement of dissolution rate of alumina in cryolite melt. *In:* Bohner, H. O., (éd.) Light Metals 1985. Warrendale, PA, É.-U.: The Metallurgical Society of AIME, pp. 763-780.

McGeer, J. P. & Zwicker, J. D. 1982. Alumina: Calcination Control and Smelting Use. *JOM,* 34(5), pp. 50-54, https://doi.org/10.1007/bf03339150.

Metson, J. B., Hyland, M. M. & Groutso, T. 2005. Alumina phase distribution, structural hydroxyl and performance of smelter grade aluminas in the reduction cell. *In:* Kvande,

H., (éd.) Light Metals 2005. Warrendale, PA, É.-U.: The Minerals, Metals & Materials Society, pp. 127-131.

Meyer, A., Børset, O., Sommerseth, C., Osen, K., Rosenkilde, C. & Kristiansen, L. 2012. Examination of drop in bath acidity due to change-over of alumina qualities in the sunndal aluminium smelter, Norway. Proceedings of the 9th International Alumina Quality Workshop, Perth, Australia. Sidney, Australie: AQW Inc., pp. 316-321.

Moxnes, B. P., Aga, B. E. & Skaar, J. H. 1998. How to obtain open feeder holes by installing anodes with tracks. *In:* Welch, B. J., (éd.) Light Metals 1998. Warrendale, PA, É.-U.: The Minerals, Metals & Materials Society, pp. 247-255.

Moxnes, B. P., Solheim, A., Liane, M., Svinsås, E. & Halkjelsvik, A. 2009. Improved cell operation by redistribution of the alumina feeding. *In:* Bearne, G., (éd.) Light Metals 2009. Warrendale, PA, É.-U.: The Minerals, Metals & Materials Society, pp. 461-466.

Novak, B., Ratvik, A. P., Wang, Z. & Grande, T. 2018. Formation of Aluminium Carbide in Hall-Héroult Electrolysis Cell Environments. Light Metals 2018. Cham, Suisse: Springer International Publishing, pp. 1215-1222, https://doi.org/10.1007/978-3-319-72284-9_159.

Novak, B., Tschöpe, K., Ratvik, A. P. & Grande, T. 2012. Fundamentals of Aluminium Carbide Formation. *In:* Suarez, C. E., (éd.) Light Metals 2012. Hoboken, NJ, É.-U.: John Wiley & Sons, Inc., pp. 1343-1348, https://doi.org/10.1007/978-3-319-48179-1_232.

Ødegård, R., Roenning, S., Rolseth, S. & Thonstad, J. 1985. Crust formation in aluminum cells. *JOM,* 37(11), pp. 25-28, https://doi.org/10.1007/BF03258735.

Ødegård, R., Roenning, S., Rolseth, S. & Thonstad, J. 2013a. On alumina phase transformation and crust formation in aluminum cells. *In:* Bearne, G., Dupuis, M. & Tarcy, G. (éds.) *Essential Readings in Light Metals.* Vol. 2, Hoboken, NJ, É.-U.: John Wiley & Sons, Inc., pp. 622-629, https://doi.org/10.1002/9781118647851.ch92.

Ødegård, R., Sterten, Å. & Thonstad, J. 2013b. On the solubility of aluminium carbide in cryolitic melts - influence on cell performance. *In:* Bearne, G., Dupuis, M. & Tarcy, G. (éds.) *Essential Readings in Light Metals.* Vol. 2, Hoboken, NJ, É.-U.: John Wiley and Sons Inc., pp. 25-32, https://doi.org/10.1002/9781118647851.ch4.

Pawlek, R. P. 2010. Wettable cathodes: an update. *In:* Johnson, J. A., (éd.) Light Metals 2010. Warrendale, PA, É.-U.: The Minerals, Metals & Materials Society, pp. 377-382.

Richards, N. E. 2007. Evolution of Electrolytes for Hall-Héroult Cells. *In:* Peterson, W. S. & Miller, R. E. (éds.) *Hall-Héroult Centennial.* Hoboken, NJ, É.-U.: John Wiley & Sons, Inc., pp. 114-119, https://doi.org/10.1002/9781118788011.ch9.

Rivoaland, L. 2016. Development of a new type of cathode for aluminium electrolysis. Proceedings of ICSOBA 2016 Conference. Quebec City, QC, Canada: ICSOBA-RioTinto-REGAL, pp. 9.

Robelin, C. & Chartrand, P. 2011. A viscosity model for the (NaF + AlF3 + CaF2 + Al2O3) electrolyte. *The Journal of Chemical Thermodynamics,* 43(5), pp. 764-774, https://doi.org/10.1016/j.jct.2010.12.017.

Robilliard, K. R. & Rolofs, B. 2013. A demand feed strategy for aluminium electrolysis cells. *In:* Bearne, G., Dupuis, M. & Tarcy, G. (éds.) *Essential Readings in Light Metals.* Vol. 2, Hoboken, NJ, É.-U.: John Wiley & Sons, Inc., pp. 747-751, https://doi.org/10.1002/9781118647851.ch111.

Rye, K. A., Rolseth, S., Thonstad, J. & Zhanling, K. 1990. Behaviour of alumina on addition to cryolitic baths. Proceedings of the 2nd International Alumina Quality Workshop. Perth, Australie: AQW Inc., pp. 24-37.

Schubert Severo, D. & Gusberti, V. 2017. Heat exchanger for alumina preheating in aluminium reduction cells. Proceedings of ICSOBA 2017 Conference. Hamburg, Germany: ICSOBA, pp. 1059-1069.

Sele, T. 1977. Instabilities of the metal surface in electrolytic alumina reduction cells. *Metallurgical Transactions B,* 8(4), pp. 613-618, https://doi.org/10.1007/BF02669338.

Senanu, S., Wang, Z., Ratvik, A. P. & Grande, T. 2019. Carbon Cathode Wear in Aluminium Electrolysis Cells. *JOM,* 72(1), pp. 210-217, https://doi.org/10.1007/s11837-019-03717-z.

Siew, E. F., Ireland-Hay, T., Stephens, G. T., Chen, J. J. J. & Taylor, M. P. 2005. A study of the fundamentals of pothole formation. *In:* Kvande, H., (éd.) Light Metals 2005. Warrendale, PA, É.-U.: Minerals, Metals & Materials Society, pp. 763-769.

Singh, R., Das, K., Mishra, A. K. & Kalo, N. 2017. An approach for estimation of cathode voltage drop in an aluminum reduction cell with an inclined carbon block and a copper Insert. *Transactions of the Indian Institute of Metals,* 70(7), pp. 1795-1804, https://doi.org/10.1007/s12666-016-0978-5.

Skybakmoen, E., Rørvik, S., Solheim, A., Holm, K. R., Tiefenbach, P. & Østrem, Ø. 2011. Measurement of Cathode Surface Wear Profiles by Laser Scanning. *In:* Lindsay, S. J., (éd.) Light Metals 2011. Hoboken, NJ, É.-U.: John Wiley & Sons, Inc., pp. 1059-1066, https://doi.org/10.1007/978-3-319-48160-9_180.

Sleppy, W. C. & Cochran, C. N. 2013. Bench scale electrolysis of alumina in sodium fluoride–aluminum fluoride melts below 900°C. *In:* Bearne, G., Dupuis, M. & Tarcy, G. (éds.) *Essential Readings in Light Metals.* Vol. 2, Hoboken, NJ, É.-U.: John Wiley & Sons, Inc., pp. 1089-1094, https://doi.org/10.1002/9781118647851.ch159.

Solheim, A. 2002. Crystallization of cryolite and alumina at the metal-bath interface in aluminium reduction cells. *In:* Schneider, W., (éd.) Light Metals 2002. Warrendale, PA, É.-U.: The Minerals, Metals & Materials Society, pp. 225-230.

Solheim, A. 2014. A novel design criterion for alumina feeders in aluminium electrolysis cells. *In:* Grandfield, J., (éd.) Light Metals 2014. Hoboken, NJ, É.-U.: John Wiley & Sons, Inc., pp. 709-716, https://doi.org/10.1002/9781118888438.ch119.

Solheim, A. 2018. Inert anodes—the blind alley to environmental friendliness? *In:* Martin, O., (éd.) Light Metals 2018. Cham, Suisse: Springer International Publishing, pp. 1253-1260, https://doi.org/10.1007/978-3-319-72284-9_164.

Song, Y., Peng, J., Di, Y., Wang, Y. & Feng, N. 2017a. Metal flow performance in aluminium electrolytic cells with different side-wall types. *Canadian Metallurgical Quarterly,* 57(3), pp. 1-9, https://doi.org/10.1080/00084433.2017.1414107.

Song, Y., Peng, J., Di, Y., Wang, Y. & Feng, N. 2017b. Performance of the cathodes with trapezoidal protrusions in aluminum electrolysis cells. *JOM,* 69(12), pp. 2844-2850, https://doi.org/10.1007/s11837-017-2615-0.

Song, Y., Peng, J., Di, Y., Wang, Y., Li, B. & Feng, N. 2016. The impact of cathode material and shape on current density in an aluminum electrolysis cell. *JOM,* 68(2), pp. 593-599, https://doi.org/10.1007/s11837-015-1719-7.

Sørlie, M. & Øye, H. A. 2010. *Cathodes in Aluminium Electrolysis,* Düsseldorf, Allemagne: Aluminium Verlag GmbH, 662 p.

Stam, M. A., Taylor, M. P., Chen, J. J. J., Mulder, A. & Rodrigo, R. 2008. Common behaviour and abnormalities in aluminium reduction cells. *In:* Deyoung, D. H., (éd.) Light metals 2008. Warrendale, PA, É.-U.: The Minerals, Metals & Materials Society, pp. 309-314.

Tabereaux, A. T. 2000. Prebake cell technology: a global review. *JOM,* 52(2), pp. 23-29, https://doi.org/10.1007/s11837-000-0043-y.

Tabereaux, A. T. & Peterson, R. D. 2014. Aluminum production. *In:* Seetharaman, S. (éd.) *Treatise on Process Metallurgy.* Vol. 3, Boston, MA, É.-U.: Elsevier, pp. 839-917, https://doi.org/10.1016/B978-0-08-096988-6.00023-7.

Tarapore, E. D. 2013. The effect of some operating variables on flow in aluminum reduction cells. *In:* Bearne, G., Dupuis, M. & Tarcy, G. (éds.) *Essential Readings in Light Metals.* Vol. 2, Hoboken, NJ, É.-U.: John Wiley & Sons, Inc., pp. 322-329, https://doi.org/10.1002/9781118647851.ch46.

Tarcy, G. P., Kvande, H. & Tabereaux, A. 2011. Advancing the industrial aluminum process: 20th century breakthrough inventions and developments. *JOM,* 63(8), pp. 101-108, https://doi.org/10.1007/s11837-011-0120-4.

Taylor, M. P. 1997. Challenges in optimizing and controlling the electrolyte in aluminum smelters. Proceedings of the International Conference on Molten Slags, Fluxes and Salts. Warrendale, PA, É.-U.: Iron and Steel Society of AIME, pp. 659-674.

Taylor, M. P., Liu, X., Fraser, K. & Welch, B. J. 1990. Dynamics and performance of reduction cell electrolytes. *In:* Bickert, C., (éd.) Light Metals 1990. Warrendale, PA, É.-U.: The Minerals, Metals & Materials Society, pp. 259-266.

Taylor, M. P. & Welch, B. J. 2004. The future outlook and challenges for smelting aluminium. *Aluminium International Today,* 16(2), pp. 20-24.

Tessier, J., Tarcy, G. P., Batista, E., Wang, X. & Doiron, P. 2013. Improvement of Alumina Dissolution Rate through Alumina Feeder Pipe Modification. *In:* Sadler, B. A., (éd.) Light Metals 2013, Hoboken, NJ, USA. : John Wiley & Sons, Inc., pp. 711-717, https://doi.org/10.1002/9781118663189.ch122.

Thonstad, J. 1977. Semicontinuous determination of the concentration of alumina in the electrolyte of aluminum cells. *Metallurgical Transactions B,* 8(1), pp. 125-130, https://doi.org/10.1007/bf02656361.

Thonstad, J., Fellner, P., Haarberg, G. M., Híveš, J., Kvande, H. & Sterten, Å. 2001. *Aluminium Electrolysis: Fundamentals of the Hall-Héroult Process,* Düsseldorf, Allemagne: Aluminium-Verlag, 359 p.

Thonstad, J., Johansen, P. & Kristensen, E. W. 1980. Some properties of alumina sludge. *In:* McMinn, C. J., (éd.) Light Metals 1980. Warrendale, PA, É.-U.: The Metallurgical Society of AIME, pp. 227-239.

Thonstad, J., Nordmo, F. & Paulsen, J. B. 1972. Dissolution of alumina in molten cryolite. *Metallurgical Transactions,* 3(2), pp. 407-412, https://doi.org/10.1007/BF02642044.

Thonstad, J., Roenning, S. & Entner, P. 1982. Formation of bottom crusts in aluminum pots. a laboratory study. *In:* Andersen, J. E., (éd.) Light Metals 1982. Warrendale, PA, É.-U.: The Metallurgical Society of AIME, pp. 485-497.

Thonstad, J., Solheim, A., Rolseth, S. & Skar, O. 2013. The dissolution of alumina in cryolite melts. *In:* Bearne, G., Dupuis, M. & Tarcy, G. (éds.) *Essential Readings in Light Metals.* Vol. 2, Hoboken, NJ, É.-U.: John Wiley & Sons, Inc., pp. 105-111, https://doi.org/10.1002/9781118647851.ch14.

Torklep, K., Kalgraf, K. & Nordbo, T. 1997. Alumina distribution in point-fed Hall-Heroult Cells. *In:* Huglen, R., (éd.) Light Metals 1997. Warrendale, PA, É.-U.: Minerals, Metals & Materials Society, pp. 377-386.

Tschöpe, K., Støre, A., Rørvik, S., Solheim, A., Skybakmoen, E., Grande, T. & Ratvik, A. P. 2012. Investigation of the Cathode Wear Mechanism in a Laboratory Test Cell. *In:* Suarez, C. E., (éd.) Light Metals 2012. Hoboken, NJ, É.-U.: John Wiley & Sons, Inc., pp. 1349-1354, https://doi.org/10.1007/978-3-319-48179-1_233.

Tschöpe, K., Støre, A., Skybakmoen, E., Solheim, A., Grande, T. & Ratvik, A. P. 2013. Critical Reflections on Laboratory Wear Tests for Ranking Commercial Cathode Materials in

Aluminium Cells. *In:* Sadler, B. A., (éd.) Light Metals 2013. Hoboken, NJ, É.-U.: John Wiley & Sons, Inc., pp. 1251-1256, https://doi.org/10.1007/978-3-319-65136-1_211.

Utigard, T. A. 1987. Mass transfer in Hall-Heroult Electrolysis induced by interfacial tension gradients. *Aluminium,* 63(6), pp. 608-613.

Utigard, T. A. 1993. An analysis of the effect of bath density variations on the behaviour of Hall-Heroult Cells. *Canadian Metallurgical Quarterly,* 32(4), pp. 327-333, https://doi.org/10.1179/cmq.1993.32.4.327.

Utigard, T. A. 1999. Why best pots operate between 955 and 970 °C. *In:* Eckert, C. E., (éd.) Light Metals 1999. Warrendale, PA, É.-U.: The Minerals, Metals & Materials Society, pp. 319-326.

Utigard, T. A., Rolsetht, S., Thonstad, J. & Toguri, J. M. 1989. Interfacial phenomena in aluminum electrolysis. *In:* Closset, B. (éd.) *Production and Electrolysis of Light Metals.* Oxford, R.-U.: Pergamon, pp. 189-199, https://doi.org/10.1016/B978-0-08-037295-2.50022-3.

Utigard, T. A. & Toguri, J. M. 1985. Interfacial tension of aluminum in cryolite melts. *Metallurgical Transactions B,* 16(2), pp. 333-338, https://doi.org/10.1007/bf02679724.

Utigard, T. A. & Toguri, J. M. 1991. Marangoni flow in the Hall-Heroult Cell. *In:* Rooy, E., (éd.) Light Metals 1991. Warrendale, PA, É.-U.: The Minerals, Metals & Materials Society, pp. 273-281.

Veneraki, I. E., Romanko, K. S., Urda, N. N. & Semenov, V. S. 1973. Thermal conductivity of materials of aluminum electrolytic cells. *Energetika i Elektrifikatsiya,* (2), pp. 52-54.

Von Kaenel, R., Bugnion, L., Von Kaenel, L., Spinetti, G. & Pfeffer, M. 2017. The use of copper in cathodes of aluminium reduction cells. Proceedings of ICSOBA 2017 Conference. Hamburg, Germany: ICSOBA, pp. 879-889.

Walker, D. I., Utigard, T. A. & Taylor, M. P. 1995. Alumina agglomerates in aluminum smelters. *In:* Evans, J. W., (éd.) Light Metals 1995. Warrendale, PA, É.-U.: The Minerals, Metals & Materials Society, pp. 425-434.

Walker, M. L., Purdie, J. M., Wai-Poi, N. S., Welch, B. J. & Chen, J. J. J. 2013. Design considerations for selecting the number of point feeders in modern reduction cells. *In:* Bearne, G., Dupuis, M. & Tarcy, G. (éds.) *Essential Readings in Light Metals.* Vol. 2, Hoboken, NJ, É.-U.: John Wiley & Sons, Inc., pp. 752-759, https://doi.org/10.1002/9781118647851.ch112.

Wang, L., Tabereaux, A. T. & Richards, N. E. 1994. Electrical conductivity of cryolitic melts containing aluminum carbide. *In:* Mannweiler, U., (éd.) Light metals 1994. Warrendale, PA, É.-U.: The Minerals, Metals & Materials Society, pp. 177-185.

Wang, Q., Li, B., He, Z. & Feng, N. 2014. Simulation of magnetohydrodynamic multiphase flow phenomena and interface fluctuation in aluminum electrolytic cell with innovative cathode. *Metallurgical and Materials Transactions B,* 45(1), pp. 272-294, https://doi.org/10.1007/s11663-013-0001-z.

Wang, X. 2009. Alumina dissolution in aluminum smelting electrolyte. *In:* Bearne, G., (éd.) Light Metals 2009. Warrendale, PA, É.-U.: The Minerals, Metals & Materials Society, pp. 383-388.

Wang, Z., Nobakhtghalati, S., Støre, A., Solheim, A., Tschöpe, K., Ratvik, A. P. & Grande, T. 2016. Cathode Wear in Electrowinning of Aluminum Investigated by a Laboratory Test Cell. *In:* Williams, E., (éd.) Light Metals 2016. Hoboken, NJ, É.-U.: John Wiley & Sons, Inc., pp. 895-902, https://doi.org/10.1002/9781119274780.ch151.

Wang, Z., Skybakmoen, E. & Grande, T. 2009. Spent Si3N4 bonded SiC sidelining materials in aluminium electrolysis cells. *In:* Bearne, G., (éd.) Light Metals 2009. Warrendale, PA, É.-U.: The Minerals, Metals & Materials Society, pp. 353-358.

Welch, B. J. 1990. The role cell design and cell operating conditions can play in reducing problems from alumina. Proceedings of the 2nd International Alumina Quality Workshop. Perth, Australie: AQW Inc., pp. 15-22.

Welch, B. J. 1995. Sludge/muck in smelting cells. Proceedings of the 5th Australasian Aluminum Smelter Technology Workshop. Sidney, Australie: Royal Australian Chemical Institute and University of South Wales, pp. 651–659.

Welch, B. J. 2007. Gaining that extra 2 percent current efficiency. *In:* Peterson, W. S. & Miller, R. E. (éds.) *Hall-Héroult Centennial.* Hoboken, NJ, É.-U.: John Wiley & Sons, Inc., pp. 120-129, https://doi.org/10.1002/9781118788011.ch10.

Welch, B. J. & Grjotheim, K. 1988. Alumina's and cell feeding technologies. Proceedings of the 1st International Alumina Quality Workshop. Gladstone, Australie: AQW Inc., pp. 75-86.

Welch, B. J. & Kinery, J. T. 2000. Advancing the hall heroult electrolytic process. *In:* Peterson, R. D., (éd.) Light Metals 2000. Warrendale, PA, É.-U.: The Minerals, Metals & Materials Society, pp. 17-25.

Welch, B. J. & Kuschel, G. I. 2007. Crust and alumina powder dissolution in aluminum smelting electrolytes. *JOM,* 59(5), pp. 50-54.

Whitfield, D., Skyllas-Kazacos, M., Welch, B. J. & McFadden, F. S. 2004. Aspects of alumina control in aluminium reduction cells. *In:* Tabereaux, A. T., (éd.) Light Metals 2004. Warrendale, PA, É.-U.: The Minerals, Metals & Materials Society, pp. 249-255.

Yang, Y., Gao, B., Wang, Z., Shi, Z. & Hu, X. 2015. Study on the dissolution of alumina in cryolite electrolyte using the see-through cell. *In:* Hyland, M., (éd.) Light Metals 2015.

Hoboken, NJ, É.-U.: John Wiley & Sons, Inc., pp. 583-588, https://doi.org/10.1002/9781119093435.ch97.

Yurkov, A. 2015. Refractories and Carbon Cathode Materials for Aluminium Reduction Cells. *In:* Yurkov, A. (éd.) *Refractories for Aluminium: Electrolysis and the Cast House.* Cham, Suisse: Springer International Publishing, pp. 65-208, https://doi.org/10.1007/978-3-319-11442-2_2.

Zhan, S., Li, M., Zhou, J., Yang, J. & Zhou, Y. 2014. CFD simulation of dissolution process of alumina in an aluminum reduction cell with two-particle phase population balance model. *Applied Thermal Engineering,* 73(1), pp. 805-818, https://doi.org/10.1016/j.applthermaleng.2014.08.040.

Zhang, X., Tang, Y., Zhang, F. & Lee, C.-S. 2016. A Novel Aluminum–Graphite Dual-Ion Battery. *Advanced Energy Materials,* 6(11), pp. 1502588-n/a, https://doi.org/10.1002/aenm.201502588.

Zoukel, A., Chartrand, P. & Soucy, G. 2009. Study of aluminum carbide formation in Hall-Heroult electrolytic cells. *In:* Bearne, G., (éd.) Light metals 2009. Warrendale, PA, É.-U.: The Minerals, Metals & Materials Society, pp. 1123-1128.